

Multiple Chromisms Associated with Dithizone

by

Lumanyano L. A. Ntoi

A dissertation submitted in accordance with the requirements of the degree of

Magister Scientiae

in the

Department of Chemistry

Faculty of Natural and Agricultural Sciences

at the



University of the Free State

P.O BOX 9301

Bloemfontein, South Africa

Supervisor

Prof. K.G. von Eschwege

2016

ACKNOWLEDGEMENTS

This has been an enormous period that has helped me develop and grow, not only on scientific level but also on a personal level. There has been a lot of challenges but now when I look back they were learning curves to me. However, I have enjoyed this study, it was a life changing opportunity that I am grateful to have experienced, and the company around me during this research period was excellent. Most of all I would like to thank God for everything and I would like to extend my deepest gratitude to the following individuals that have been with me right through this journey:

- Prof. K. G. von Eschwege, thank you for giving me this opportunity to work with you. I really appreciate your guidance, enthusiasm, motivation and allowing me to engage; your knowledge and support has helped me complete this study. I cannot imagine a humorous supervisor better than you. *“Same procedure as last year”*
- The analytical group; Q. Vilakazi, S. Xaba, M. Nete, L. Mona, T. Chiweshe, A. Ngcephe, R. Kankwanzi, S. Kumar, and A. Kannan. Thank you for the great environment that we all shared. I would also like to thank my mentor Ms. O Mbatyazwa.
- The National Research Foundation for the financial support.
- Prof. J. C. Swarts and Dr. B. Buitendach for assistance with the electrochemistry and the use of equipment.
- Dr. A. Brink and O. Alexander, for the use of the X-ray diffractometer and assistance in solving the crystal structures.
- My family, Mr N. D. P. Ntoi, Mrs E. N. Ntoi, and Mrs K. Gutyingwa, without your love, courage and support I wouldn't be where I am today. You mean a lot to me and I will forever be grateful for all the efforts and sacrifices you have made for my academic life. *“Ndiyabulela”*

“If a man is properly motivated, he can do almost anything”

Table of Contents

1. INTRODUCTION	1
1.1. SYNTHESIS	2
1.2. CHROMISM	3
1.3. ANALYTICAL APPLICATIONS	4
1.4. KINETICS	4
1.5. X-RAY CRYSTALLOGRAPHY	4
2. LITERATURE SURVEY	5
2.1. INTRODUCTION	5
2.2. DITHIZONE and its METAL COMPLEXES	5
2.2.1. Discovery, Synthesis and Solubility	5
2.2.2. Structure and Geometry	11
2.3. CHROMISM	17
2.3.1. Photochromism	17
2.3.2. Solvatochromism	23
2.3.3. Electrochromism	26
2.3.4. Halochromism	29
2.3.5. Thermochromism	31
2.3.6. Concentratochromism	33
2.3.7. Chronochromism	34
2.4. ANALYTICAL APPLICATIONS	35
2.4.1. Metal Dithizonates	35
2.4.2. Mole Ratio Method	37
2.4.3. Continuous variation Method	39
3. RESULTS AND DISCUSSION	41
3.1. INTRODUCTION	41
3.2. SYNTHESIS	41
3.2.1. Dithizone derivatives	41
3.2.1.1. (<i>p</i> -COOH)dithizone	41
3.2.1.2. (<i>p</i> -SO ₃)nitroformazan	43
3.2.1.3. (<i>p</i> -Sulfonylacetamide)nitroformazan	44

3.2.2.	Metal Dithizonate	45
3.2.2.1.	(<i>p</i> -COOH)dithizonatophenylmercury(II), PhHg(<i>p</i> -COOH-HDz)	45
3.2.2.2.	PhHg(<i>p</i> -COOPhHg -HDz)	45
3.2.2.3.	<i>Tris</i> -(<i>p</i> -COOH)dithizonatocobalt(III)	46
3.2.2.4.	<i>Tris</i> -dithizonatocobalt(III)	47
3.2.2.5.	<i>tris</i> -(<i>p</i> -COOH)dithizonatonickel(II)	48
3.2.2.6.	<i>Bis</i> -dithizonatonickel(II)	48
3.2.2.7.	(<i>p</i> -COOH)dithizonatolead(II)	49
3.2.2.8.	<i>bis</i> -dithizonatolead(II)	49
3.2.2.9.	(<i>p</i> -COOH)dithizonatosilver(I)	50
3.2.2.10.	Dithizonatosilver(I)	50
3.2.3.	Discussion	51
3.2.3.1.	Dithizone Derivatives	51
3.2.3.2.	Metal Dithizonates	53
3.3.	X-RAY CRYSTALLOGRAPHY	60
3.3.1.	<i>p</i> -COOH(nitroformazan) crystal	60
3.4.	SPECTROMETRIC DETERMINATION OF COMPLEX IONS	65
3.4.1.	Mole Ratio Method	65
3.4.1.1.	Co(<i>p</i> -COOH-HDz) ₃ & Co(HDz) ₃	66
3.4.1.2.	Ni(<i>p</i> -COOH-HDz) ₃ & Ni(HDz) ₂	67
3.4.1.3.	Pb(<i>p</i> -COOH-HDz) & Pb(HDz) ₂	70
3.4.1.4.	Ag(<i>p</i> -COOH-HDz) & Ag(HDz)	71
3.4.1.5.	Hg(<i>p</i> -COOH-HDz)	72
3.4.2.	Method of Continuous Variation	73
3.4.2.1.	Co(<i>p</i> -COOH-HDz) ₃	74
3.4.2.2.	Ni(<i>p</i> -COOH-HDz) ₃ & Ni(HDz) ₂	74
3.5.	CHROMISM	76
3.5.1.	Photochromism and reaction kinetics	79
3.5.2.	Solvatochromism	85
3.5.3.	Electrochromism	89
3.5.4.	Halochromism	94
3.5.5.	Concentratochromism	98
3.5.6.	Thermochromism	101
3.5.7.	Chronochromism	101
4.	ABSTRACT AND	103
5.	FUTURE PERSPECTIVES	104
6.	APPENDIX : X-Ray Crystallographic Data	I

1. Introduction

It has been noticeable that organic chemistry is merging into analytical procedures of qualitative and quantitative analysis. For instance, some organic compounds that are generally used for analysis, like the chelating agent dimethylglyoxime and pH indicators, are now part of analytical chemistry. Organic reagents may be used to speed up, simplify, and also improve accuracy in analytical methods. These organic analytical reagents are also applicable to trace metal analysis. Diphenylthiocarbazone (dithizone) is one of these organic analytical reagents that has been reported to be important for detection of metals at low concentration. Preparation of this dithizone compound is fairly simple and direct, although there has been some challenges in getting pure product.¹ Dithizone is known to be a versatile analytical reagent that reacts with a variety of metals to form intensely coloured metal complexes. It has been widely applied in research fields that focus on qualitative and quantitative determination of heavy metals. This ligand has two sites for coordination with a metal, either via its sulfur or both the sulfur and nitrogen atoms.²

Even at trace levels many elements in the sea have been affecting humans and other living organisms. This effect has encouraged more studies in fields like biochemistry, geology and chemistry to determine these trace elements.³ In approximately one third of all proteins the vital elements are metals, and these metals take part in virtually all biological processes. The metal ions in metalloproteins are generally quantified by inductive coupled plasma mass spectrometry and atomic absorption spectrometry, because these techniques are reliable and have good sensitivity. Like any other instrument these have limitations, like being costly, time consuming and not always readily available. Simple spectroscopy like the ultraviolet-visible (UV-Vis) is an alternative because it is less costly and labour-intensive. In this technique the absorption spectrum of a chromophoric chelator on binding the desired metal is of importance, as determination of trace metals by UV-Vis relies on it. Ligands like 2,2'-bipyridyl and dithizone have been used to form coloured complexes with Fe(II) and Zn(II), as a means to determine these metals spectrophotometrically.⁴ The intrinsic sensitivity and potential selectivity of organic complexing reagents have made these reagents to be important in analytical chemistry. Organic reagents may also aid in the precipitation of metals. Dithizone is one of the widely used organic complexing agents for extracting metals of interest from their interfering ions, e.g. from water to

¹ W. E. White, *J. Chem. Edu.*, 369, (1936).

² A. A. Pasynskii, A. N. Il'in, S. S. Shaovalov and Yu. V. Torubaev, *J. Inorg. Chem.*, 939, **52** (2007).

³ Y. -S Kim, Y. -S Choi and K. In, *Bull. Korean Chem. Soc.*, 137, **21** (2000).

⁴ P. S. Mehta and V. B. Patel, *Int. J. Pharmaceutical Research and Analysis*, 87, **2** (2012).

chloroform.⁵ Dithizone has an intense violet-black colour in its solid state, and it is thus an excellent selective reagent for quantitative trace metal analysis. Colorimetric and spectrometric analysis of metals in microgram quantities depend on the intense colour of this reagent in solution and that of the metal complexes it forms – its extreme sensitivity has to be emphasised. Controlling the pH and making use of masking agents improve the selectivity of this reagent.⁶ Observed colour changes associated with dithizone chemistry, is an important feature which has led to the present study of its multiple chromisms. There has been a number of reports in literature that illustrates its photochromic properties when complexed with metals. This behaviour is stimulated by photo-excitation of the molecule, the back reaction being spontaneous and thermally reversible.⁷

The initial aim of this study was to also investigate analytical applications of water-soluble dithizone, like the mole-ratio and the continuous-variation methods. Both these methods rely on the intense colour that this compound exhibits when complexed with a metal. However, during these experiments it was discovered that the dithizone ligand also features other chromic phenomena which became of interest. This study consequently reports on synthesis, chromism and analytical applications of dithizone and its derivatives.

1.1. Synthesis

In literature dithizone has been reported as a compound that is not soluble in water but rather readily soluble in aqueous alkali medium, and soluble in organic solvents like chloroform. Very little information is reported on water-soluble dithizone and studies of such derivatives. This study explored synthetic methods to synthesize water-soluble dithizone derivatives.

Synthesis of three water-soluble dithizone derivatives with symmetrically placed (i.e. on both phenyl rings) substituents with the potential to make dithizone water-soluble were attempted. All three dithizones were *para*-substituted and were to be synthesized from the following anilines:

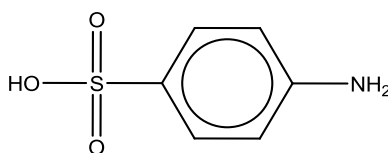


Figure 1.1: Chemical structure of Sulfanilic acid.

⁵ D. A. Skoog, D. M. West, F. J. Holler and S. R. Crouch, *Fundamentals of Analytical Chemistry*, Thomson Brooks/Cole (Canada) 8th ed., (2004).

⁶ G. H. Jeffery, J. Bassett, J. Mendham, and R. C. Denney, *Quantitative Chemical Analysis*, Thames Polytechnic (London) 5th ed., (1989).

⁷ K. G. von Eschwege, *J. Photochemistry and Photobiology A: Chemistry*, 159, **252** (2013).

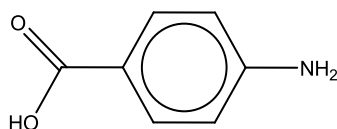


Figure 1.2: Chemical structure of 4-aminobenzoic acid.

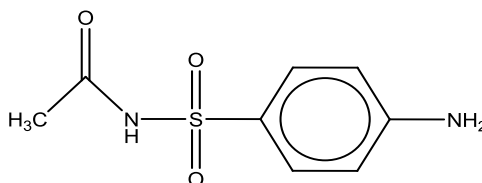


Figure 1.3: Chemical structure of Sulfacetamide.

Successfully synthesized water-soluble dithizone derivatives were then complexed with some metals that have been reported to form dithizonato complexes. Some of these metal complexes were involved in metal-to-ligand mole-ratio studies, and also studied with regard to their exhibited chromic behaviour.

1.2. Chromism

In the late 17th century Sir Isaac Newton recognised the relationship between light and colour, which then improved understanding of the hard science concerning colour. After that the level of sophistication and the myriad applications of colour have been increasing gradually up until today.^{8,9} Both chemical and physical forces may be involved in stimulating colour change. Colour change of a substance, often reversible, that is caused by an external stimulus, is defined as chromism. There are a number of external stimuli which may be involved by chromic phenomena, like light – which is called photochromism, heat (thermochromism), change in pH (halochromism), electrical current (electrochromism), solvent polarity (solvatochromism), and change in concentration (concentratochromism).¹⁰ In this study the dithizone ligand and dithizonate complex are shown to exhibit these types of chromism.

⁸ H. Nakazumi in *Chemistry and Applications of Leuco Dyes*, R. Muthyala (Ed.), Plenum Press, New York, 1997, pp. 1–45.

⁹ S. Maeda, in *Organic Photochromic and Thermochromic Compounds, Volume 1, Main Photochromic Families*, J.C. Crano and R.J. Guglielmetti (Eds.), Plenum Press, New York, 1999, pp. 85–109.

¹⁰ P. Bamfield, *Chromic Phenomena*, Royal society of chemistry, Britain, (2001).

1.3. Analytical Applications

For the sake of both qualitative and quantitative analyses in spectrophotometry, one may take advantage of a chromophoric reagent (i.e. dithizone) to react with a nonabsorbing analyte (i.e. metal ion), to form products that absorb strongly in the UV-Vis region of the spectrum. The composition of a complex and its formation constant in solution can also be determined by spectrophotometric means. Quantitative measurements of absorption can be made without any disturbance in the equilibria under consideration. The mole ratio, continuous variation (Job's method) and slope ratio methods are the three commonly employed techniques in complex ions studies.⁵ In this study the mole ratio and Job's methods were used to investigate the ratio of dithizonato metal complexes in aqueous alkali medium, using the unsubstituted dithizone and also 4,4-dithizone carboxylate as colour-development reagents.

1.4. Kinetics

Meriwether et al¹¹ conducted a study on nine photochromic dithizonato metal complexes and observed that the back reactions vary in speed. These observations then gave interest in following the mechanism involved in the activated form of these complexes. One technique that was used is the kinetic study of the return reaction of metal dithizonate complexes. It has been observed that temperature, solvent polarity and concentration play an important role in these studies.¹² A kinetic study that was conducted by Von Eschwege⁷ reveals how these factors affect the back reaction of the activated dithizonate complexes. He also reported how the phenyl-substituted dithizonates behave. With all this information at hand, the effect of the dicarboxylic acid substituent on the phenyl rings of the dithizonatomercury complex was studied kinetically.

1.5. X-ray Crystallography

During this investigation crystal-growth was attempted as part of supplementary characterisation of the structure and geometry of all products along syntheses routes, i.e. nitroformazans, dithizones, as well as its metal complexes. In line with previous findings by Von Eschwege *et al.*¹³ only nitroformazan crystals could successfully be grown to the size required by X-ray diffractometry.

¹¹ L. S. Meriwether, E. C. Breitner, C. L. Sloan, *J. Am. Chem. Soc.*, 4441 **87** (1965).

¹² L. S. Meriwether, E. C. Breitner, N. B. Colthup, *J. Am. Chem. Soc.*, 4448, **87** (1965).

¹³ K. G. Von Eschwege, F. Muller and E. C. Hosten, *Acta Cryst. Sect. E* **68** (2012).

2. Literature Survey

2.1. Introduction

Diphenylthiocarbazon (dithizone) is an organic compound which is also classified an organic analytical reagent. This compound has earned its place in analytical chemistry because it forms colorful complexes with numerous metals, with consequent use in trace metal analyses, extraction methods and precipitation of metals. In this chapter this ligand is examined step by step, beginning with its discovery, synthesis, geometry and structure, as well as that of its metal complexes. Secondly, the interesting chromic nature of this ligand and its metal complexes are discussed. Chromism is applicable in analytical chemistry, i.e. when using techniques like molecular absorption or ultraviolet visible (UV-vis) spectroscopy to determine the composition of complex ions in selected metal complexes. Lastly, the photochromic nature of the mercury dithizonate complex extends this investigation into studying its back-reaction kinetically.

2.2. Dithizone and its Metal Complexes

2.2.1. Discovery, Synthesis and Solubility

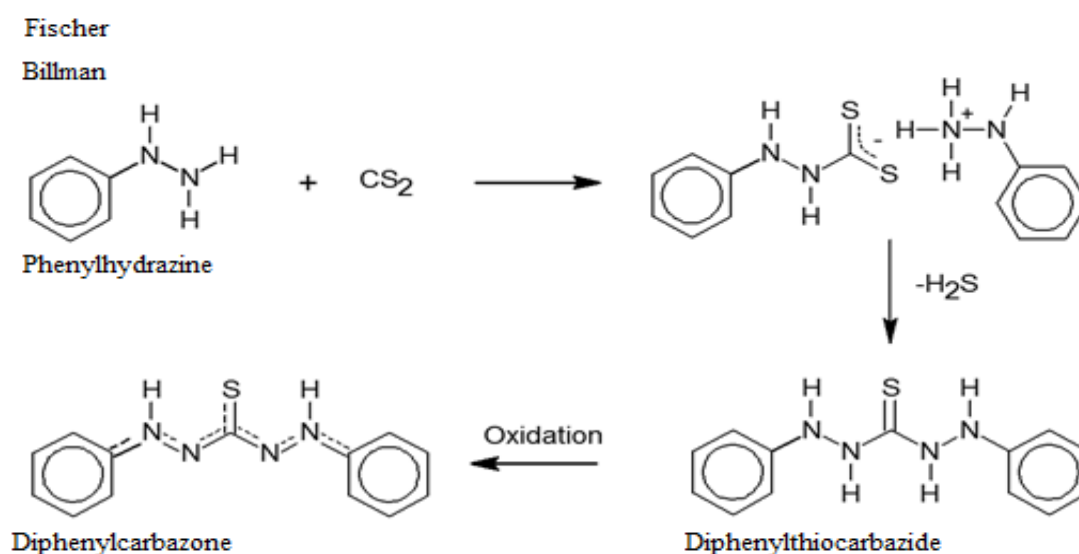
Diphenylthiocarbazon, 3-mercapto-1,5-diphenylformazan or 1,5-diphenylthiocarbazon, which is generally called dithizone and abbreviated as H₂Dz, is a violet-black crystalline powder with a metallic reflex. Dithizone has a chemical formula, C₁₃H₁₂N₄S, molar mass of 256.33 g mol⁻¹, density of 1.35 g.cm⁻³ and a melting point of 169 °C, at which it decomposes.¹⁴ The synthetic part of this organic reagent was first introduced by Emil Fischer,¹⁵ while doing an extensive study on derivatives of phenylhydrazine. He noticed the formation of an unstable white salt when mixing carbon disulphide and phenylhydrazine solutions. When these solutions were carefully heated, hydrogen sulphide was lost and ‘diphenylsulfocarbazid’ formed. Oxidization resulted when warmed with dilute alkali medium. Although this method was successful it had the limitation of producing very low yields. Yields were however improved by the condensation of phenylhydrazine with carbon disulfide, to form β-phenyldithiocarbazic acid. Heating of the latter forms diphenylthiocarbazide, which was dissolved in alcoholic sodium hydroxide to undergo mutual oxidation-reduction to form diphenylthiocarbazon.¹⁶ In their extensive study of

¹⁴ H. M. N. H. Irving, Analytical Science Monographs No. 5, The Chemical Society, London, (1977).

¹⁵ E. Fischer, Annalen, 67, **190** (1878).

¹⁶ O. Grummitt, R.Stickle, *Industrial and Engineering Chem.*, 1300, **14** (1942).

dithizone, Billman and Cleland¹⁷ proposed a method to improve the yields even further. This method used solvent-free conditions. At the first step of β -phenyldithiocarbamic acid formation no changes were made, but at the second step which involved removal of hydrogen sulphide, it was found that the temperature had an effect on the yields. Through a series of experiments that were conducted, by only varying the temperature, it was found that the optimum working temperature was 96-98 °C. Then, in the final oxidation step the effect of time and solvent was studied. Best yields were obtained when using methanolic potassium solution. The final product, after drying, was calculated to be 52-66 % yield. The above-mentioned synthetic methods are illustrated in Scheme 2.1, here below.



Scheme 2.1. The synthetic method of dithizone that was introduced by E. Fischer, then finally improved by Billman and Cleland.

Bamberger¹⁸ and Tarbell¹⁹ again, independently reported a different synthetic method which excludes the preparation from hydrazine, but begins with an aniline, in preparation of diazonium salts in dilute hydrochloric at 0°C, by slow addition of sodium nitrite. The diazonium salts are coupled by the addition of nitromethane to precipitate the nitroformazyl product. The coupling step was improved by use of a buffer with 40 % acetic acid at pH 4.5 in the coupling stage. Hubbard and Scott²⁰ used a similar method when preparing a series of dithizone derivatives containing double-ring phenyls, naphthyldithizone derivatives. The latter method was further modified by Pelkis *et al.*²¹ The change was in the final oxidation step; 2 % alcoholic alkali was added to the thiocarbazide and 1 % dilute hydrochloric acid added to precipitate the dithizone

¹⁷ J. H. Billman, E. S. Cleland, *J. Am. Chem. Soc.*, 1300, **65** (1943).

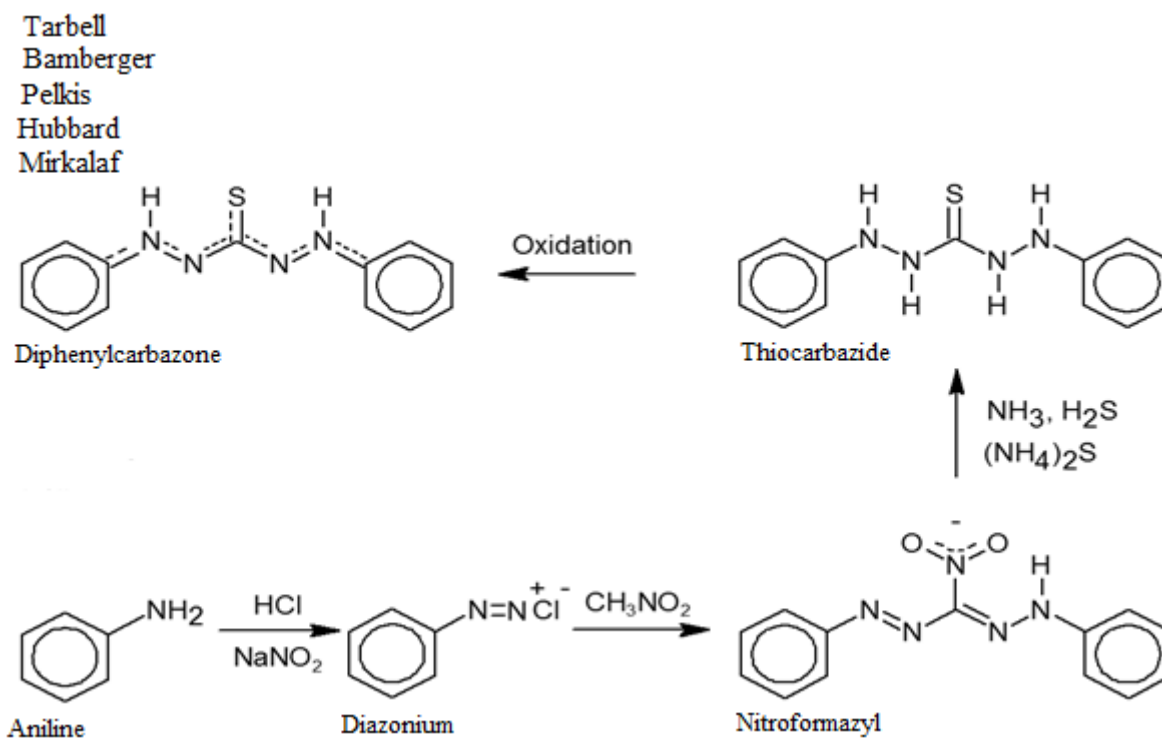
¹⁸ E. Bamberger, R. Padova, E. Omerod, *Lieb. Ann.* 307, **260**, (1926).

¹⁹ D. S. Tarbell, C. W. Todd, M. C. Paulson, E. G. Lindstrom, V. P. Wystrach, *J. Am. Chem. Soc.*, 1381, **70** (1948).

²⁰ D. M. Hubbard, E. W. Scott, *J. Am. Chem. Soc.*, 2390, **65** (1943).

²¹ P. S. Pelkis, R. G. Dubenko, L. S. Pupko, *J. Org. Chem. USSR.*, 2190, **27** (1957).

product. Instead of using NH_3 and H_2S , which are toxic gasses, Mirkhalaf *et al.*²² used 20 % $(\text{NH}_4)_2\text{S}$ solution to convert the nitroformazyl to the thiocarbazide intermediate product. Good yields of electron withdrawing and donating derivatives of dithizone were obtained with this method. Here below follows a schematic illustration for the synthesis of dithizone by various authors, following the same basic route, but various modifications, as mentioned above.



Scheme 2.2. Synthesis of dithizone by various indicated authors.

Not all dithizone derivatives have been synthesized by the method shown in Scheme 2.2. Water-soluble dithizone has been synthesized by the method illustrated in Scheme 2.1. For example, the sulphonic acid derivative of dithizone was claimed to have been prepared, and apparently stable as its sodium salt both in aqueous medium and in dry state, but unstable as the free acid.²³ Shaw *et al.*²⁴ used a modified method based on that developed by Tanaka *et al.*²³ to also synthesize the water-soluble sulfonate and some new carboxylate analogues of dithizone. These two water-soluble dithizone derivatives were developed as highly sensitive chromogenic ligands for ion chromatography in determining inorganic and organo-mercury in aqueous matrices. 4-Hydrazinobenzenesulphonic acid was used to prepare the sulphonic acid derivative, and 4-hydrazinobenzoic acid for the carboxylate derivative of dithizone. The method begins by dissolving 4-hydrazinobenzenesulphonic acid or 4-hydrazinobenzoic acid in aqueous sodium

²² F. Mirkhalaf, D. Whittaker, D. J. Schiffrin, *J. Electro. Anal. Chem.*, 203, **452** (1998).

²³ H. Tanaka, M. Chinuka, A. Harda, T. Ueda, S. Yube, *Talanta*, 489, **23** (1976).

²⁴ M. J. Shaw, P. Jones, P. R. Haddad, *Analyst*, 1209, **128** (2003).

hydroxide solution, followed by refluxing in a solution of ethanol and carbon disulphide. After 3 hours the solution was cooled and ethanol added to attain an intermediate product which was dissolved in a minimum amount of water and transferred into an ethanolic solution of sodium hydroxide. This solution was aerated with an air pump while stirring. After an hour cold n-butanol was added, followed by filtration and washing of the collected dithizone sulfonate with dried ether. When preparing the dithizone carboxylate derivative, after the intermediate product was aerated and agitated, the product was precipitated with addition of dilute hydrochloric acid (at pH 4.5-5), and washed with large amounts of water. The final product, dithizone carboxylate, was then collected by filtration (structures shown below). Mirkhalaf *et al.*²² also prepared the carboxylic acid derivative of dithizone by the method illustrated in Scheme 2.2. This compound was used for chemical modification of indium tin oxide and gold electrodes.

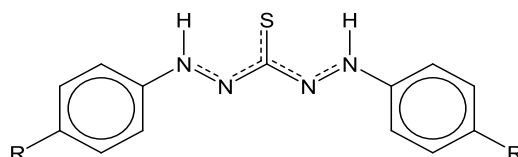


Figure 2.1: Water-soluble dithizone derivatives, where R = COOH or SO₃Na.

Knowledge of the complexation of dithizone is just as important, since dithizone is commonly known to form complexes with a wide variety of metals. In 2013 Von Eschwege²⁵ reported a general convenient procedure for complexing dithizone whereby dithizone was deprotonated with a weak base (i.e. trimethylamine) before reaction with a metal salt (i.e. phenylmercury(II) chloride); the complexation reaction is instantaneous. Recrystallization by the overlaying of solvents usually precipitates out a clean product.

Careful selection of an appropriate solvent for the reaction or characterization under investigation is also essential. Hence it is of analytical importance to discuss the solubility of dithizone in organic solvents and its behavior in two-phase extraction systems. From the data provided in Table 2.1 it is seen that the highest solubilities are achieved in chlorinated paraffins, like CHCl₃ and CH₂Cl₂, followed by the aromatic hydrocarbons. Alcohols, ketones, paraffinic and alicyclic hydrocarbons have low solubilities. Dithizone solutions are deeply colored and often not transparent, even at low concentrations. In saturated solutions it is therefore difficult to be certain whether there is an excess of solids present or not. Special care is needed when filtering, to ensure that no metallic impurities are introduced by the filtering medium. Molar absorption coefficient data or the absorbance of suitably dilute aliquots, is thus to be used for calculating concentration.

²⁵ K. G. von Eschwege, *J. Photochem. and Photobiology A: Chem.*, 159, **252** (2013).

Table 2.1. Solubility of dithizone in selected organic solvents.¹⁴

Solvent	Solubility (g l ⁻¹)			
	0 °C	20 °C	30 °C	35 °C
Chloroform	13.7	16.9	20.3	19.0
Dichloromethane	-	-	12.6	-
Benzene	-	1.24	4.24	-
Acetonitrile	-	1.0	-	-
Toluene	0.35	0.95	-	1.87
Acetone	-	0.93	-	-
Diethyl ether	-	0.4	-	-
Ethanol	-	0.3	-	-
n-Hexane	-	0.04	-	-
Water, pH<7	-	5 x 10 ⁻⁵	-	-

Dithizone is insoluble in water, but readily soluble in aqueous alkali above pH 7. In two-phase equilibria, when two immiscible solvents are used to equilibrate dithizone, a certain amount of the non-extractable anion, HDz⁻, with $\lambda_{\max} = 470$ nm will be produced given that the aqueous phase is alkaline. The distribution ratio is then decreased due to the readjustment of the equilibrium, see Figure 2.2. In this study the abbreviation, H₂Dz, will be used for the dithizone reagent, HDz⁻ and Dz²⁻ for the two conjugate bases, while H₃Dz⁺ represents the conjugate acid.¹⁴

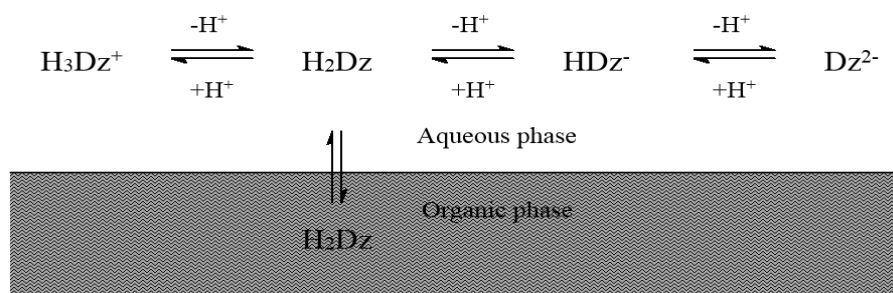


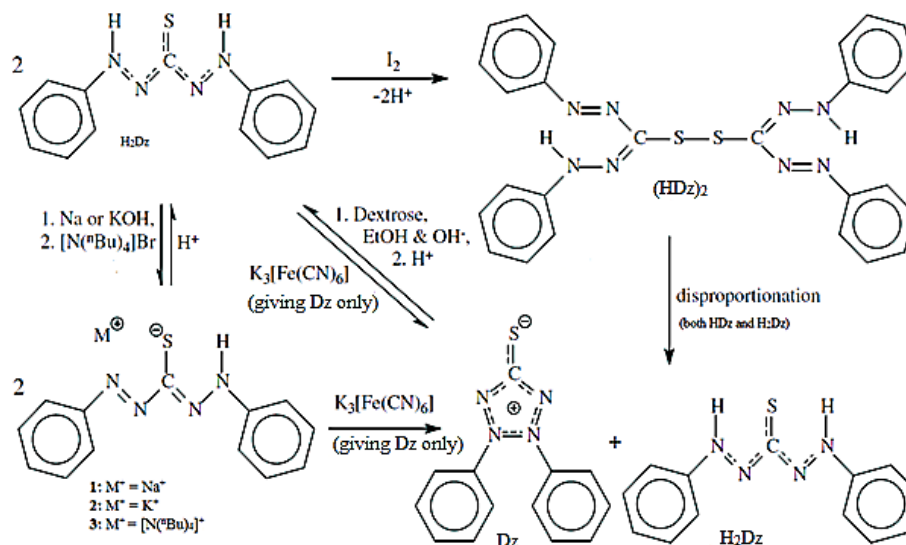
Figure 2.2. Dithizone partitioning between two immiscible solvents.

The solubility product constant ($pK_{\text{sol}} = 11.04$) was obtained by the method of Dyrssen and Hök,²⁶ where $K_{\text{sol}} = [\text{H}^+][\text{HDz}^-]$. Absorption spectra of dithizone in 1.5 M NaOH and that of weaker solutions did not differ. However, 10 M KOH gave a red-violet color, which might have been due to the formation of Dz²⁻.²⁷ It was observed that when H₂Dz is chemically oxidized by I₂ it ultimately forms monomeric dehydrodithizone, Dz, although it initially forms an isolatable disulfide-bridged species, (HDz)₂, see Scheme 2.3. However, with K₃[Fe(CN)₆] only the monomeric dehydrodithizone was formed, compared to oxidation by I₂ where disproportionation

²⁶ D. Dyrssen, B. Hök., *Svensk. Kem. Tidskr.*, 80, **64** (1952).

²⁷ R.W. Geiger, E. B. Sandell., *Analyt. Chim. Acta.*, 197, **8** (1953).

of $(\text{HDz})_2$ into H_2Dz and Dz results. Dz can be chemically reduced back to H_2Dz again. Electrochemically, two oxidation processes were indeed observed for dithizone. On the overall path of oxidation, six species were identified electrochemically: H_3Dz^- , H_3Dz , H_2Dz , HDz^\bullet , $(\text{HDz})_2$, and $(\text{HDz}^+)_2$ oxidized. UV-Vis characterisation (λ_{max}) clearly shows differences between most of these species, having different colours in solution: H_2Dz is green (444 and 610 nm), Dz is yellow (456 nm), HDz^- is orange (501 nm), and $(\text{HDz})_2$ is red (412 nm), in acetone.^{28,29} Scheme 2.3 shows the related electrochemistry.



Scheme 2.3. Chemical oxidation and reduction of dithizone, H_2Dz .²⁹

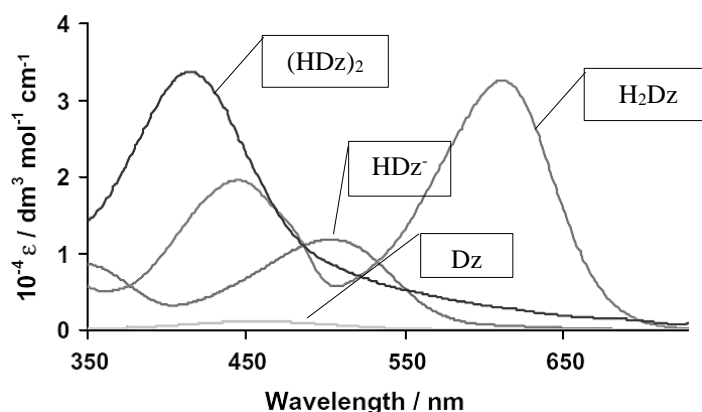


Figure 2.3. UV-Vis spectra of $(\text{HDz})_2$ (412 nm), Dz (456 nm), H_2Dz (444 and 610 nm) and HDz^- (501 nm) dissolved in acetone.²⁹

²⁸ J. W. Ogilvie, A. H. Crowin, *J. Am. Chem. Soc.*, 5023, **83** (1961).

²⁹ K. G. von Eschwege, J. C. Swarts, *Polyhedron*, 1727, **29** (2010).

2.2.2. Structure and Geometry

X-ray crystallography study is the best way to characterize a compound's chemical structure. The structure of the dithizone precursor, nitroformazan, has been well established by X-ray crystallography. The most common are amongst the *ortho*-substituted nitroformazans, like the *ortho*-methyl³⁰, *ortho*-methoxy³¹ and *ortho*-S-methyl derivatives.³² The *ortho*-S-methyl nitroformazan crystals obtained from acetone overlaid with hexane gave a monoclinic crystal system in the $P2_1/c$ space group ($Z=4$), but for the same compound, crystals obtained from a tetrahydrofuran-methanol solution were found to yield a triclinic crystal system in the $P-1$ space group ($Z=2$). These two different polymorphs did not occur due to temperature effects seeing that data collections were performed both at 298 K and 200 K, and no significant changes were observed. Unlike H_2Dz which has a linear back-bone geometry, the nitroformazan has a bent geometry in the solid state. The single imine proton provides a strong intramolecular hydrogen bond between nitrogens, (N11)H and N13, with bond distance 1.976 Å, thereby maintaining the bent geometry, see Figure 2.4. As a result of the unsymmetrical occurrence of only one single imine proton, as opposed to the symmetrically spaced two imine protons of dithizone, the nitroformazan precursor does not exhibit conjugation along its backbone. The formazan molecule is largely planar, with the NO_2 and S12 atoms coplanar to the backbone of the formazan molecular backbone. Bond lengths are typically representative of either single or double bonds.²⁵

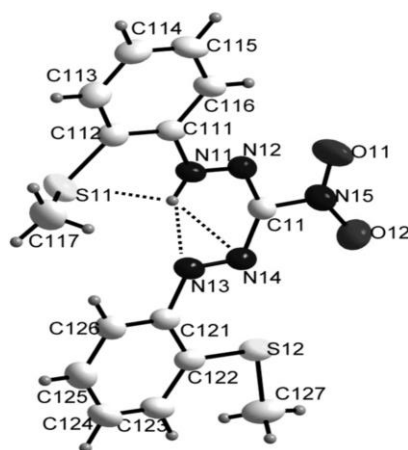


Figure 2.4. *Ortho*-S-methyl nitroformazan crystal structure obtained from tetrahydrofuran-methanol solution. Dotted lines depict intramolecular H-bonds. The structure has been drawn at 50% probability level.²⁵

Crystals of 2- and 4-phenoxy nitroformazans were grown independently from diethyl ether overlaid with hexanes, yielding monoclinic crystals in the $P2_1/c$ space group ($z = 4$ and 8,

³⁰ K. G. Von Eschwege, E.C. Hosten, A. Muller, *Acta Cryst.*, o425, **E68** (2012).

³¹ K. G. Von Eschwege, F. Muller, T.N. Hill, *Acta Cryst.*, o609, **E68** (2012).

³² K. G. Von Eschwege, F. Muller, E.C. Hosten, *Acta Cryst.*, o199, **E68** (2012).

respectively). The phenyl moieties in the substituent are twisted out of the plane due to steric hindrance and the formazan back-bones are typically flat with the nitro-groups at the apex slightly twisted. Along the formazan backbone (N1–N2–C1–N3–N4) there are partially delocalised π -electrons, with double bonds longer and single bonds shorter than what is otherwise typical. In the 4-phenoxyformazan structure similar bond lengths were obtained for both N1–N2 and N3–N4; this is an indication of the imine proton being shared by N1 and N4 atoms. This imine proton mostly resides on the N1 position, as suggested by the slightly shorter bond of C1–N2 (1.332 Å) in comparison to C1–N3 (1.348 Å), see Figure 2.5.³³

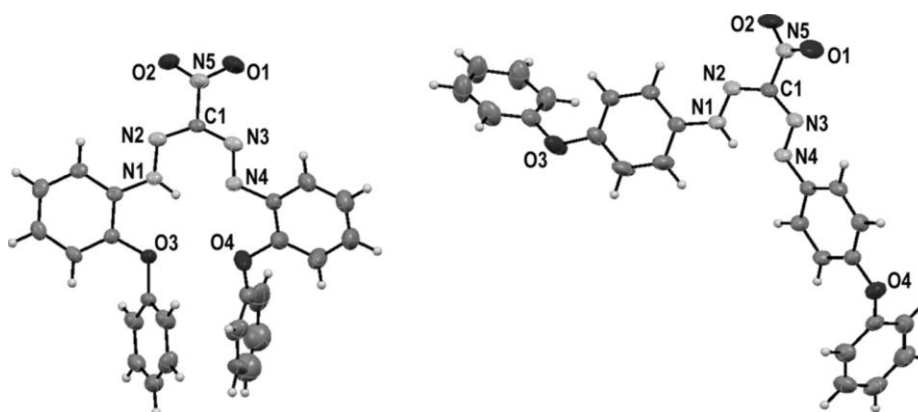


Figure 2.5. X-ray structures of 2-phenoxyformazan (left) and 4-phenoxyformazan (right). ORTEP views with thermal ellipsoids are drawn at 50% probability level.³³

X-ray crystallography studies suggested that dithizone in its solid state is almost perfectly planar. Dithizone crystals are very thin, fragile laths, usually stretching along the a axis and rarely formed as single crystals. They are most likely twinned which then inhibits accurate and precise determination of the β angle, therefore affecting the intensity of measurements negatively. Aslop³⁴ showed that the molecule was effectively coplanar and has a bond distance of 1.74 Å at the C-S bond. He concluded that the conjugation along the $N - N - C - N - N$ back-bone extends to both phenyl rings of the molecule.

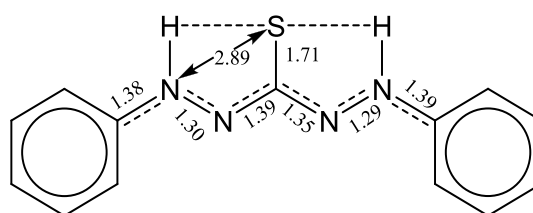


Figure 2.6. Symmetric structure (nearly planar) of the dithizone molecule with its bond distance (Å) of the back-bone chain.

³³ E. Alabaraoye, K. G. von Eschwege, N. Loganathan, *J. Phys. Chem. A*, 10894, **118** (2014).

³⁴ P. A. Aslop, Ph.D. Thesis, London, (1971).

A relatively good single crystal from chloroform solution of dithizone was obtained by Laing.³⁵ He also found it to be nearly planar with the phenyl rings slightly twisted out of the mean plane. The measured bond-lengths in Figure 2.6 give evidence that π -electrons are delocalised along the back-bone chain of the molecule, which means that there are no localised single or double bonds. The assumption was made that the two imino-hydrogen atoms, illustrated in Figure 2.7, are partially positively charged and the charge on the conjugated chain will be $N^{\delta-}-N^{\delta+}-C^{\delta-}-N^{\delta+}-N^{\delta-}$, i.e. with alteration of charge.¹⁴ Imino hydrogen atoms form hydrogen bonds at the intersection of the mirror where the C–S bond lies. This is known as the thione structure. In some organic solvents when the concentration is high enough, dithizone has two peaks in the visible spectrum, see Figure 2.8. These two peaks brought about the assumption that this reagent exists as an equilibrium mixture of the two tautomeric forms, thione and thiol, see Figure 2.8. The thiol structure is not supported by experimental evidence. An attempt was made to establish the thiol form by acidifying a sodium dithizonate solution and shake it up with an immiscible organic solvent. From the organic phase the typical double peak spectrum of dithizone was still obtained, with no evidence for the conversion of the thiol as it was initially expected to form.³⁶

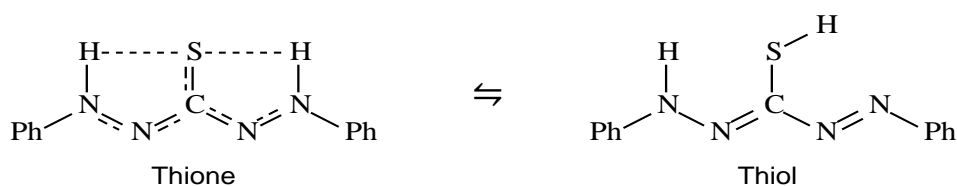


Figure 2.7. Proposed structural forms of dithizone.

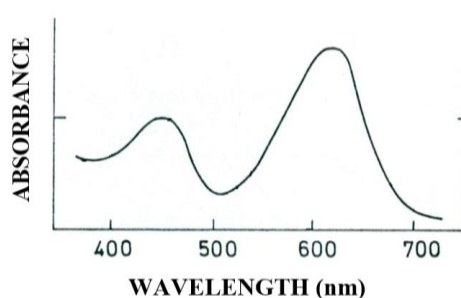


Figure 2.8. Dithizone spectrum in organic solvent (chloroform).

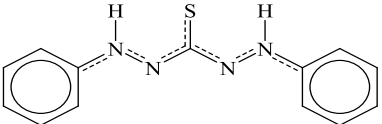
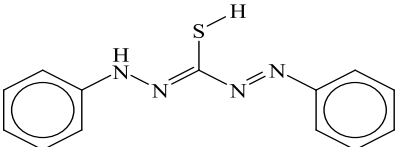
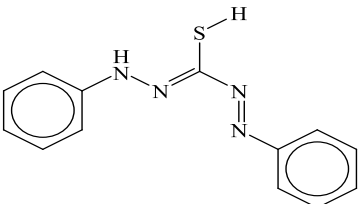
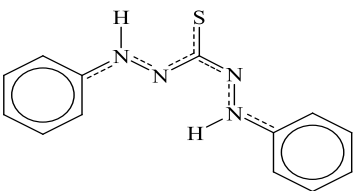
Quantum computational chemistry is an ideal technique to establish energetically favored geometries as it lays a foundation for explaining or predicting reaction pathways, charge distribution and energy transitions in species and reactions. Therefore this tool was applied to establish the possible tautomers of dithizone. The relative energies were calculated by means of

³⁵ M. Laing, *J.C.S. Perkin II*, 1248, (1977).

³⁶ H. M. N. H. Irving, A. T. Hutton, *Analyt. Chim. Acta.*, 311, **141** (1982).

the Amsterdam Density Functional (ADF) package, in gas phase, to determine the energetically most favored tautomer of dithizone. Resulting energy values agree with experimental evidence previously reported in literature³⁷, namely that the structure of the molecule is symmetrical. The tautomers in Table 2.2 are tabulated in increasing order of energies up until the fourth tautomer, i.e. tautomer 1 is the most favoured structure in both the solvent and gas phase. Although there were six possible tautomers reported, only the four with lowest energies are shown here. The relative molecular energy of tautomer 1 was normalized to be zero. Solvent energies, relative to the gas phase energies, are 16.8 and 18.8 kJ mol⁻¹ for dichloromethane (DCM) and methanol, respectively.³⁸

Table 2.2. Four possible tautomeric structures and its ADF optimized energies, in gas phase and solvent environment. Energies of tautomer 1 are normalized to zero.³⁸

Tautomers of dithizone, H ₂ Dz.	Relative energy (kJ mol ⁻¹)		
	Gas	DCM	Methanol
(1) 	0	0	0
(2) 	27.5	39.2	40.5
(3) 	62.2	46.2	42.6
(4) 	64.6	74.0	74.3

³⁷ K. G. von Eschwege Ph.D. Dissertation, (2006).

³⁸ K. G. Von Eschwege, J. Conradie, A. Kuhn, *J. Phys. Chem. A*, 1463, **115** (2011).

As far as its metal complexes are concerned, in most cases the dithizone ligand is bidentately coordinated to the metal, *via* its S and N atoms. There are some exceptions, like in $\text{In}(\text{HDz})_3$,³⁹ where the third ligand only coordinates monodentately through sulfur alone. Although the ligand is mostly coordinated in linear configuration, in an osmium cluster the ligands are in a bent configuration, i.e. rotated 180° around one C-N bond, as a consequence of steric hindrances. In the osmium cluster it has been observed that the dithizonato sulfur uniquely bridged two metal centres. The configuration is illustrated in Figure 2.9, the metals being about 90° with respect to the sulphur atom.³⁷

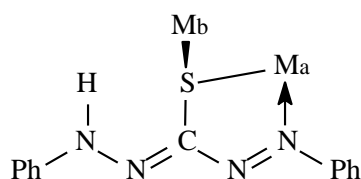


Figure 2.9. Configuration of two metals bridged by the sulfur compound.

Dithizone complexes formed from nickel, palladium and platinum have been grouped as unusual and characterised by multiple absorption bands in the visible spectrum⁴⁰ and with very high formation constant.⁴¹ An attempt was done to grow nickel dithizonate, $\text{Ni}(\text{HDz})_2$, from chloroform, which yielded very fine irregular black laths. The crystals are triclinic with space group $P\bar{1}$ ($Z=1$), with the nickel atom again bonded to sulphur ($\text{Ni}-\text{S}$, 2.19 Å) and nitrogen ($\text{Ni}-\text{N}$, 1.87 Å), see Figure 2.10. The $\text{Ni}(\text{HDz})_2$ molecule is centrosymmetric and configuration about the Ni atom is square planar, with the non-phenyl hydrogen atom uniquely located along the back bones of the ligands.⁴²

Tris-dithizonatocobalt(III), $\text{Co}(\text{HDz})_3$, is the product of the reaction between H_2Dz or K^+HDz^- and any of a variety of Co(II) salts in methanol or acetone. The advantage of using the potassium dithizonate salt, KHDz , is that no base is required to strip the ligand of a proton during metal complexation. Regardless of whether stoichiometric or limiting amounts of KHDz were used, Co(II) is always auto-oxidized to Co(III), with three ligands coordinated to the central metal. The structure was confirmed by X-ray crystallography, see Figure 2.9. The crystal was dark brown in colour, with a triclinic crystal system with space group $P-1$ ($Z=2$), having all three dithizonate ligands bidentately coordinated through the N and S atoms to give a slightly distorted octahedral coordination geometry. A facial geometry is seen, as all three sulfur atoms of the

³⁹ M. L. Niven, H. M. N. H. Irving, L. R. Nassimbeni, *Acta Cryst.*, 2140, **B38** (1982).

⁴⁰ H. Irvin, J. J. Cox, *J. Chem. Soc.*, 1470, 1961.

⁴¹ K. S. Math, Q. Fernando, H. Freiser, *Analyt. Chem.*, 1962, **36** (1964).

⁴² M. Laing, P. Sommerville, P. A. Aslop, *J. Chem. Soc. (A)*, 1247 (1971).

dithizonate ligands are coordinated on one side of the cobalt metal, while the nitrogen atoms are on the other side.⁴³

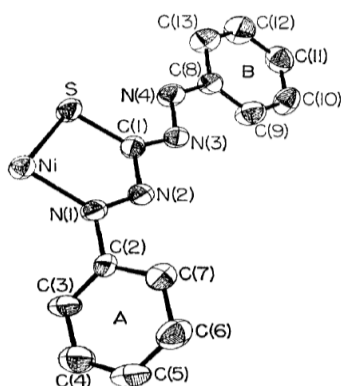


Figure 2.10: Nickeldithizonate, Ni(HDz)₂, structure with thermal vibration ellipsoids indicated.

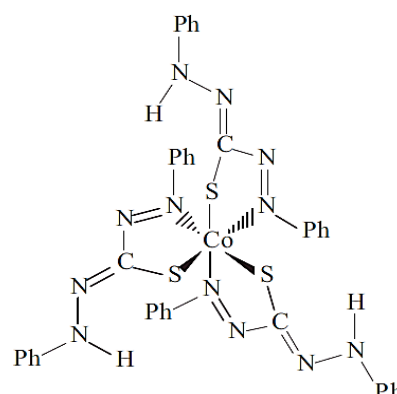


Figure 2.11. Structure of *tris*-dithizonatocobalt(III). For simplicity sake a schematic diagram is given.

The geometry around the mercury atom in dithizonatophenylmercury(II), DPM or PhHg(HDz), is T-shaped with an irregular planar three co-ordination. This T-shaped geometry involves strong bonds of Hg-C with bond length 2.10(2) Å, and Hg-S bond length of 2.37(1) Å, with the near linear angle of S-Hg-C being 168.0(7)°. Perpendicular to the former there is a weak Hg-N bond with bond distance of 2.66(2) Å. In this complex, delocalisation is not as pronounced along the ligand back-bone as in the dithizone structure.^{44,45} Regardless of a substitution on the S-site, coordination of S-methylated-dithizone with mercury(II) nevertheless still takes place, with the dative covalent bond shifted from N to S. A strong base such as NaOH has to be added to strip this ligand of its remaining single imine proton, in order for metal complexation to take place, see Figure 2.1 (left).⁴⁶

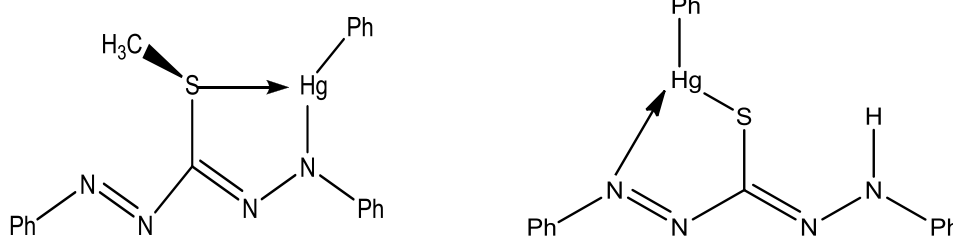


Figure 2.12. S-Methylated-dithizonatophenylmercury (left) and Dithizonatophenylmercury(II) (right).

⁴³ K. G. von Eschwege, L. van As, C. C. Joubert, J. C. Swarts, M. A. S. Aquino, T. S. Cameron, *Electrochimica Acta.*, 747, **112** (2013).

⁴⁴ A. T. Hutton, H. M. N. H. Irving, *Chem. Commun.*, 1113, (1979).

⁴⁵ E. Botha, M.Sc. Dissertation, (2010).

⁴⁶ H. M. N. H. Irving, A. H. Nabilsi, S. S. Sahota, *Analyt. Chim. Acta.*, 135, **67** (1973).

2.3. Chromism

2.3.1. Photochromism

Photochromism can be defined as the light-induced reversible transformation of chemical species in one or both directions, between two forms that have different absorption spectra, by absorption of electromagnetic radiation. The word is derived from Greek words; *phos*, meaning light, and *chroma*, which is color. Photochromism has become common simply because of its applicability in our daily lives. One example is in spectacles that goes darker when exposed to sunlight and recover transparency in diffuse light. Initially the lenses of these spectacles were impregnated with inorganic salts, mainly silver, but they were uncomfortable to wear because of weight. For this reason organic photochromic lenses became more popular, although having a limited lifetime. In 1867 Fritzsche⁴⁷ reported the first photochromism, which he observed from the bleaching of an orange-colored solution of tetracene in daylight, the color reverted back in darkness. The word photochromism was suggested by Hirshberg⁴⁸ to describe this phenomenon, and it is still in use until today.

In 1945 Reith and Gerritsma⁴⁹ observed the photochromic nature of mercury dithizonate and also noted that the colour immediately reverted back to yellow when shaking with aqueous acid. While studying traces of mercury Irving *et al.*⁵⁰ observed the photochromic behavior of mercury dithizonate solution in chloroform. When exposed to direct sunlight this solution changed from orange-yellow to an intense royal blue colour, and the colour change was reversed when the solution was placed in the dark. Independently, Webb *et al.*⁵¹ reported the same photochromism in mercuric dithizonate solution in chloroform or benzene when irradiated or placed in direct sunlight. A follow-up study on these observations was made on twenty-four metal dithizonate complexes. These dithizonate complexes were studied at room temperature and at -80 °C, in 16 different solvents. Nine of these metal complexes were found to be photochromic under steady illumination, having various colour changes (see Table 2.3). It was observed that the colour change was not dependent on the metal, this then indicates that the ligand in the reaction was of primary importance. Colour changes were usually from orange to blue, violet, or red. Return rates to the resting state colour was shown to be largely dependent on the metal, and return rates varied from a half-life of about 30 seconds for the mercury complex to less than 1 second for cadmium and lead complexes, even when cooled to -80 °C. In benzene at 25 °C with 80-90% of

⁴⁷ J. Fritzsche, *Comptes Rendus Acad. Sci., Paris*, 1035, **69** (1867).

⁴⁸ Y. Hirshberg, *Compt. Rend. Acad. Sci., Paris*, 903, **231** (1950).

⁴⁹ J. F. Reith, K. W. Gerritsma, *Rec. Trav. Chim.*, 41, **64** (1945).

⁵⁰ H. Irving, G. Andrew, E. J. Risdon, *J. Chem. Soc.*, 541, (1949).

⁵¹ J. L. A. Webb, I. S. Bhatia, A. H. Corwin, A. G. Sharp, *J. Am. Chem. Soc.*, 91, **72** (1950).

the mercury complex it was possible to achieve a steady photo-excited state system concentration at high levels of illumination. Similar conditions applied for cadmium or lead complexes, gave steady state concentrations of only 0.1% of the normal form. Dry and non-polar solvents like benzene, toluene and chloroform were observed to give the strongest photochromic effects, while hydroxylic solvents, organic acids and bases accelerated the back reactions.⁵²

Table 2.3. Photochromic metal dithizonates upon illumination with visible light.

Complex	Solvent	Color and absorbance maxima (nm)		Temp. (°C)	Approx. return time (s)
		Normal form	Activated form		
Pd(HDz) ₂	Chloroform	Green (450, 640)	Blue (450, 520, 570, 630)	25	5-10
	Benzene	Green	Orange	25	5-10
	Dichloromethane	Green	Orange	-10	1-2
Pt(HDz) ₂	Benzene & carbon tetrachloride	Yellow (490, 708)	Red	25	1-2
AgHDz·H ₂ O	Tetrahydrofuran	Yellow (470)	Violet	25	2-5
				10	40-60
Zn(HDz) ₂	Dichloromethane	Red (530)	Violet-blue	25	1-2
	Tetrahydrofuran & ethylacetate	Red	Violet-blue	-40	< 1
Cd(HDz) ₂	Tetrahydrofuran & acetone	Orange (500)	Violet	-80	<1
Hg(HDz) ₂	Benzene & chloroform	Orange (490)	Blue (605)	25	30-90
Pb(HDz) ₂	Tetrahydrofuran	Red (520)	Blue	-80	< 1
Bi(HDz) ₃	Dichloromethane, xylene, ethyl acetate & methanol	Orange (498)	Violet	-30	< 1
	Pyridine	Orange	Violet	-30	10
BiCl(HDz) ₂	Tetrahydrofuran & dichloromethane	Orange (490)	Blue (605)	-40	2-5

In 1965 Meriwether *et al*⁵³ did a kinetic study on the photochromic return reactions of mercury and silver dithizonates. The thermal back-reaction of the mercury dithizonate complex follow first-order kinetics in benzene at 25°C. The return rate decreased threefold as a consequence of N-deuteration of the complexes, while the total complex and water concentration showed a direct linear dependence. Since the thermal back-reaction is radiationless, its rate is affected by temperature, solvent, ligand substituent and the presence of impurities. It is therefore necessary to measure the rates of return at different temperatures, solvents and concentrations in order to quantify these observations. These measurements show that there is an exponential correlation

⁵² L. S. Meriwether, E. C. Breitner, C. L. Sloan, *J. Am. Chem. Soc.*, 4441 **87** (1965).

⁵³ L. S. Meriwether, E. C. Breitner, N. B. Colthup, *J. Am. Chem. Soc.*, 4448, **87** (1965).

between the rate of isomerization and temperature, while higher return rates were observed with decrease in molar mass and increase in solvent polarity. From the series of electronically altered PhHg(HDz) complexes kinetics disclosed highest rates of 0.0106 s^{-1} for the derivative with methoxy groups on the *meta* phenyl ring positions of dithizone, and lowest rate of 0.0002 s^{-1} for the *ortho*-methyl derivative.²⁵ When investigating steric effects on the photochromic reactions of mercury dithizonate it was found that these effects do not decrease return rates. In fact, large substituents like phenoxy groups increase the rate because large molecules have an increased number of degrees of vibrational freedom, which is argued to help overcome the transitional energy barrier during the back reaction, see Figures 2.13 and 2.14. This is consistent with a temperature study on the 4-phenoxydithizonatophenylmercury, PhHg(4-OPh), complex with half-life of 2 min. 8 sec., revealing an exponential relationship between the return rate and temperature. Varying solvent polarity revealed an almost perfect linear relationship between the rate of the back-reaction and solvent properties, like the dipole moment, dielectric constant and molar mass (roughly).³³

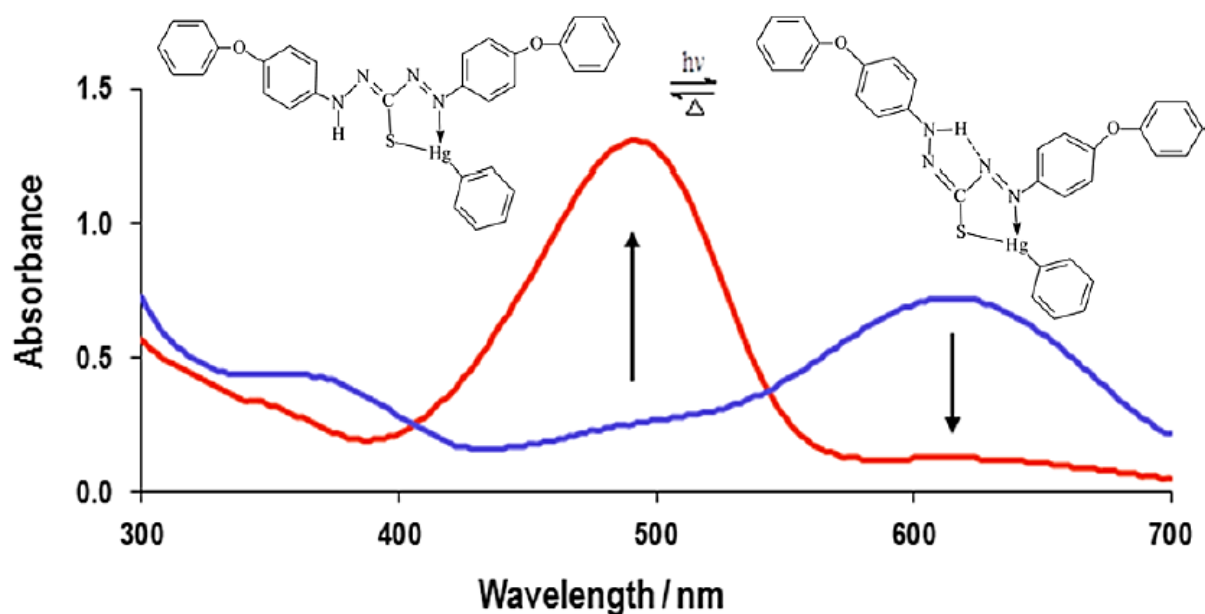


Figure 2.13. Photochromic reaction of 4-phenoxydithizonatophenylmercury in toluene; radiationless thermal back-reaction reverting back to its ground state.³³

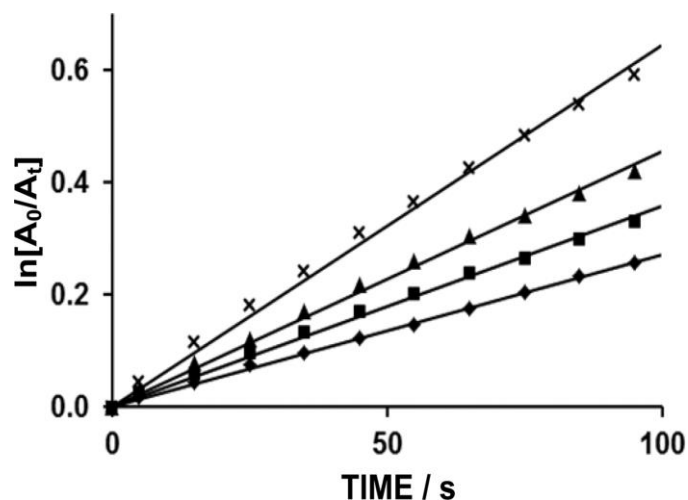


Figure 2.14. First-order kinetics of the back-reaction of 4-phenoxydithizonatophenylmercury in toluene at 20 °C at different concentrations.³³

Since PhHg(HDz) is well known for its photochromic nature a quantum computational study was done to determine the structure of the blue photo-excited form. Density function theory (DFT) methods were used to do theoretical studies of the molecular structure and electronic spectra of the blue and orange isomers of the photochromic mercury(II) dithizonate. Previously reported X-ray crystal⁵⁴ data of the orange isomer in ground state are in agreement with computed structural results. Confidence in these DFT calculations and its accuracy was gained by computing the ground state structure of the orange mercury dithizonate complex, in comparison with the experimentally obtained crystal structure. As a result of very good agreement, efforts were made to determine the unknown structure of the photo-excited blue mercury dithizonate. In Figure 2.15 three possible structures for the blue excited isomer are shown. These were investigated in order to determine the most favourable one. Figure 2.15a represents the historically favoured geometry, referred to as N2H. Figure 2.15b and 2.15c are the proposed alternatives referred to as S1H and N4H, respectively. The main difference between the two structures, N4H and N2H, is the position of the backbone amine proton that is situated on the N4 position for the newly proposed structure, rather than on the N2 position as previously hypothesized. Structure S1H was the least favoured of three investigated structures. The historically hypothesized geometry of the blue excited state form (N2H) is less favoured by more than 35 kJ mol⁻¹ relative to the new proposed structure (N4H) of the blue photo-excited state. The imine proton in structure N2H is not intra- or inter-molecularly transferred as speculated earlier, but stays intact on the N4 position during the reversible photochromic reaction. The ADF/PW91 and crystal structures give both a slightly bent conformation of the dithizonato backbone for the orange isomer. This slightly bent conformation is also observed for the blue

⁵⁴ A. T. Hutton, H. M. N. H. Irving, L. R. Nassimbeni, *Acta Cryst.*, 2064, **B36** (1980).

isomer as given by ADF/PW91 and is favoured over the linear structure computed by G03/B3LYP. In both the orange and blue isomers the mercury phenyl moieties lie almost perpendicular to the ligand. Another observation was that the same bathochromic shifts observed experimentally as determined by UV-vis spectroscopy were also obtained as excitation energies for the blue isomer from the time dependent density functional theory as implemented in the Amsterdam Density Functional (ADF) and Gaussian 03 (G03) program system. Best approximations of experimentally observed electronic spectra were given by B3LYP calculated excitation energies and oscillator strengths for both isomers.⁵⁵ Figure 2.14 shows the photochromic reaction of the mercury(II) dithizonate complex.

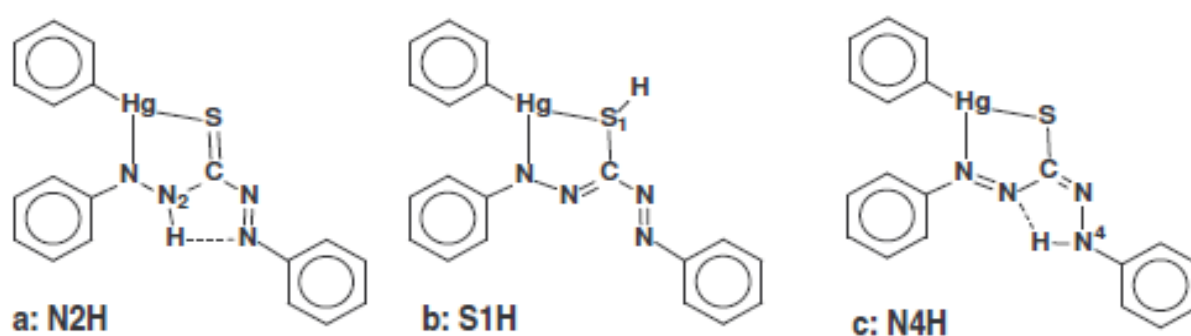


Figure 2.15. Three different possible photo-excited isomers of the blue PhHg(HDz) complex.⁵⁵

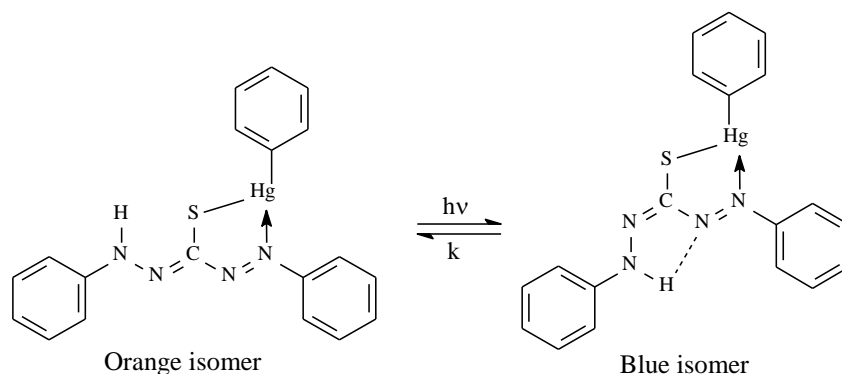


Figure 2.16. Photochromic reaction of PhHg(HDz).

Involving the latest technology in scientific instrumentation, an investigation was done by means of femtosecond transient absorption spectroscopy to establish aspects of the initial photochromic reaction of the dithizonate complex in solution. By employing these ultrafast techniques, photochromism of the mercury dithizonate complex was observed for the first time in strongly polar solvents like methanol. This is an indication that in many other similar complexes photoreactions may occur, but not visibly observed, due to the very high rate of return reactions. A series of mercury (II) dithizonate complexes were synthesised to investigate the effect of

⁵⁵ K. G. von Eschwege, J. Conradie, J. C. Swarts, *J. Phys. Chem. A*, 221, **112** (2008).

electronically different substituents on the ultrafast dynamics of the photochromic reaction. These electronically different substituents were symmetrically substituted on both phenyl rings of dithizone, but at different positions on the phenyl group. From these investigations it was observed that these substituents remarkably altered both wavelength of light absorption and ultrafast time dynamics throughout the photochromic reaction of the phenylmercury complexes that were studied. Electronic alterations, steric effects and inertia were attributes ascribed as reasons for these changes. A solvatochromic effect in the excited state was observed for the first time and the ultrafast rates were proven to be dependent on solvent polarity. Ultrafast excitation by 40 fs laser pulses took place in less than 100 fs, with a time constant of 1.5 ps in the 180° photo-isomerization process. It was postulated that an orthogonally (90°) twisted excited state bifurcates towards the orange *cis* and blue *trans* configurations, below the funnel of the conical intersection, see Figure 2.17.⁵⁶ During the 40 fs laser pulse ($\lambda = 470$ nm) PhHg(HDz) in ground state S_0 gets photo-excited to the excited state S_1 surface that is vertically above the orange ground state. The molecule then moves towards the conical intersection between S_1 and S_0 , where it is twisted in its orthogonal geometry, and internally redistributes its added energy vibrationally. The latter results in a 1 ps delay before the molecule penetrates the S_0 surface.⁵⁷

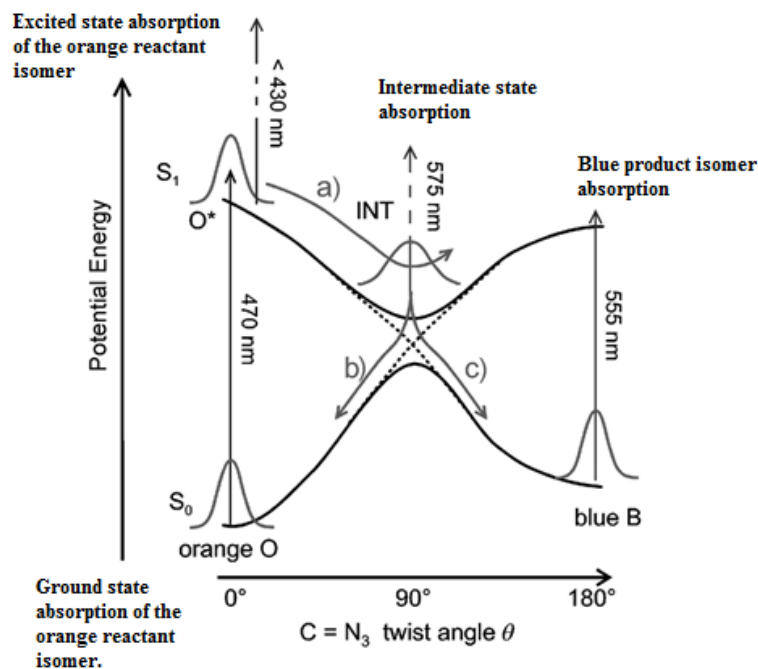


Figure 2.17. The proposed energy of the ground and excited states as the PhHg(HDz) complex rotates. The reaction pathway is initiated at ground state, S_0 , becomes photo-excited at S_1 , and then starts twisting along its downwards energy path towards the conical intersection with S_0 , where it bifurcates in two ground state pathways, path b (orange form) and path c (blue form), along S_0 after fast vibrational relaxation.⁵⁷

⁵⁶ K. G. von Eschwe, G. Bosman, J. Conradie, H. Schwoerer, *J. Phys. Chem. A*, 844, **118** (2014)

⁵⁷ H. Schwoerer, K. G. von Eschwe, G. Bosman, P. Krok, and J. Conradie, *ChemPhysChem*, 2653, **12** (2011).

2.3.2. Solvatochromism

A phenomenon whereby a compound changes color when dissolved in solvents with different polarities, either by a change in the absorption or emission spectra of the molecule, is called solvatochromism.⁵⁸ In reality solvatochromic shifts are not simple univocal indices, but rather reflections of extremely complex phenomenon. There are many different intermolecular forces involved, including both the molecular probe and the solvent. More evidence is observed in emission spectra where environment effects influences the energy of the excited state and also governs which state has the lowest energy.⁵⁹

Although it is necessary to classify organic and inorganic solvents due to their physical and chemical differences in various classes, the overlapping of these classes cannot be avoided.

The various classes are:

- Hydrogen bond donating (HBD) solvents; they contain proton donor groups (water, ammonia, alcohols, primary amides and carboxylic acids).
- Hydrogen bond accepting (HBA) solvents; they contain proton acceptor groups (amines, ethers, ketones and sulfoxides).
- Aprotic solvents; they are without proton-donor groups (DMSO, DMF, THF, CCl₄, CS₂, C₆H₆ and dioxane).
- Amphiprotic solvents; they act both as hydrogen bond acceptor and hydrogen bond donors (water, alcohols and amides).

A dipole-dipole interaction which can be formed in molecules can be assumed to be hydrogen bond.^{60,61} Depending on the nature of the solute and that of the solvent, these bonds can be inter- or intramolecular in nature. The structure of the chromophore is the most useful classification of dyes, which can also be divided into various classes.

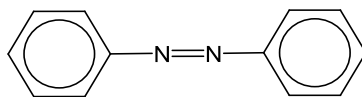


Figure 2.18. Chemical structure of an Azo dye.

The azo dye is one of the major types of dyes used in many processes, and has $-N=N-$ double bonds, with two substituents attached to at least one aromatic group (benzene or naphthalene), but usually on both sides (see Figures 2.18 & 2.19). Azo dyes mostly have a polar nature which

⁵⁸ P. Bamfield, *Chromic Phenomena*, Royal Society of Chemistry, Britain, (2001).

⁵⁹ A. Marini, A. Muñoz-Losa, A. Biancardi, B. Mennucci, *J. Phys. Chem. B*, 17128, **114** (2010).

⁶⁰ C. Reichardt, T. Welton, *Solvent and Solvent Effects in Organic Chemistry*, Wiley-VCH, Weinheim (Germany) 4th ed., (2010).

⁶¹ S. J. Grabowski, *Hydrogen Bonding – New insights*, Springer, USA, (2006).

makes them suitable for studying solvatochromism, using different techniques and in a variety of solvents.⁶²

Regarding the solvent-solute interaction, its nature can have a profound effect on the spectral behavior of the solute in a given solution, since the equilibrium between either the tautomeric forms or the resonance structures of the solute can be dictated by the polarity of the solvent. For instance, species with a high dipole moment will be favored by polar solvents and structures with low charge distribution will be stabilized by non-polar solvents. Furthermore, the solvent can alter the electronics of the solute, and is reflected in the spectral shifts of the solution. Here the solvent interacts with the HOMO/LUMO orbitals of the solute to stabilize its ground or excited state. Spectroscopic characteristics of four triarylmethane dyes (Crystal Violet, Ethyl Violet, Victoria Blue R and Victoria Pure Blue BO) are examples of such interactions. These characteristics were investigated in a variety of polar solvents, and observations were that the absorption spectra of the compounds displaying lower symmetry were different from those of highly symmetric compounds. The distinct nature of the overlapping absorption bands' characteristics of these two sets of dyes was the justification of the differences observed.⁶³ On the other hand, solvents with different polarities were used to investigate the electronic absorption spectra of 2',4'-dihydroxy-methoxyazobenzene and 4,2',4'-tri-hydroxyazobenzene. The conclusions made were that important factors for the observed solvatochromism were both the electronic character and chemical nature of the solvent and that of the solute substituents.⁶⁴

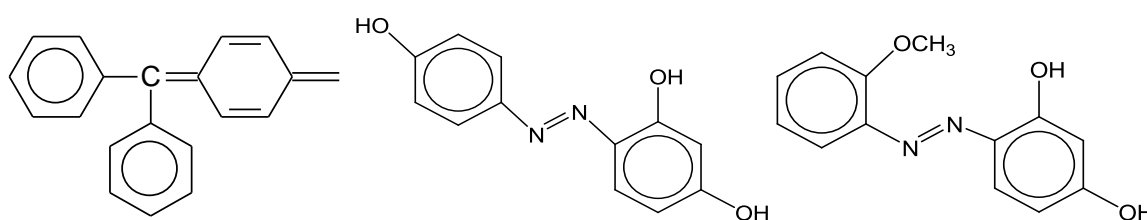


Figure 2.19. Triarylmethane (left), 2',4'-dihydroxy-methoxyazobenzene (middle) and 4,2',4'-tri-hydroxyazobenzene chemical structures (right).

As a result of the application of time dependent density function theory (TDDFT) to the observed orange colour in methanol and green in dichloromethane, for the first time a satisfactory explanation for the solvatochromic properties of dithizone could be given. Computed B3LYP-TDDFT results have proven that tautomer 2 (see Table 2.2 and Figure 2.20) is causing the methanol solution to appear orange. It happens to be the tautomer with the second lowest energy. More evidence is given by the close agreement of experimental UV-Vis spectroscopic results

⁶² M. A. Rauf, S. Hisaindee, *J. Mol. Struct.*, 45, **1042** (2013).

⁶³ L. M. Lewis, G. L. Indig, *Dyes Pigm.*, 145, **46** (2000).

⁶⁴ I. Sidir, E. Tasal, Y. Gulseven, T. Gungor, H. Berber, C. Ogretir, *Intr. J. Hydrogen Energy*, 5267, **34** (2009).

with the computed orbitals and oscillators, see Figure 2.20 in combination with Figure 2.27. A significant difference was observed in the oscillator peak patterns of all tautomers in Table 2.2, with an undisputed correlation between the oscillator and experimental peak patterns in methanol of tautomer 2. The experimental peak at *ca.* 450 nm is in excellent agreement with the oscillator at 446 nm. The same is observed at shorter wavelength oscillators. Tautomer 2 only requires the intramolecular transfer of the imine proton to its neighboring sulfur. Figure 2.20 shows UV-Vis spectra of these two tautomers in the two different solvents (DCM and methanol). Transfer of the imine proton to its neighboring sulfur in methanol with respect to tautomer 1 in DCM is unrelated to the calculated relative energies of these two tautomers.³⁸

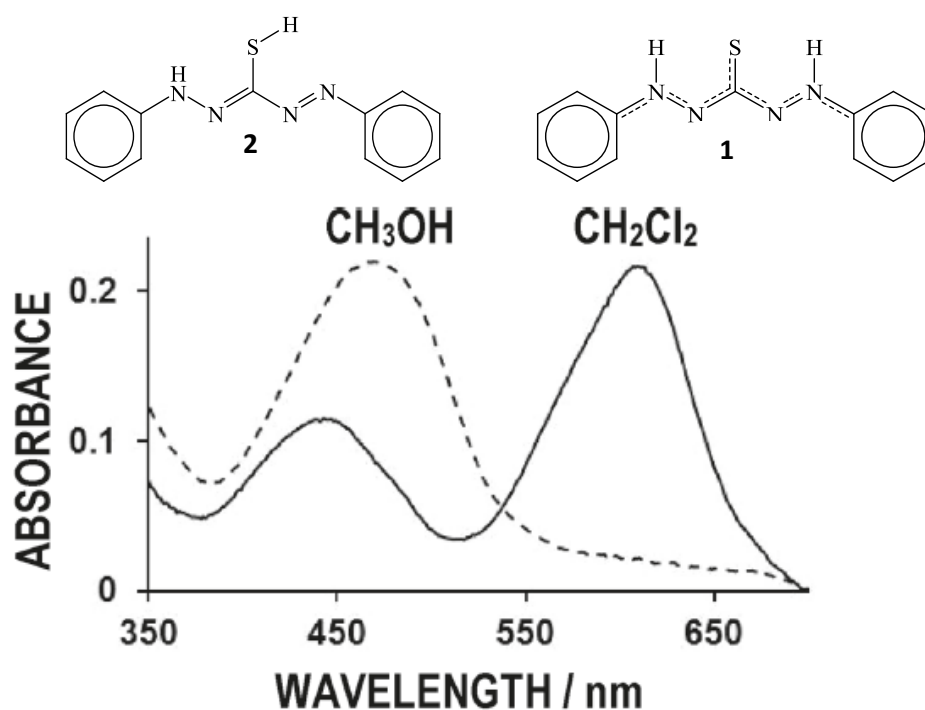


Figure 2.20. Experimental spectra at low concentration of H₂Dz in methanol and DCM. Related tautomers are indicated.

Results that were obtained from dithizone absorption spectra in various solvents and their binary mixtures were investigated in terms of solvent-solute interactions. From these electronic absorption spectra it was observed that the absorption maxima of dithizone were dependent on the solvent polarity. Interaction of the probe molecule with the solvent was indicated by the change in peak position of the long wavelength absorption band. For instance, it shifted with a change in solvent polarity from 597 nm in iso-propanol to 626 nm in n-heptane.⁶⁵

⁶⁵ M. A. Rauf, S. Hisaindee, J. P. Graham, A. Al-Zamly, *J. Mol. Liq.*, 332, **211** (2015).

2.3.3. Electrochromism

Electrochromism is the reversible color change of an electroactive species upon electron transfer or oxidation/reduction process and it normally involves the passage of an electric current or potential. A color can form on one or on both electrodes or in the electrolyte adjacent to the electrodes by passing a charge in one direction during the process of coloration in electrochromic cells. Cathodic coloration is when the color is formed by reduction at a negative electrode (cathode) and anodic coloration is at a positive electrode (anode).⁶⁶ In 1969 electrochromic devices (ECD) were first described, based on the observations of a reversible color change in thin films of tungsten trioxide.⁶⁷ This was followed by advancements on various components of ECDs of an array of materials spanning the entire visible spectrum that were later refined and optimized. Single layer and dual layer are the two main types of transmissive ECD. Both have films of conductive material deposited on a substrate, i.e. a film of electrochromic (EC) material and a layer of electrolyte material.⁶⁸ The charge from a power source to the EC material is carried by the conductive material. Completion of the circuit that facilitates the transfer of electrons between electrodes is ensured by the electrolyte material. The π or d-electron state of the EC material can be changed by applying a potential difference (ranging from -3 to +3 V) and a color change will be induced.⁶⁹

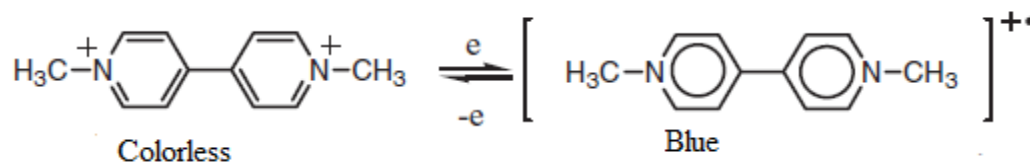


Figure 2.21. Chemical structure of methyl viologen as dication (left) and radical cation (right).

Electrochromic materials consist of three main classes; organic polymers, organic small molecules and inorganics. Organic electrochromic polymers (OEPs) have several advantages over inorganics, in that they are highly conjugated systems with band gaps commonly ranging from 0.5 to 3.0 eV. These advantages include; band gap that is tuneable, same material with multiple coloration, stability is high, efficiency of coloration is good, rapid switching times, high flexibility, and low cost.⁷⁰ An example of solution electrochrome is the dimethyl-4,4'-bipyridylium dication (methyl viologen, see Figure 2.21) which changes colour to the bright blue

⁶⁶ M. Green, *Chem. Ind.*, 611, (1996).

⁶⁷ S. K. Debb, *Appl. Opt. Suppl.*, 192, **3** (1969).

⁶⁸ H. J. Byker, *Electrochim. Acta*, 2015, **46** (2001).

⁶⁹ G. A. Sotzing, J. L. Reddinger, A. R. Katritzky, J. Soloduch, R. Musgrave, J. R. Reynolds, P. J. Steel, *Chem. Mater.*, 1578, **9** (1997).

⁷⁰ G. Sonmez, F. Wudl, *J. Mater. Chem.*, 20, **15** (2005).

coloured radical cation when it undergoes a one-electron reduction. Fe(III) thiocyanate is another example of aqueous phase electrochrome, and also hexacyanoferrates and quinones.^{71,72}

When studying electroactive species the most effective electroanalytical technique to be used is cyclic voltammetry, as it is versatile and easy to do measurements. This technique has been applicable in various fields like electrochemistry, organic chemistry, inorganic chemistry and also in biochemistry. Redox behavior of molecules that are observed can be effective over a wide potential range using this technique.^{73,74}

In 1975 Tomscanyi⁷⁵ was the first to study dithizone electrochemically in aqueous medium, utilizing a hanging mercury drop electrode in basic aqueous solution. The mechanisms of the electrochemical and aerial oxidation of dithizone were considered, two weak oxidation processes and two strong reductive processes were identified. Dithizone can be reduced and oxidized electrochemically, as its redox properties are governed by its thiol group and formazan structure. It is also known to be a weak reducing agent. Another electrochemical study was done on dithizone, under non-aqueous medium, where chemical oxidation and reduction of this versatile ligand were compared. From this comparison it was concluded that chemical and electrochemical behavior of dithizone correlates well.²⁹

Non-aqueous electrochemistry of metallo complexes have become a field of interest. In doing so, a comparison was done between the electrochemical properties of dithizone and its dithizonato metal complexes. Dithizonatophenylmercury(II), PhHg(HDz), is formed by the reaction between dithizone, H₂Dz, or potassium dithizonate, K⁺HDz⁻, and phenylmercury(II) chloride. Electrochemically it has been observed that H₂Dz and PhHg(HDz) have different oxidation states on the cyclic voltammetry time scale. H₂Dz itself is oxidized in two one-electron transfer steps, the first step being where the disulphide is produced and then, HDz⁺ is produced in the second oxidation step. On the other hand, PhHg(HDz) revealed only one ligand-based oxidation step. Upon electrochemical oxidation, disulphide formation in PhHg(HDz) is effectively prevented by the mercaptan group in the ligand which becomes a stable “metal thioether”, Hg-S-C, upon complexation with the phenyl mercury. A comparative study of cyclic voltammetry and the spectroelectrochemical studies of H₂Dz and PhHg(HDz) were done in CH₂Cl₂ containing 0.1 mol dm⁻³ [NⁿBu]₄][B(C₆F₅)₄] employing a glassy carbon electrode working electrode at 20°C, see Figure 2.22 (left). As opposed to the oxidation processes, at least

⁷¹ P. M. S. Monk, R. J. Mortimer, D. R. Rosseinsky, *Electrochromism: Fundamentals and applications*, VCH, Weinheim, (1995).

⁷² P. M. S. Monk, *The Viologens: Synthesis, Physicochemical properties and Applications of the Salts of 4,4'-Bipyridine*, Wiley, Chichester, (1998).

⁷³ P. T. Kissinger, W. R. Heineman, *J. Chem. Ed.*, 702, **60** (1983).

⁷⁴ D. H. Evans, K. M. O'Connell, R. A. Peterson, M. J. Kelly, *J. Chem. Ed.*, 290, **60** (1983).

⁷⁵ L. Tomscayi, *Anal. Chim. Acta*, 411, **70** (1974); 371, **88** (1977) and 409, **89** (1977).

two reduction waves were observed for both H_2Dz and $\text{PhHg}(\text{HDz})$. Spectroelectrochemistry of $\text{PhHg}(\text{HDz})$ was also done to establish its electrochromic behavior over a range of both positive and negative potentials, see Figure 2.22 (right). A DCM solution of 0.3 mol dm^{-3} $\text{PhHg}(\text{HDz})$ with 0.1 mol dm^{-3} $[\text{N}(\text{nBu})_4][\text{B}(\text{C}_6\text{F}_5)_4]$ was placed in an OTTLE cell and potential difference of 0 to 2.200 V was slowly applied against Ag wire at a rate of $0.25/0.5 \text{ mVs}^{-1}$. There was no evidence of a colored chromophore for $(\text{PhHg}(\text{HDz}))^+$, as there is no absorption band between 380 and 800 nm, but only the decomposition of the products at higher potentials. However, when the potential reached 1.000 V a spectrum for $(\text{PhHg}(\text{HDz}))^+$ was obtained. As for reduction studies, the same conditions and reactants were applied, decreasing from 0 to -2.500 V. The complex was reduced at -0.750 V, generating $(\text{PhHg}(\text{HDz}))^-$ and gave a spectrum with $\lambda_{\text{max}} = 505 \text{ nm}$. This intermediate product was further reduced between -0.900 V and -1.300 V, to form $(\text{PhHg}(\text{HDz}))^{2-}$.⁷⁶

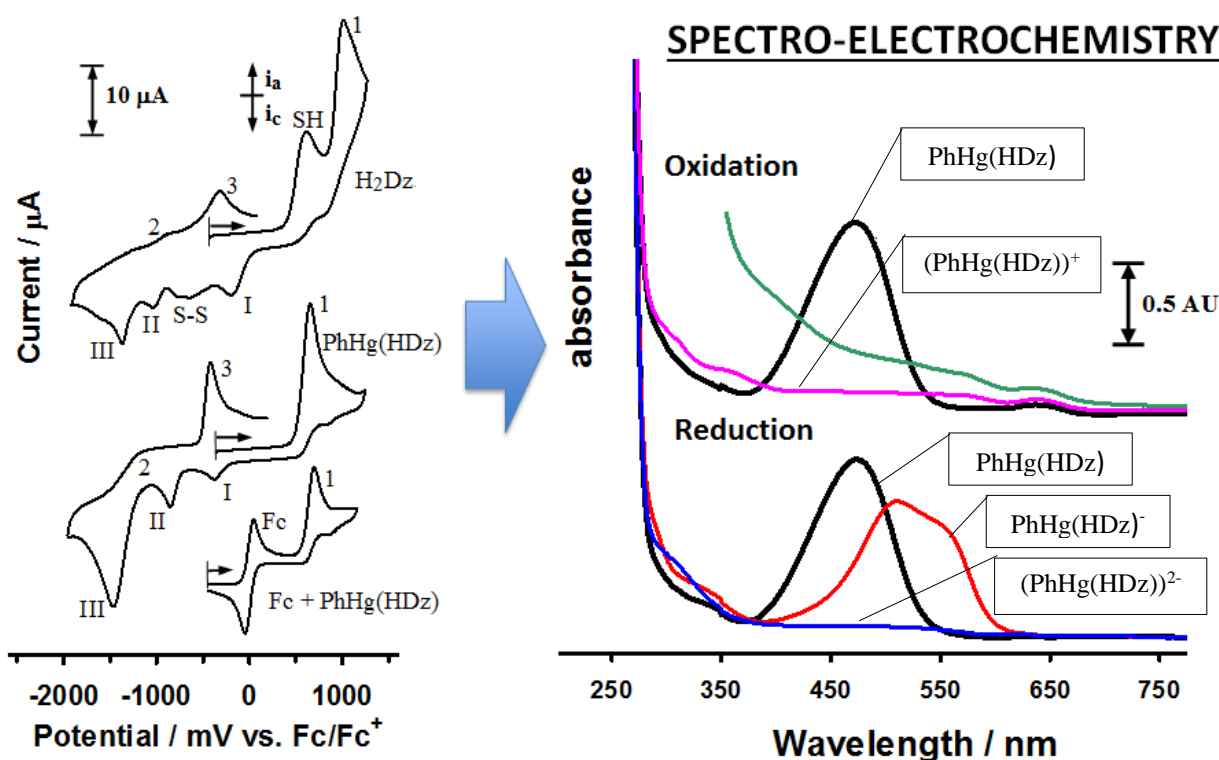


Figure 2.22. Left: Cyclic voltammetry at 0.500 Vs^{-1} of dithizone, H_2Dz , mercury(II) dithizonate, $\text{PhHg}(\text{HDz})$, and in the presence of ferrocene, Fc, as internal standard. The arrows indicate scans initiated in the positive direction. Right: UV-Vis spectra of $\text{PhHg}(\text{HDz})$ in the OTTLE cell, with oxidative studies at the top and reductive studies at the bottom.⁷⁶

In contrast to the *mono*-dithizonatomercury complexes, related electro- and spectro-electrochemistry were observed for the *tris*-dithizonatocobalt(III), $\text{Co}(\text{HDz})_3$, complex. The

⁷⁶ K. G. von Eschwege, L. van As, J. C. Swarts, *Electrochim. Acta*, 10064, **56** (2011).

metal of this product is redox active, which forms three stable metal thioethers, Co-S-C, and each of its three HDz⁻ ligands shows a one-electron oxidation process. Two one-electron reductions occur. For every redox process observed electrochemically, there were spectral changes. Upon reduction, the complex behaviour was more pronounced electrochromically, but only mildly so upon oxidation.⁴³

2.3.4. Halochromism

Color change in a compound that is induced by a change in pH is called halochromism. In analytical chemistry halochromic materials are used extensively, otherwise best known as pH-sensitive dyes or indicators. When these materials are combined with pH modifiers such as carboxylic acid, they can be used as humidity indicators.⁷⁷ When this phenomenon was first introduced in 1902 with a chemical reaction that transforms a colorless compound into a coloured compound, it was simply defined as the color change of a dissolved compound on addition of acid or base.⁷⁸ In the application of pH-sensitive dyes on various textile materials, textile pH-sensors have been developed. It has been observed that halochromic dyes can be integrated into conventional textiles by a conventional dyeing technique. A clear color change was observed with pH-variation on the majority of the materials that were developed. In halochromism of dyes the surrounding textile matrix should always be considered.⁷⁹

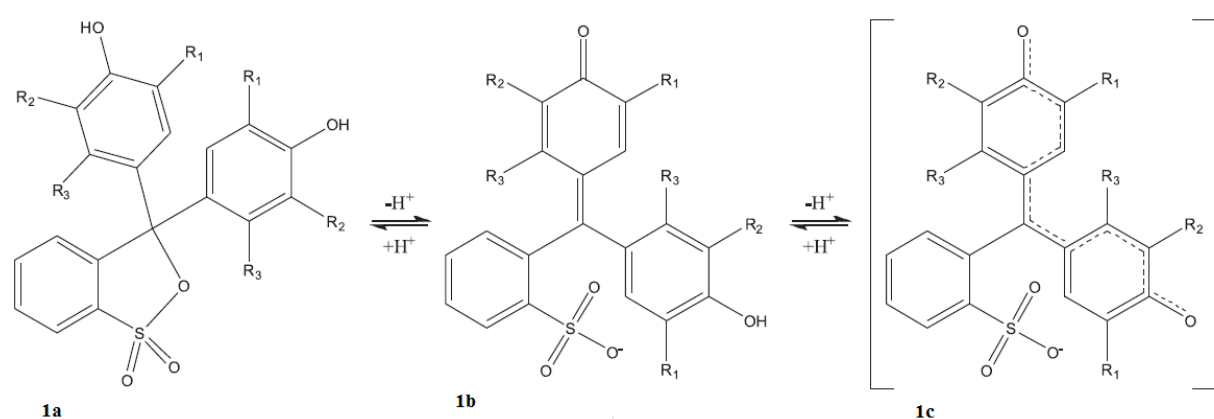


Figure 2.23. General reaction scheme of sulfonphthaleine dyes. **1a** is the neutral structure observed only in very acidic solutions or powder. The colour change of this dye can be ascribed to the protonation/deprotonation reaction of the single anionic form, **1b**, to the double anion, **1c**.

⁷⁷ P. Bamfield, M. G. Hutchings, *Chromic Phenomena: Technological Applications of Colour Chemistry*, RSC Publishing, Cambridge UK, 2nd ed., (2010).

⁷⁸ A. Baeyer, V. Villiger, *Ber. Dtsch. Chem. Soc.*, 4728, **111** (1899).

⁷⁹ L. van Schueren, K. De Clerck, *Advances in Science and Technology*, 47, **80** (2013).

Two distinct methods were used to graft sets of ten pH-sensitive sulfonphthaleine dyes onto polyamide 6, see Table 2.4. The first method used was conventional dyeing of fabrics, where it was observed that halochromicity is largely influenced by substituents. Sulfonphthaleine dyes with halogen substituents were the only ones that still displayed pH-sensitive behavior, see Figure 2.23. It was proposed that halogen bonding is an important contribution to the overall interaction, as dyes with halogen substituents showed this type of bonding. Results showed the importance of halogen substituents on sulfonphthaleines in the development of pH-sensitive sensors.⁸⁰ In aqueous environment hydrogen bonds are easily broken while halogen bonds are less affected by its environment.

Table 2.4. Substituents of selected sulfonphthaleine dye molecules and their pK_a values.

Dye	R ₁	R ₂	R ₃	pK _a
Phenol Red	H	H	H	8.0
Cresol Red	CH ₃	H	H	8.3
m-Cresol Purple	H	H	CH ₃	8.5
Xylenol Blue	CH ₃	H	CH ₃	9.1
Thymol Blue	i-Pr	H	CH ₃	8.9
Chlorophenol Red	Cl	H	H	6.7
Bromophenol Blue	Br	Br	H	4.1
Bromocresol purple	Br	CH ₃	H	6.3
Bromocresol Green	Br	Br	CH ₃	4.8
Bromothymol blue	i-Pr	Br	CH ₃	7.4

Halochromism is a subclass of a more general phenomenon called ionochromism, whereby a color change of a compound is induced by the interaction with an ionic species. The terms halochromic, acidochromic, or pH sensors are often used in species that change color due to hydrogen ion solvation. Other common ion species are metal ions and onium cations like tertiary ammonium and phosphonium. Ionochromic organic structures are called ionochromes or ionophores. There are three main classes of commercially important pH sensitive dyes; phthalides, triarylmethanes and fluorans. Although, there are also other chromophores that undergo useful color changes on protonation, these include simple neutral azo dyes, styryl dyes and indophenols. The phthalide structured pH indicator dyes fall into two types which are phthaleins and sulfophthaleins. Their changes in pH is best exemplified by their dihydroxy derivative that has the trivial name of phenolphthalein. Color changes of this parent derivative are reversible, providing an easily visible method for measuring pH in the ranges, 8.5 – 9.0. Similar ionization reactions are observed for sulfophthaleins.⁸¹

⁸⁰ T. De Meyer, I. Steyaert, K. Hemelsoet, R. Hoogenboom, V. Van Speybroeck, K. De Clerck, *Dyes and Pigments*, 249, 124 (2016).

⁸¹ I.J. Fletcher and R. Zink, *The Chemistry and Applications of Leuco Dyes*, R. Muthyala (Ed.), Plenum, New York, 1997, pp. 97–123.

Dithizone itself readily also undergo acid-base reactions, exhibiting a color change from blue-green to orange when deprotonated. Under extreme conditions, i.e. in the presence of sodium metal, H_2Dz may even be stripped of its second proton. The synthesis intermediate, H_4Dz , is usually dirty white, H_2Dz is green, HDz^- form orange-red solutions, and Dz is yellow.

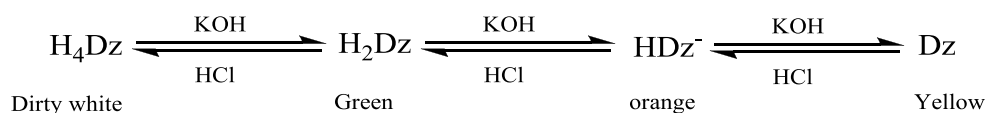


Figure 2.24. Schematic representation of dithizone halochromism.

2.3.5. Thermochromism

Thermochromism was once defined by Day as “an easily noticeable reversible color change brought about by the boiling point of each liquid, the boiling point of the solvent in the case of a solution or the melting point for solids”.⁸² For many inorganic and organic materials this definition is academically accurate, and also in other important technical areas that involve other external influences as well as heat in the observed color change (i.e. thermochromic pigments), the label “thermochromic” is applied. A more appropriate technical approach is to separate reversible organic thermochromism into ‘intrinsic’ systems, where heat is the only stimulus for color.⁸³ For example, on heating, the red color of rubies transforms into a shiny green when a sufficient temperature is exceeded, but returns upon cooling. Scientists studied this phenomenon for centuries.⁸⁴ In reversible intrinsically thermochromic organic systems, color changes of chromophores are caused by heating alone, without any other external stimulus. When the heat source is removed, the color of the chromophore reverts back to its thermally more stable state. An example of this system is spirooxazines, known for molecular rearrangement of molecules by breaking of covalent bonds. This bond breaking is observed in ring opening of spiropyrans that is induced by heating either the solid or solution to produce a highly colored merocyanine form. Polarity of the solvent also has an effect, where a polar solvent favors the formation of the more polar merocyanine form.⁸⁵

⁸² J. H. Day, *Chem. Rev.*, 65, 63 (1963).

⁸³ S.M. Burkinshaw, J. Griffiths, A.D. Towns, *Colour Science '98. Vol. 1: Dye and Pigment Chemistry*, J. Griffiths (Ed.), University of Leeds, 1999, pp. 174–183.

⁸⁴ C. F. Schönbein, *Ann. Phys. Chem.*, 263, 45 (1838).

⁸⁵ B. Hellrung, H. Balli, *Helv. Chim. Acta*, 1583, 72 (1989).

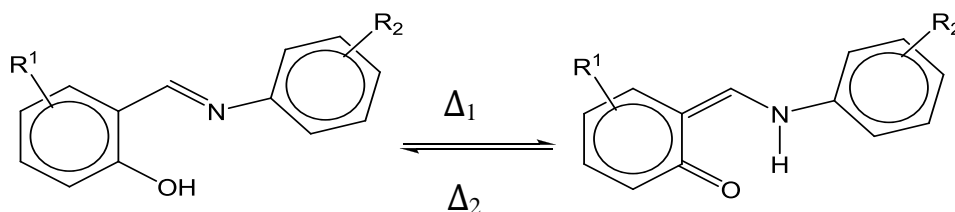


Figure 2.25. Thermochromic reaction of Schiff bases.

Another example is the bianthrylidene system, where bianthrones undergo reversible thermochromic reactions by interchanging between stereoisomers that have different colors. On heating, the tautomer that forms is green, and at room temperature it is yellow. The energy barrier between the stereoisomers can be raised by a bulky substituent, to an extent that it does not exhibit thermochromism.⁸⁶

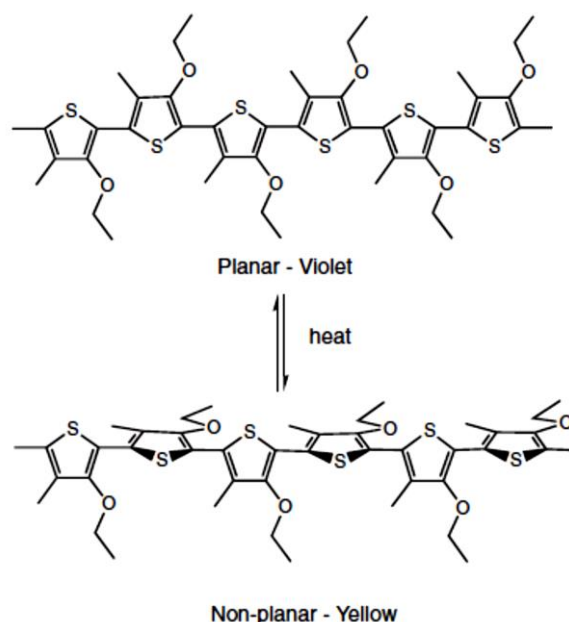


Figure 2.26. Thermochromic reaction of conjugated poly(thiophene)s.⁸⁷

Another class of intrinsic systems is the macromolecular conjugated polymers system, which includes poly(3-alkylthiophene)s and poly(3-alkoxythiophene)s. They also exhibit reversible thermochromism in both the solid state and in solution. A phenomenon known as negative thermochromism, blue-shift or hypsochromic, is observed in poly[3-oligo(oxyethylene)-4-methio-phenene], where the absorption band at room temperature is at 550 nm and is decreased to another band appearing at 426 nm on heating, which then becomes the only band when reaching 100°C. The color changes from violet to yellow, because at low temperature the polymer is assembled in a highly conjugated (planar) form. When heated it becomes disordered and less

⁸⁶ A. Samat, V. Lokshin, in *Organic Photochromic and Thermochromic Compounds, Vol. 2, Physicochemical Studies, Biological Applications, and Thermochromism*, J.C. Crano and R.J. Guglielmetti (Eds.), Plenum Press, New York, 1999, pp. 415–466.

conjugated (either twisted or non-planar), as indicated in Figure 2.26 above. By changing the length and flexibility of the side chains the temperature range of color changes can be altered.⁸⁷ Only liquid crystals and conjugated polymers of the intrinsically thermochromic organic materials have found important practical applications. A practical example where conjugated polymers are used is in optical temperature indicators and thermal recording.⁸⁸

2.3.6. Concentratorchromism

Concentratorchromism is the very rare color change phenomenon that occurs as a result of a change in concentration. One such an example is that of polythienylacetylene in THF solution. These solutions gave a continuous red-shift as the solute concentration increases. A logarithmic concentration dependence was observed, meaning, by simply changing the concentration the optical transitions of the molecule is predictably tunable.⁸⁹

A second example is that of bathochromic shifts which were observed in UV-Vis spectra with increase in fullerene concentration in solutions. Fullerene molecules that are in solution aggregate into nanoclusters. These nanoclusters increase their average sizes with an increase in concentration. This suggests that concentratorchromism is the result of formation and growth of fullerene nanoaggregates.⁹⁰

Discovery of concentratorchromism also in dithizone solutions in our group recently, was very surprising, revealing a third class of concentratorchromic compounds. When the concentration of dithizone in methanol solution is significantly high the solution is green, but upon dilution it turns orange. This is observed in the UV-vis spectra, whereby the peak at 600 nm of the green solution starts fading away, while the second characteristic dithizone peak at 455 nm undergoes a red-shift to 475 nm, see Figure 2.27. This is concentratorchromism of dithizone in methanol solutions. However, in DCM the color remains green regardless of diluted concentration of dithizone.³⁸ Quantum computational chemistry results as seen from time-dependant density functional oscillator calculations indicates that the origin of the green to yellow color change should have an explanation similar to that seen in dithizone's observed solvatochromism (as discussed in par.2.3.2); tautomer **2** is responsible for the orange color, and **1** for the green color. However, the precise reason for this phenomenon occurring at low dithizone concentrations is as yet unknown.

⁸⁷ M. LeClerc, *Adv. Mater.*, 1491, **11** (1999).

⁸⁸ N. Hirota, N. Hisamatsu, S. Maeda, H. Tsuahara, K. Hyodo, *Synth. Met.*, 67, **80** (1996).

⁸⁹ B. Tang, W. Poon, H. Peng, *Chin. J. Polym. Sci.*, 81, **17** (1999).

⁹⁰ H. Peng, F. S. M. Leung, A. X. Wu, Y. Dong, Y. Dong, N. Yu, X. Feng, B. Z. Tang, *Chem. Mater.*, 4790, **16** (2004).

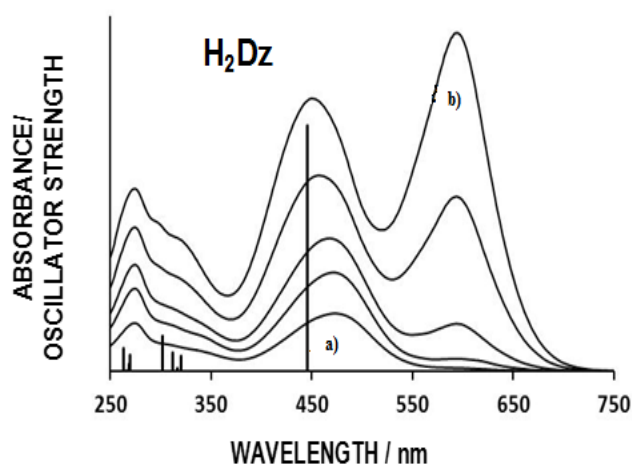


Figure 2.27. Comparison of computed B3LYP TDDFT (vertical bars) and experimental UV-Vis spectral results of tautomers **1** and **2** in methanol solution. a) Low concentration (orange solution, tautomer **2**), b) high concentration (green solution, tautomer **1**) of H₂Dz.

2.3.7. Chronochromism

Color change that takes place over a predetermined period of time is called chronochromism. Such systems usually employ pH indicators.⁵⁸ Technically all chromic phenomena are chronochromic, as they require a certain period of time to proceed. This type of system is an example of indirect chromism.

It is usually employed for two purposes: self-destruction, and real-time mimicking and indication of dynamic processes. The first purpose can be viewed as the opposite of self-healing materials that are capable of self-repairing damage caused by an external environment.⁹¹ An example where this system has been applied to is in hydrochromic dyes that isomerize in the presence of water, by changing back to the initial colorless form. These can be employed in printing, e.g. in rewritable paper, where the printed text vanishes and the process can be accelerated by an increase in temperature. At ambient temperature and humidity the self-erasing process takes roughly a day but at 70°C it takes 30 seconds.⁹²

As for the second purpose, one may consider food safety. Food quality is highly dependent on the temperature history during the custody chain and is inevitably a major threat for spontaneous spoilage of perishable products. Time-temperature indicators (TTIs) can be of use to document the temperature history for advanced quality control and assessment. Poor programmability and high cost is however the reason for limited use of TTIs. These limits have been addressed by the construction of plasmonic nanocrystals as general, kinetically programmable, and cost efficient

⁹¹ M. D. Hager, P. Greil, C. Leyens, S. van der Zwang, U. S. Schubert, *Adv. Mater.*, 5424, **22** (2010)..

⁹² L. Sheng, M. Li, S. Zhu, H. Li, G. Xi, Y.G. Li, Y. Wang, Q. Li, S. Laing, K. Zhong, S. X. Zhang, *Nat. Commun.*, 2044, **5** (2014).

TTI protocol. They are based on chronochromic behavior during heteroepitaxy of Ag shell on Au nanorods, as they go from red to green. Flexible programmability of this system is given by simply varying the concentrations of the relevant reagents to get wide tune-ability of the kinetic rate and apparent activation energy of these self-evolving systems. The deterioration processes of numerous perishables may be tracked by this TTI. A practical example is an investigation done to mimic the growth of milk E. Coli over time at two different temperatures where milk is usually stored, see Figure 2.28.⁹³

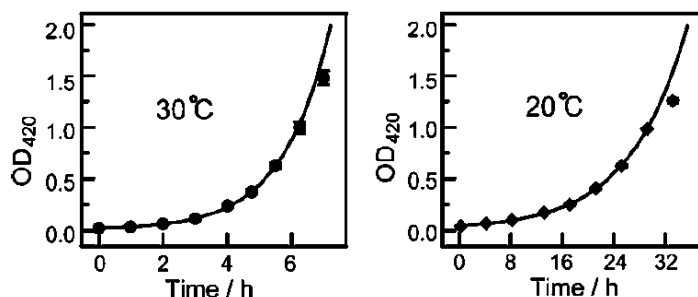


Figure 2.28. Plot of optical density at 420 nm against time in hours for the growth rate of E. coli at to different temperatures over time.

2.4. Analytical Applications

2.4.1. Metal Dithizonates

Dithizone is serving in the field of analytical chemistry since its introduction by H. Fischer⁹⁴ as a new organic reagent. Ever since then it has had a great impact on analytical procedures. In trace metal analyses he showed its applicability in titrimetric procedures and developed mono-color and mixed-color procedures to determine traces of metal dithizonates. This method was then refined and improved as the availability of spectrophotometers increased. He introduced this organic reagent to analytical procedures by exploiting the special features of this compound, like the intensely colored complexes it forms with metals, its solubility in a range of organic solvents, and insolubility in water while readily soluble in alkali water. He then used these properties in techniques based on liquid-liquid extractions by adjusting pH in the aqueous phase. Dithizone has a comparative advantage over 8-quinolinol and many organic reagents that have been introduced, because it is selective in its reactions. The majority of cations that it forms stable complexes with can be precipitated as sulphides from aqueous solutions, but often they do not form extractable dithizonates, see Figure 2.29. Fortunately, elements which are important for determination in trace quantities may be extracted as sulphides. A combination of certain metals

⁹³ C. Zhang, A. Yin, R. Jiang, J. Rong, L. Dong, T. Zhao, L. Sun, J. Wang, X. Chen, C. Yan, *J. Am. Chem. Soc.*, 4561, **7** (2013).

⁹⁴ H. Fischer, *Wiss. Veröffentlich. Siemens-Werken*, 158, **24** (1925).

with alkyl or aryl groups, e.g. PhHg^+ , Et_2Sn^+ , Bu_2Ga^+ , Ph_3Pb^+ , or Me_2TI^+ , form strongly coloured complexes with dithizone and can be determined spectrophotometrically by extraction into organic solvents.¹⁴

H																		He
Li	Be											B	C	N	O	F	Ne	
Na	Mg											Al	Si	P	S	Cl	Ar	
K	Ca	Sc	Ti	Y	Cr	Mn	Fe	Co	Ni	Cu	Zn	Ga	Ge	As	Se	Br	Kr	
Rb	Sr	Y	Zr	Nb	Mo	Tc	Ru	Rh	Pd	Ag	Cd	In	Sn	Sb	Te	I	Xe	
Cs	Ba	La	Hf	Ta	W	Re	Os	Ir	Pt	Au	Hg	Tl	Pb	Bi	Po	At	Rn	
Fr	Ra	Ac	Th	Pa	U													

Figure 2.29. Metals extractable by dithizone (within solid border) and metals (shaded) that can be precipitated as sulphides from aqueous solution.¹⁴

Trace metal analysis of toxic heavy metals was and is an important area of analytical chemistry. Over the years dithizone has been used to determine mercury at trace levels.⁹⁵ A number of the heavy metals that dithizone forms complexes with, including mercury, are photochromic and photoacoustic spectroscopy (PAS) has been quite successful for the analysis of these species.⁹⁶ Due to the fact that preparation of solid samples for PAS is time consuming, a novel technique was established. In this technique polystyrene latex micro-particles are impregnated with dithizone, with aqueous Hg(II) being sequestered onto the particles. An added advantage to this method is that samples can be quantified simultaneously, fast and simple. Mercury can be determined at picomole levels in aqueous samples by using this method. The sensitivity of the technique is good for environmental analysis and the particles can easily be converted into solid samples, to be analyzed by photochromism-induced-PAS (PC-PAS). In the PC-PAS technique there is good selectivity for Hg(HDz)_2 over other toxic heavy metals. In water streams heavy metals contamination can be observed visually by applying a packed column of these microparticles, since there is a visual color change during reaction with heavy metals.⁹⁷

Dithizone forms colored complexes with copper(II), which forms the basis for a number of titrimetric and spectrometric determinations. However, the reaction lacks selectivity, but is sensitive at ppm levels. This reaction has been used to determine trace amounts of copper(II) directly in the aqueous phase, thus overcoming the limitation of dithizone and its copper(II)

⁹⁵ E. B. Sandel, H. Onishi, *Colorimetric Determination of Traces of metals*, 4th ed., Wiley-Interscience, New York, 1978, p 391.

⁹⁶ N. Chen, R. Guo, E. P. C. Lai, *Anal. Chem.*, 2435, **60** (1988).

⁹⁷ V. A. VanderNoot, E. P. C. Lai, *Anal. Chem.*, 3187, **64** (1992)

complexes' insolubility in water, while avoiding extraction into toxic solvents like chloroform.⁹⁸ Other reports show how solvent extraction steps to determine Zn(II) are by-passed; instead it makes use of inexpensive anionic micelles. In this micellar medium trace amounts of Zn(II) are determined directly using dithizone. Other advantages to this method is that it is simple, rapid, has greater sensitivity, better selectivity and improved precision. The results obtained by this method were comparable to those obtained with the flame absorption spectroscopy (FAAS) method, with no significant difference at 95% confidence level between the two methods.⁹⁹ There are various spectrophotometric methods that focus on the determination of trace metals in aqueous phase. An example of these metals is lead, which has been studied extensively for its toxicity and its trace amounts are important industrially as a biological nutrient, environmental pollutant and occupational hazard. For the first time a non-extractive direct spectrophotometric method for trace determination of lead(II) in aqueous biological samples was reported. This method does not require any "clean-up" step, it is very simple, ultra-sensitive and fairly selective at ultra-trace levels of lead(II). Determinations are done in the presence of aqueous micellar solutions using dithizone. A stoichiometry of 1:2 was observed for Pb:dithizone. The results from this method were in close agreement with those obtained when using atomic absorption spectroscopy (AAS).¹⁰⁰

2.4.2. Mole Ratio Method

Selection of most suitable complexing agents is enabled by determination of mole ratio's in different metal complexes, as well as their formation constants. Yoe and Jones^{101,102} were the researchers who first introduced the mole ratio method. In this method one reactant's (usually cation) analytical concentration is held constant while that of the other is varied by making use of a series of solutions. From these solutions absorbance is plotted versus mole ratio of the reactants. The plot gives a curve with two straight lines, see Figure 2.28. These lines then give the combining ratio in the complex, by intersecting at a corresponding mole ratio.¹⁰³ A minor disadvantage to this method is when the complex is weak, formation constant of such complexes appear to be decreasing as the curvature increases. This then results in uncertainty in the identification of the molar ratio of the components of these complexes. Another problem

⁹⁸ B. Kumar, H. B. Singh, M. Katyal, R. L. Sharma, *Mikrochim. Acta.*, 79 (1991).

⁹⁹ G. A. Shar, M. I. Bhangar, *J. Chem. Soc. Pak.*, 74, **23** (2001)

¹⁰⁰ H. Khan, M. Jamaluddin, M. I. Bhangar, *Spectroscopy*, 285, **20** (2006).

¹⁰¹ J. H. Yoe, A. L. Jones, *Ind. Eng. Chem. Anal. Ed.*, 11, **16** (1944).

¹⁰² J.H. Yoe, A.E. Harvey, *J. Am. Chem. Soc.*, 648, **70** (1948).

¹⁰³ D. A. Skoog, D. M. West, F. J. Holler, S. R. Crouch, *Fundamentals of Analytical Chemistry*, Thomson Brooks/Cole (Canada) 8th edn., (2004).

encountered is complexes that are not completely formed at the equivalence point.¹⁰⁴ Chriswell *et al.*¹⁰⁵ discussed techniques to improve application of the mole ratio method to weak complexes.

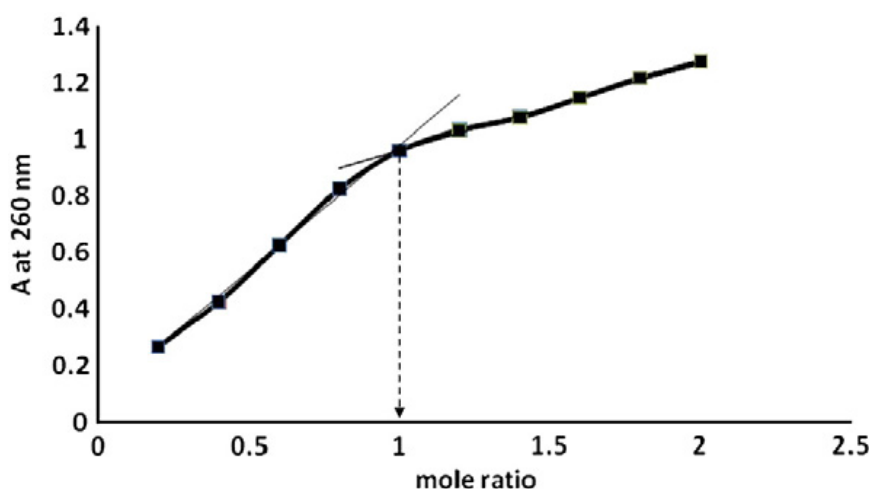


Figure 2.30. Mole ratio of Fe(III) ions with EDTA in the Fe(III)EDTA complex is 1:1 (Fe:EDTA).¹¹⁰

Limiting factors in the mole ratio method may be: stability of the formed complex, effect of the buffer, and the use of masking reagents.¹⁰⁶ The use of dual wavelength spectrometry by adding a known excess of the ligand and varying the amount of metal added, was proposed as improvement for these limitations. From this dual wavelength method the absorbance of the free ligand is then plotted against the metal concentration (x-axis). The mole ratio of the formed complex can be determined from the metal concentration on the x-axis, divided by the initial concentration of the ligand.¹⁰⁷ However, this method is also limited because it requires a significant absorbance of the ligand and that is not always the case with aliphatic ligands, etc.. Another limitation is when metal absorbance overlaps with that of the ligand or the absorbance of the formed complex at the selected wavelengths. A ligand such as EDTA has been used in an innovative ligand exchange method involving the displacement of Fe(III) or Cu(II). The determined mole ratio corresponds to the reported structure of Cu(II)-salicylate complex¹⁰⁸ as 1:2. Another validation was done by determining the mole ratio of Cu(II)-citrate complex (1:1) and Cu(II)-EDTA (1:1) complex, which agrees with related reported complexes.¹⁰⁹ The validity of the method was established, and now it is generalized for the determination of many metal complexes, using other metal complexes that are visible in the UV-Vis range. It was also successful in determining the mole ratio's of Fe(III)-citrate and Ferric EDTA, see Figure 2.30.

¹⁰⁴ A.E. Harvey, D.L. Manning, *J. Am. Chem. Soc.*, 4488, **72** (1950).

¹⁰⁵ C. D. Chriswell, A. A. Schilt, *Anal. Chem.*, 1623, **47** (1975).

¹⁰⁶ B.W. Budensinsky, *Talanta*, 323, **21** (1974).

¹⁰⁷ Z. Nan, H. Chun-Xiang, *Analyst*, 1077, **118** (1993).

¹⁰⁸ L.L. Borer, *J. Chem. Educ.* 354, **77** (2000).

¹⁰⁹ Z. Fresenius, *Anal. Chem.*, 400, **306** (1981).

This method also comes with two requirements; the formation constant of the metal complex being determined must be higher than the reagent (salicylate) metal complex and the metal complex being studied must not absorb at λ_{max} of the reagent metal complex.¹¹⁰

2.4.3. Continuous Variation Method

Ever since Job¹¹¹ introduced a method for determining the formulas and formation constants of complexes it has captured the imagination of the chemical community. When later modified it became the most widely used method for determining the composition of soluble metal complexes. One or more wavelengths can be used to measure the absorbance.¹¹² Two solutions, cation and ligand, with identical analytical concentrations are used to prepare a series of solutions where the mole ratio of reactants vary systematically. In each mixture the total moles of reactants and the total volume are kept constant. At a suitable wavelength each of the solution's absorbances are measured and the corrected absorbances plotted against the volume fraction of one reactant. The absorbance is corrected for any absorbance the mixture might exhibit if no reaction has taken place. This method is commonly known as the method of continuous variations or Job's method.¹⁰³

A triangular plot is observed from the plotted absorbance vs. mole fraction of reactants if a single stable complex forms, i.e. that is not appreciably dissociated, see Figure 2.31. However, this method cannot give reliable results for the formation constant of weak complexes. From this method, reliable results are only obtained when there is one predominant complex formed, where the reactants and complex are not involved in concomitant equilibria.¹¹³

In the dithizone system a monophasic consisting of 20 % chloroform, 70 % ethanol and 10 % water was used to introduce this method, as to verify the composition of primary zinc dithizonate, $Zn(HDz)_2$. A 1:2 complex formation was always confirmed, irrespective of the selection of wavelength; 525 or at 470 nm. A_j is the symbol used to denote the Job ordinate that is determined by the difference between the actually measured absorbance and the calculated value. This is based on the assumption that the components have merely mixed without reacting in any way. X is the mole fraction of the metal (zinc), see Figure 2.31.¹¹⁴

¹¹⁰ F. R. Mansour, N. D. Danielson, *J. Microchemical*, 74, **103** (2012).

¹¹¹ P. Job, *Ann. Chim.*, 113, **9** (1928).

¹¹² W. C. Vosburgh, G. R. Cooper, *J. Amer. Chem. Soc.*, 437, **63** (1941).

¹¹³ F. Woldbye, *Acta Chem. Scand.*, 299, **9** (1955).

¹¹⁴ H. Irving, C. F. Bell, R. J. P. Williams, *J. Chem. Soc.*, 356, (1952).

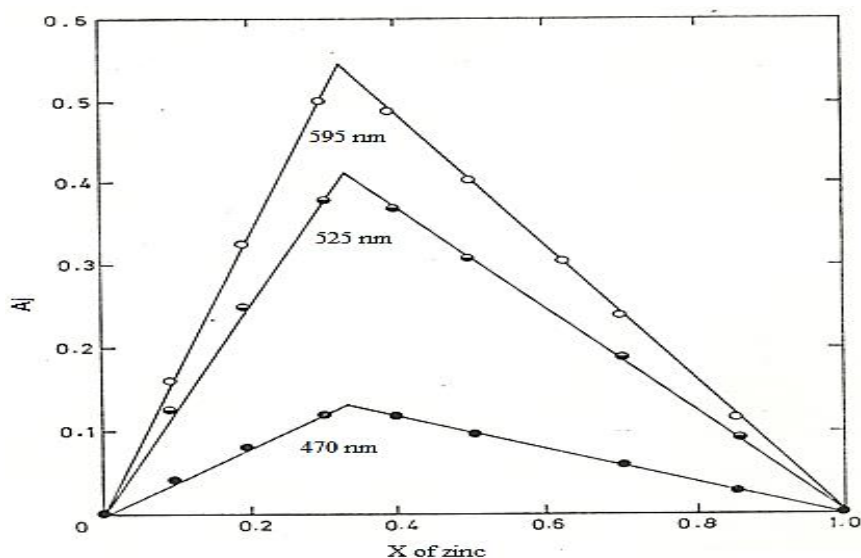


Figure 2.31. Method of continuous variations in a monophasic system. Job ordinate (A_j) against mole fraction of zinc (X).¹¹⁴

A two-phase system was also introduced, but using the organic phase to determine A_j with an advantage of establishing the composition of comparatively weak complexes. However, the limit to this two-phase system is that the metal has to be uncharged and extractable into a water immiscible solvent. The locations of the extrema are better defined with dithizone complexes since they are normally of high stability.¹¹⁵

During attempts to synthesize water-soluble dithizones, specifically also with the aim to develop new reagents for the well-known mole-ratio and continuous variation methods, a series of chromic phenomena were discovered in the carboxylic acid derivative of dithizone and its complexes. Characterization work was done accordingly, and tests were run, testing its application in the said aims.

¹¹⁵ H. Irving, T. B. Pierce, *J. Chem. Soc.*, 2565, (1959).

3. Results and Discussion

3.1. Introduction

This chapter reports experimental procedures, reaction conditions and techniques, including detailed discussions of results obtained during this study. All solvents and reagents were used without any further purification, as supplied by Sigma-Aldrich and Merck. Ultra-pure water with zero total dissolved solutes (TDS) was used for the experimental procedures. A KP250 cooling stirrer was used for cold reaction conditions and the melting points of products were determined on a Reichert Thermo-pan micro-scope with Koffler hot-stage. A Shimadzu UV-2550 spectrophotometer was used to obtain UV-visible spectrophotometric measurements. The Shimadzu instrument is fitted with a Shimadzu CPS temperature controller. During photochromism studies a 400 W mercury-halide lamp was used, simulating daylight. Spectra were drawn from solutions in an optical glass cuvette within absorbance ranges that obey Beer's law. Data was processed with Microsoft Excel. A Bruker Avance DPX 600 MHz instrument was used for ^1H NMR spectra, using deuterated dimethyl sulfoxide (DMSO-d_6).

3.2. Synthesis

3.2.1. Dithizone Derivatives

3.2.1.1. (*p*-COOH)dithizone

Nitroformazan: 4-aminobenzoic acid (4.1058 g, 30 mmol) was dissolved in a mixture of concentrated hydrochloric acid (15 mL) and water (25 mL) in a 200 mL beaker placed on a cooling stirrer ($-5 < 0$ °C). While stirring, small portions of sodium nitrite (3.1093 g, 45 mmol) were added slowly (for *ca* 30 min., to prevent temperature increase) to form a creamy yellow solution. The diazo solution was then added to a well stirred solution of sodium acetate trihydrate (60 g, 0.44 mol), glacial acetic acid (35 mL) and water (20 mL) in a 500 mL beaker, forming a yellowish slurry. Nitromethane (8.6 mL, 150 mmol) was added to the reaction mixture to achieve a brick red slurry which was stirred at room temperature for 3 hours, with periodic addition of water (200 mL) as the reaction mixture thickened. Finally the formazyl product was filtered through a sintered glass funnel, washed with large amounts of cold water and dried in an open fume hood or oven at 60 °C.

Nitroformazan: orange-red (4.8559 g, 93 %). M.p. 210 °C, UV-vis (acetone) λ_{max} 449 nm.

δ_{H} (600 MHz, DMSO-d_6)/ppm: 7.4-8.3 (8 H, Ar-H's, $2 \times \text{C}_6\text{H}_4$), 14.25 (1H, s, $1 \times \text{NH}$), 13.2 ($2 \times \text{COOH}$).

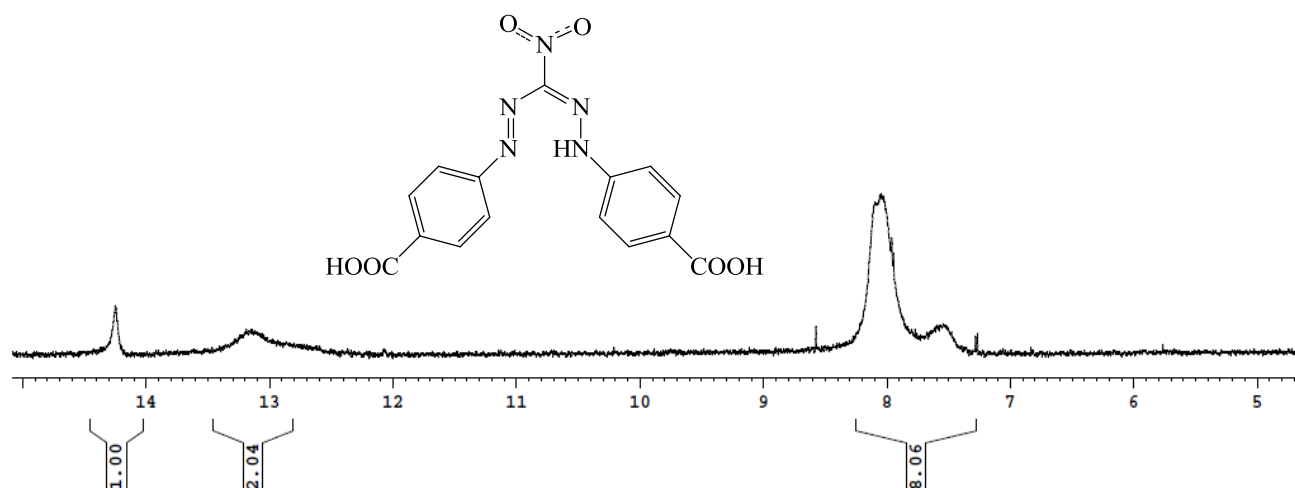


Figure 3.1. ^1H NMR spectrum of (*p*-COOH)nitroformazan.

Thiocarbazone: Nitroformazan (1.0713 g, 3 mmol) was dissolved in absolute ethanol (60 mL) in a lightly stoppered Erlen Meyer flask and stirred at 30 °C for 30 min. 20% ammonium sulphide (6 mL, 17.6 mmol) was added to the nitroformazyl solution, while stirring in the fume hood. After 20 minutes a light yellow precipitate (thiocarbazone) formed, which was filtered through a sintered glass funnel. 2% aqueous potassium hydroxide (100 mL) was periodically poured onto the precipitate in the funnel (no suction), oxidizing the yellow precipitate to a dark red potassium salt, dissolving and washing it into a clean 250 mL Erlen Meyer flask, while stirring with a spatula until complete dissolution.

Dithizone: 2 % aqueous hydrochloric acid (100 mL) was cooled down to 5 °C and slowly poured to the reddish dithizonate solution until a green precipitate was fully achieved. The product mixture was centrifuged and washed with large amounts of cold water (0 °C). The acid base step was repeated five times by re-dissolving the precipitate in 2% aqueous potassium hydroxide (100 mL) and then 2 % aqueous hydrochloric acid (100 mL, 5 °C), for purification purpose. The product was dried in an open fume hood and washed with warm DCM (50 mL x 3).

(*p*-COOH)dithizone: Dark purple (0.7403 g, 72 %), M.p. 199 °C, UV-vis (acetone) λ_{max} 452 and 634 nm, δ_{H} (600 MHz, DMSO- d_6)/ppm: 7.7 – 8.1 (8 H, Ar-H's, 2 × C₆H₄), 9.8 and 10.2 (2 × COOH).

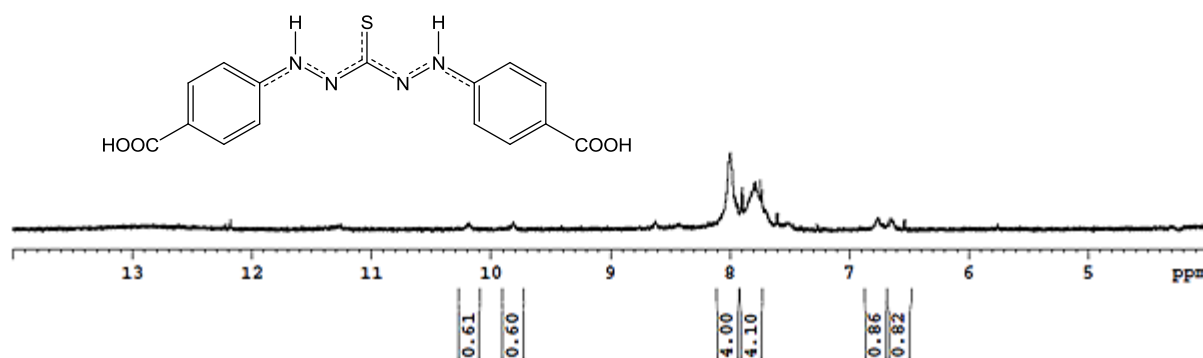


Figure 3.2. ^1H NMR spectrum of (*p*-COOH)dithizone.

3.2.1.2. (*p*-SO₃H)nitroformazan

Sulfanilic acid (1.0420 g, 6.0 mmol) was dissolved in an acidic mixture of concentrated hydrochloric acid (10 mL) and water (20 mL) in a 100 mL beaker, placed on a cooling stirrer ($-5 < 0^\circ\text{C}$). Small portions of sodium nitrite (0.6251 g, 9 mmol) were added slowly while stirring the reaction mixture to form a creamy yellow solution, diazo solution. The diazo solution was then added to a well stirred solution of sodium acetate trihydrate (60 g, 0.44 mol), glacial acetic acid (35 ml) and water (20 mL) in a 500 ml beaker. Nitromethane (8.6 ml, 150 mmol) was added to achieve a brick red reaction mixture and the stirring was continued for 2 hours at room temperature. Then left in an open fume hood to concentrate the solution overnight. The brick-red precipitate was filtered through a sintered glass funnel, washed with glacial acetic acid (50 mL x 2), immediately followed by (10 mL x 2) ethanol, and dried overnight in an open fume hood.

Nitroformazan: Orange (0.7543 g, 59 %), M.p. 230°C , UV-vis (methanol) λ_{max} 450nm.

δ_{H} (600 MHz, DMSO- d_6)/ppm: 7.76 and 7.87 (8 H, Ar- H 's, $2 \times \text{C}_6\text{H}_4$), 14.48 (1H, s, $1 \times \text{NH}$).

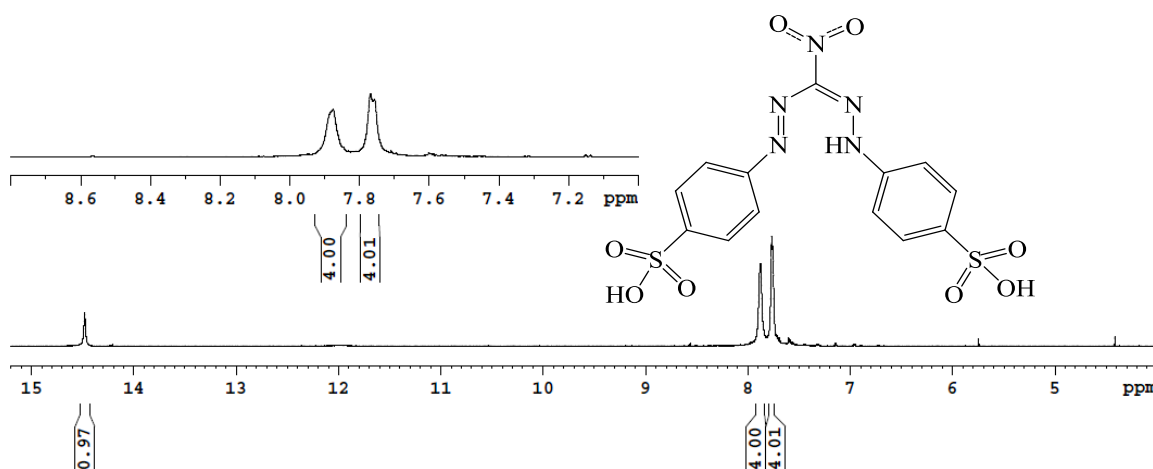


Figure 3.3. ^1H NMR spectrum of (*p*-SO₃H)nitroformazan.

(The (*p*-SO₃H)dithizone synthesis was unsuccessful at final precipitation step.)

3.2.1.3. (*p*-Sulfonylacetylamide)nitroformazan

Nitroformazans: Sulfacetamide (6.4138 g, 30 mmol) was dissolved in an acidic mixture of concentrated hydrochloric acid (7 mL) and water (12 mL) in a 100 mL beaker, placed on a cooling stirrer ($-5 < 0$ °C). Sodium nitrite (3.1240 g, 45 mmol) was added slowly in small portions while stirring, to form a creamy yellow solution (diazo solution). The diazo solution was then added to a well stirred solution of sodium acetate trihydrate (30 g, 0.44 mol), glacial acetic acid (17 mL) and water (10 mL) in a 250 mL beaker at temperature < 20 °C. Nitromethane (8.6 ml, 150 mmol) was added slowly to achieve a brick red reaction mixture, and the stirring was continued for 2 hours at room temperature. Left in an open fume hood to concentrate the solution overnight. The brick-red precipitate was filtered through a sintered glass funnel, washed with large amounts of cold water and dried overnight in an open fumehood.

Nitroformazan: Brick-red (5.3365 g, 94 %), M.p. 200 °C, UV-vis (acetone) λ_{\max} 366 and 540 nm. δ_{H} (600 MHz, DMSO- d_6)/ppm: 8.09 (8 H, Ar-H's, $2 \times \text{C}_6\text{H}_4$), 12.21 and 14.03 (2 and 1H, s, $3 \times \text{NH}$), 1.95 (6H, m, CH₃)

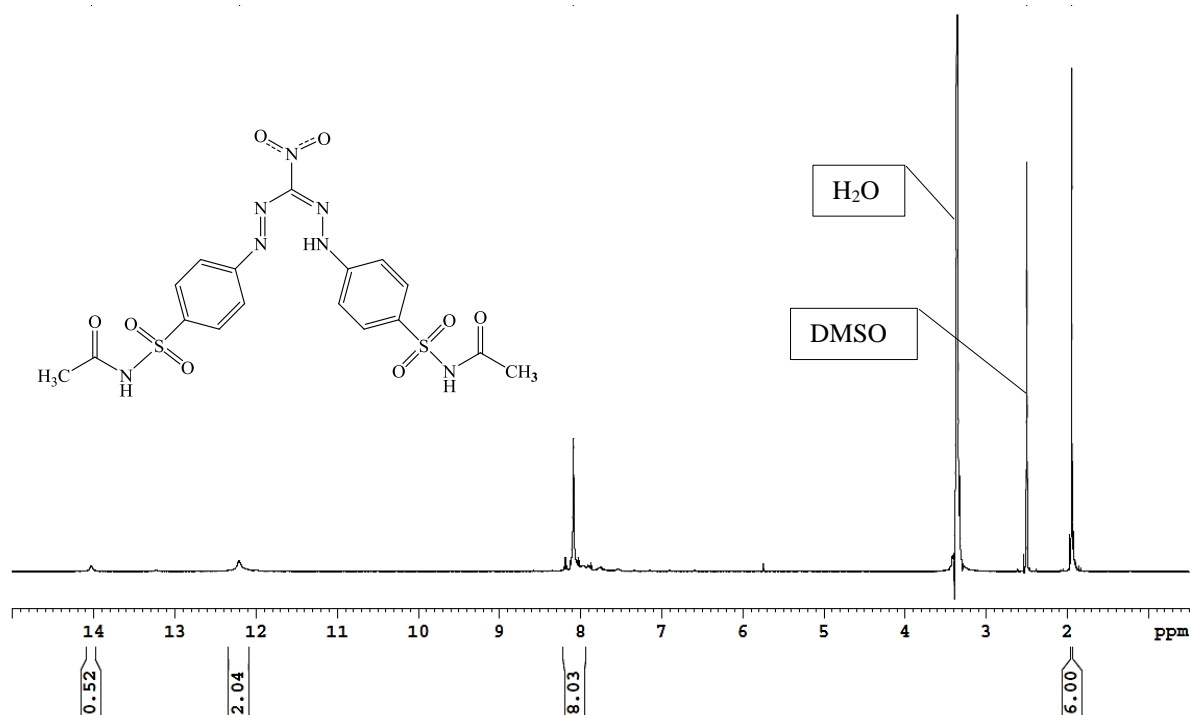


Figure 3.4. ¹H NMR spectrum of (*p*-sulfonylacetylamide)nitroformazan.

(The (*p*-sulfacetamide)dithizone synthesis was unsuccessful at final precipitation step.)

3.2.2. Metal Dithizonates

3.2.2.1. (*p*-COOH)dithizonatophenylmercury(II), PhHg(*p*-COOH-HDz)

(*p*-COOH)dithizone (0.6317 g, 1.83 mmol) was dissolved in 100 mL acetone, in a 250 mL beaker equipped with a magnetic stirrer. After 30 minutes of stirring at 30 °C, phenyl mercury acetate (0.6373 g 1.89 mmol) was added slowly in small portions, and the dark green dithizone solution immediately turned dark red. The reaction mixture was stirred for 1 hour and concentrated on the rotary evaporator under vacuum, at 50 °C. When the solution was reduced to *ca* 25 % volume, 20 mL water was added to precipitate the product. When all of the acetone was removed the aqueous solution was filtered and washed with copious amounts of warm water. The precipitate was then dried overnight in a fume hood.

PhHg(*p*-COOH-HDz): dark red (0.9678 g, 85 %). M.p. 280 °C, UV-vis (methanol) λ_{\max} 293 and 485 nm. δ_{H} (600 MHz, DMSO- d_6)/ppm: 7.2 – 8.1 (13H, Ar-H's, 1 \times C₆H₅ and 2 \times C₆H₄), 11.0 (1H, s, 2 \times NH). Product photochromic.

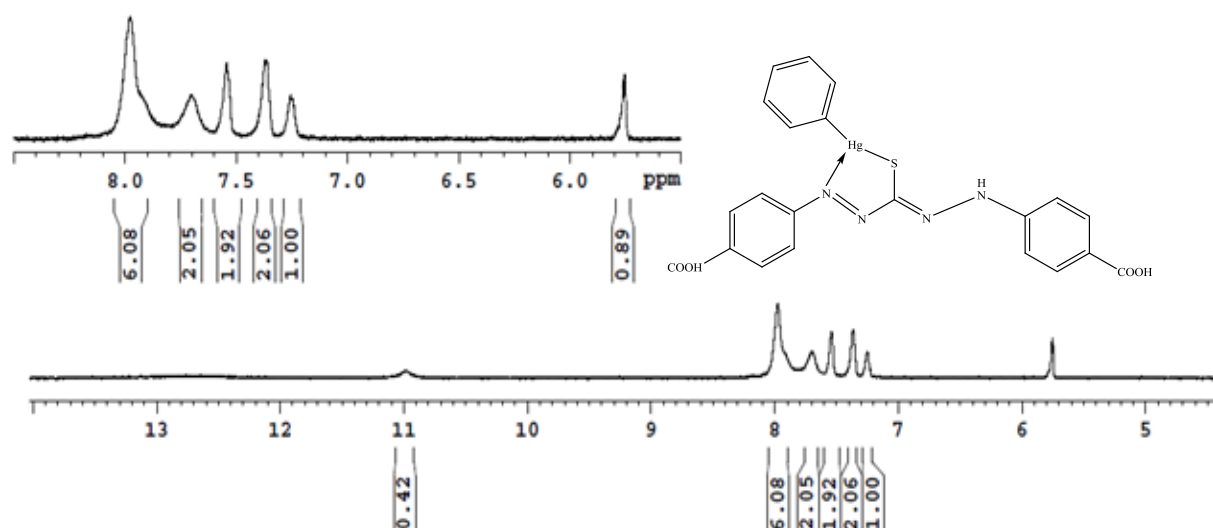


Figure 3.5. ^1H NMR spectrum of (*p*-COOH)dithizonatophenylmercury(II).

3.2.2.2. PhHg(*p*-COOPhHg -HDz)

(*p*-COOH)dithizonatophenylmercury(II) (0.1143 g, 0.18 mmol) was dissolved in 25 mL methanol, in a 250 mL beaker equipped with a magnetic stirrer. Addition of 10 mL NH_4OH (25%) resulted in a colour change from orange-red to deep purple. Phenyl mercury acetate (0.1326 g 0.39 mmol) was added in small portions to the alkali dithizonate solution. The reaction mixture was stirred for 1 hour, while remaining dark purple. The solution was then concentrated under vacuum, at 50°C, to about one quarter of the original volume and 20 mL of water was added to precipitate the product. The mixture was gravity-filtered, washed with hot water (*ca* 50 mL) and dried overnight in a fume hood.

PhHg(*p*-COOPhHg-HDz): dark blue-purple (0.1965 g, 93 %). M.p. > 360 °C,

UV-vis (methanol) λ_{\max} 296 and 500 nm. δ_{H} (600 MHz, DMSO- d_6)/ppm: 7.2 – 7.6 (15H, Ar-H's, $3 \times \text{C}_6\text{H}_5$), 7.8 and 8.0 (8H, Ar-H's, $2 \times \text{C}_6\text{H}_4$). Product not photochromic.

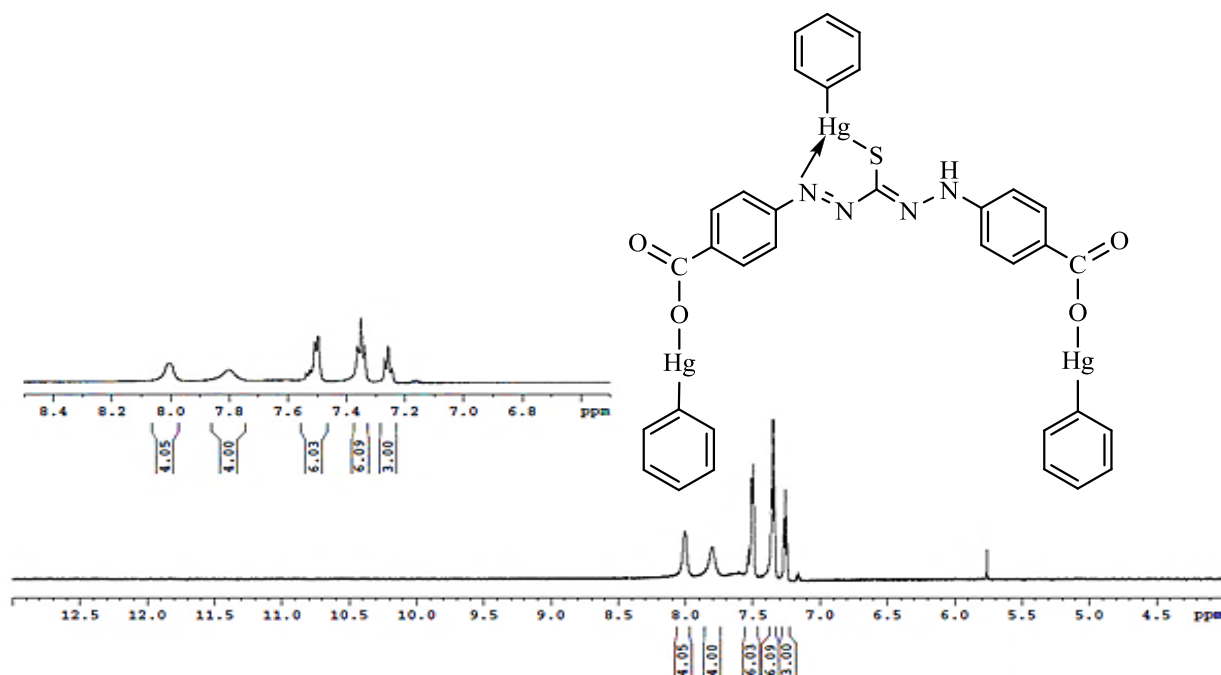


Figure 3.6. ^1H NMR spectrum of $\text{PhHg}(p\text{-COO-HDz})(\text{PhHg})_2$.

3.2.2.3. *Tris-(p-COOH)dithizonatocobalt(III)*

$(p\text{-COOH})\text{H}_2\text{Dz}$ (0.1520 g, 0.44 mmol) was dissolved in 50 mL aqueous KOH (0.5689 g, 10 mmol) solution, in a 250 mL beaker equipped with a magnetic stirrer. Cobalt(II) chloride hexahydrate, $\text{CoCl}_2 \cdot 6\text{H}_2\text{O}$, (0.0320 g, 0.13 mmol,) in 50 mL water was added to the dithizonate solution. The reaction mixture was stirred for 2 hours at room temperature, to form a deep blue solution. Glacial acetic acid (20 mL) was added to precipitate out the brown black product, and the precipitate was recovered by using a centrifuge. Acid-base purification was repeated three times by repeatedly dissolving the precipitate in 0.1 M aqueous KOH and again precipitating it out by addition of 20 mL glacial acetic acid.

$\text{Co}(p\text{-COOH-HDz})_3$: (0.1417 g, 89 %). M.p. > 360 °C. UV-vis (methanol) λ_{\max} 318 and 567 nm. δ_{H} (600 MHz, DMSO- d_6)/ppm: 7.5 – 8.2 (24H, Ar-H's, $6 \times \text{C}_6\text{H}_4$).

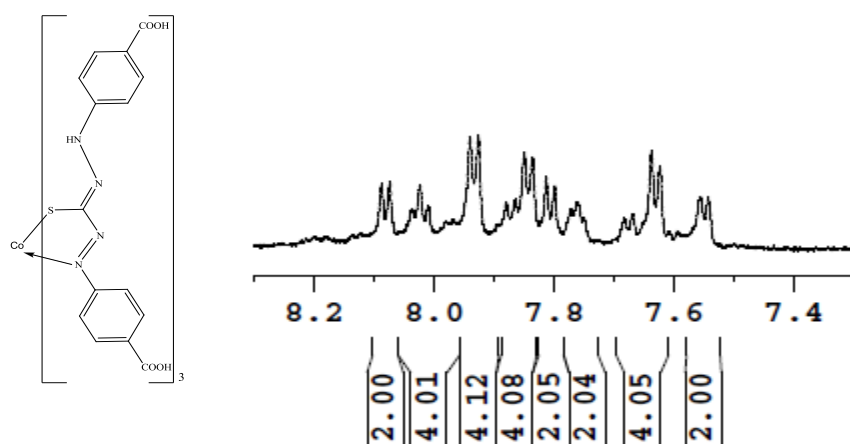


Figure 3.7. ^1H NMR spectrum of *tris*-(*p*-COOH)dithizonatocobalt(III).

3.2.2.4. *Tris*-dithizonatocobalt(III)

Dithizone, H_2Dz , (0.2520 g, 0.98 mmol) was dissolved in 10 mL aqueous KOH (0.5689 g, 10 mmol) solution in a 250 mL beaker equipped with a magnetic stirrer, then gradually increase the volume up to 50 mL with water. Cobalt(II) chloride hexahydrate, $\text{CoCl}_2 \cdot 6\text{H}_2\text{O}$, (0.0752 g, 0.31 mmol) was added to the dithizonate solution and the resultant reaction mixture was stirred at room temperature for 2 hours. The product was extracted with 100 mL DCM and washed with 100 mL 0.1 M aqueous KOH until the aqueous layer was colorless. The extract was washed with 100 mL water and dried overnight in the fume hood.

$\text{Co}(\text{HDz})_3$: (0.2163 g, 80 %). M.p. 175 °C, UV-vis (methanol) λ_{max} 448 and 556. δ_{H} (600 MHz, CDCl_3)/ppm: 6.4 – 7.45 (30H, Ar-H's, $6 \times \text{C}_6\text{H}_5$), 9.49 (3H, s, $3 \times \text{NH}$).

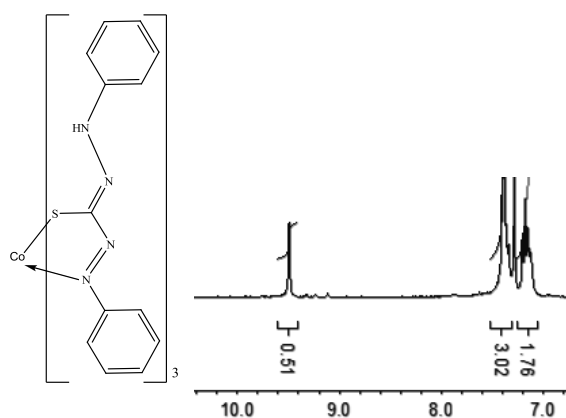


Figure 3.8. ^1H NMR spectrum of *tris*-dithizonatocobalt(III).¹¹⁶

The above synthetic procedure was used for other metal dithizonate complexes (Ni, Pb and Ag).

¹¹⁶ K. G. von Eschwege Ph.D. Dissertation, (2006).

3.2.2.5. *tris*-(*p*-COOH)dithizonatonickel(II)

(*p*-COOH) H_2Dz (0.1514 g, 0.44 mmol) was reacted with nickel(II) sulphate hexahydrate, $NiSO_4 \cdot 6H_2O$, (0.0364 g, 0.14 mmol).

$Ni(p\text{-COOH-HDz})_3$: (0.1518 g, 95 %). M.p. > 360 °C, UV-vis (methanol). λ_{max} 315 and 458 nm. δ_H (600 MHz, $DMSO-d_6$)/ppm: 7.1 – 8.3 (24H, Ar-H's, $2 \times C_6H_4$).

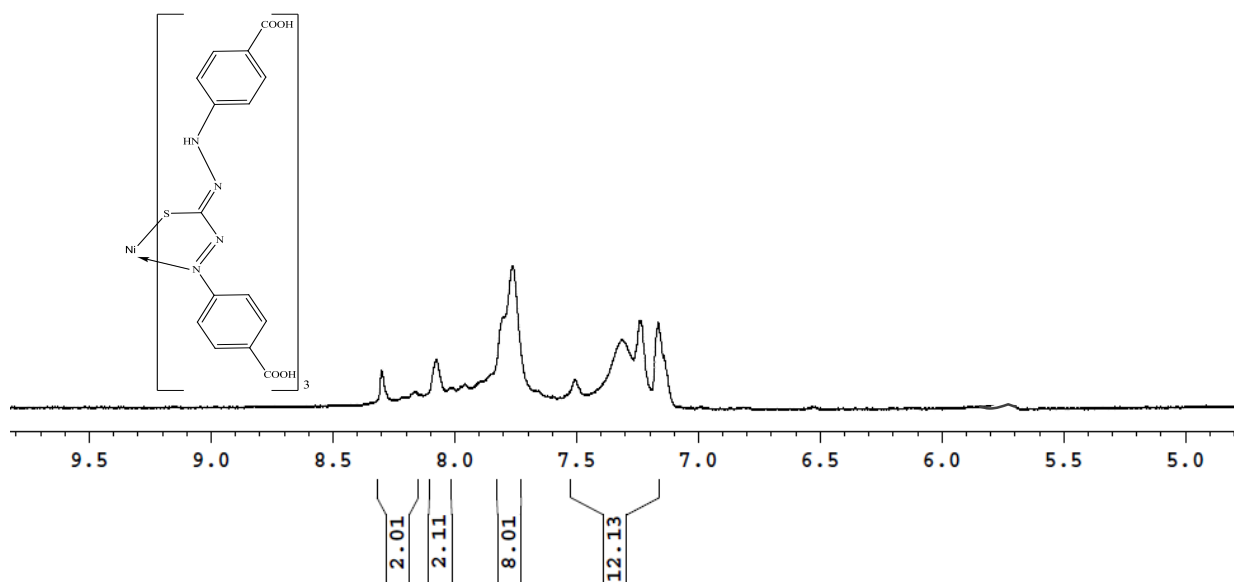


Figure 3.9. 1H NMR spectrum of *tris*-(*p*-COOH)dithizonatonickel(II). For the sake of clarity the structure is drawn as shown above.

3.2.2.6. *Bis*-dithizonatonickel(II)

H_2Dz (0.2519 g, 0.98 mmol) and nickel(II) sulphate hexahydrate, $NiSO_4 \cdot 6H_2O$, (0.1122 g, 0.41 mmol) were reacted.

$Ni(HDz)_2$: (0.2408 g, 86 %). M.p. 230 °C, UV-vis (acetone) λ_{max} 279, 456, 560 and 686 nm. δ_H (600 MHz, $DMSO-d_6$)/ppm: 6.3 – 7.4 (20H, Ar-H's, $2 \times C_6H_5$).

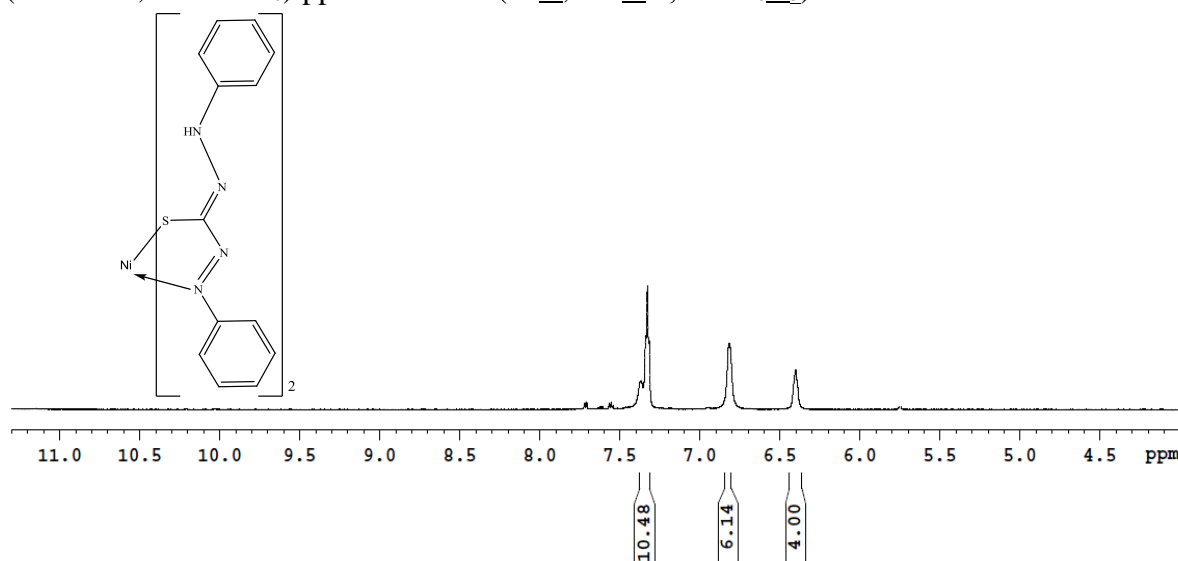


Figure 3.10. 1H NMR spectrum of *bis*-dithizonatonickel(II).

3.2.2.7. (*p*-COOH)dithizonatolead(II)

(*p*-COOH) H_2Dz (0.1533 g, 0.45 mmol) was dissolved in 0.1 M aqueous NH_4OH and reacted with lead(II) acetate trihydrate, $Pb(CH_3COO)_2 \cdot 3H_2O$, (0.1743 g, 0.46 mmol).

$Pb(p\text{-COOH-HDz})$: (0.1825 g, 74 %). M.p. > 360 °C, UV-vis (methanol) λ_{max} 300 and 507 nm. δ_H (600 MHz, $DMSO-d_6$)/ppm: 7.4 – 8.2 (8H, Ar-H's, $2 \times C_6H_4$), 10.3 (1H, s, $2 \times COOH$).

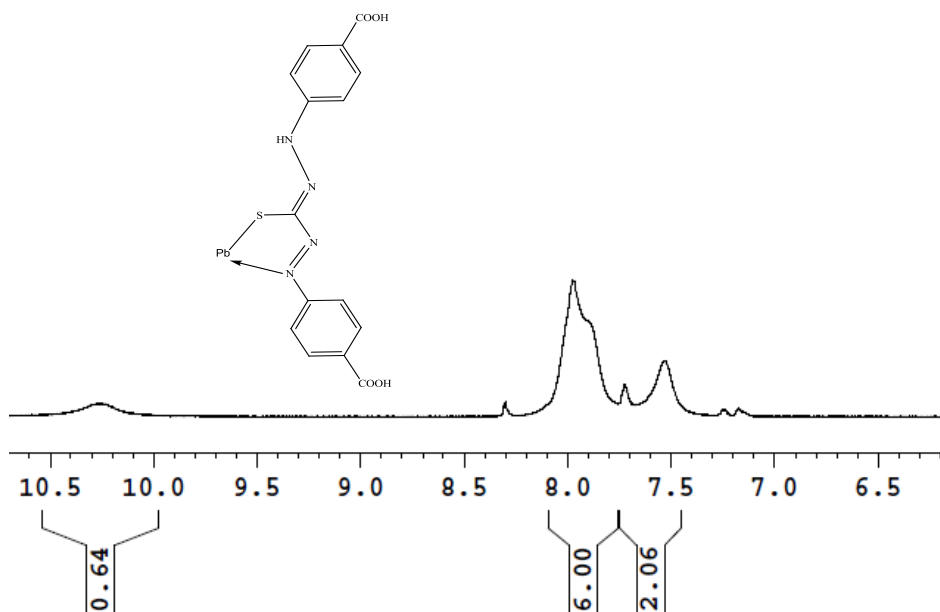


Figure 3.11. ¹H NMR spectrum of (*p*-COOH)dithizonatolead.

3.2.2.8. bis-dithizonatolead(II)

H_2Dz (0.1282 g, 0.50 mmol) was dissolved in 0.1 M aqueous NH_4OH and reacted with lead(II) acetate, $Pb(CH_3COO)_2 \cdot 3H_2O$, (0.0684 g, 0.26 mmol).

$Pb(HDz)_2$: (0.1454 g, 81 %). M.p. 210 °C, UV-vis (methanol) λ_{max} 257 and 505 nm. δ_H (600 MHz, $DMSO-d_6$)/ppm: 6.9 – 7.9 (20H, Ar-H's, $4 \times C_6H_5$), 10.00 (2H, s, $2 \times NH$).

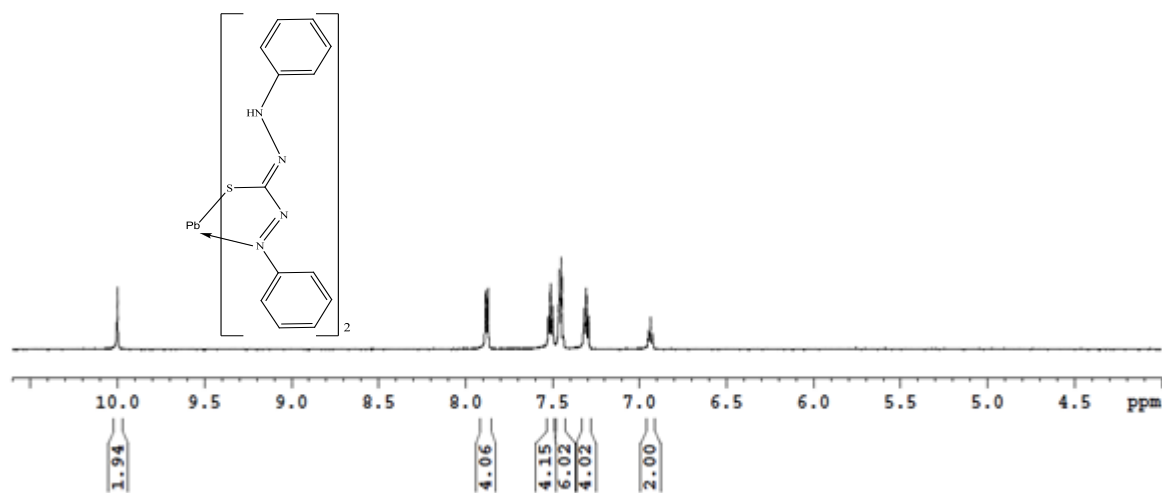


Figure 3.12. ¹H NMR spectrum of bis-dithizonatolead(II).

3.2.2.9. (*p*-COOH)dithizonatosilver(I)

(*p*-COOH) H_2Dz (0.1530 g, 0.45 mmol) was dissolved in 0.1 M aqueous NH_4OH and reacted with silver nitrate, $AgNO_3$, (0.0783 g, 0.46 mmol).

$Ag(p\text{-COOH-HDz})$: (0.1790 g, 88 %). M.p. 320 °C, UV-vis (methanol) λ_{max} 314 and 474 nm.

δ_H (600 MHz, $DMSO-d_6$)/ppm: 7.4 – 8.1 (8H, Ar-H's, $2 \times C_6H_4$), 11.07 (1H, s, $1 \times NH$), 12.6 (2H, s, $2 \times COOH$).

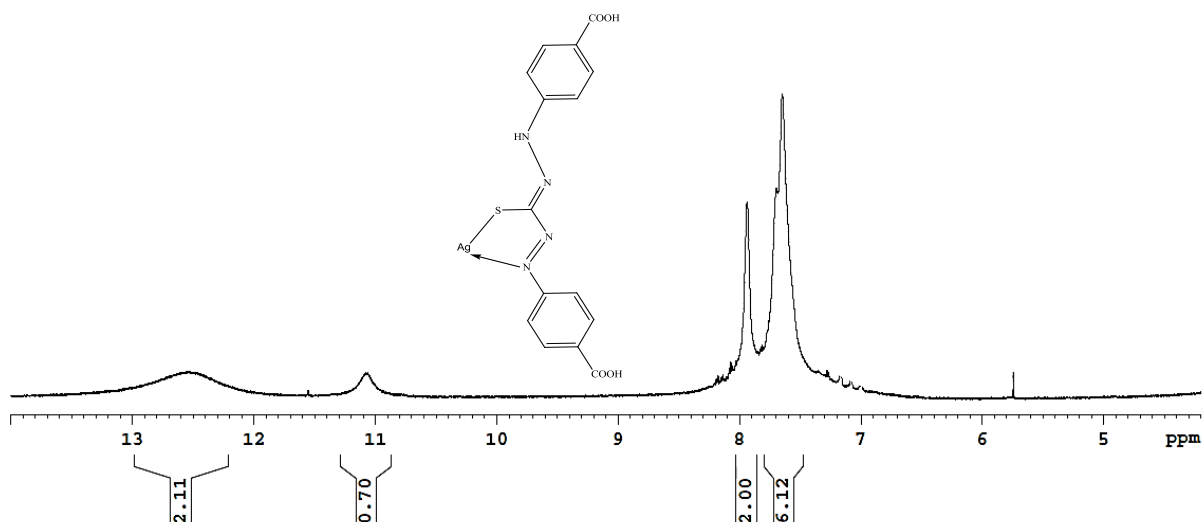


Figure 3.13. 1H NMR spectra of (*p*-COOH)dithizonatosilver(I).

3.2.2.10. Dithizonatosilver(I)

H_2Dz (0.1302 g, 0.5 mmol) and silver nitrate, $AgNO_3$, (0.0867 g, 0.51 mmol) were reacted.

Silverdithizonate: (0.1700 g, 94 %). M.p. 160 °C, UV-vis (methanol) λ_{max} 253 and 490 nm.

δ_H (600 MHz, $DMSO-d_6$)/ppm: 6.9 – 7.8 (10H, Ar-H's, $2 \times C_6H_5$), 10.38 (1H, s, $1 \times NH$).

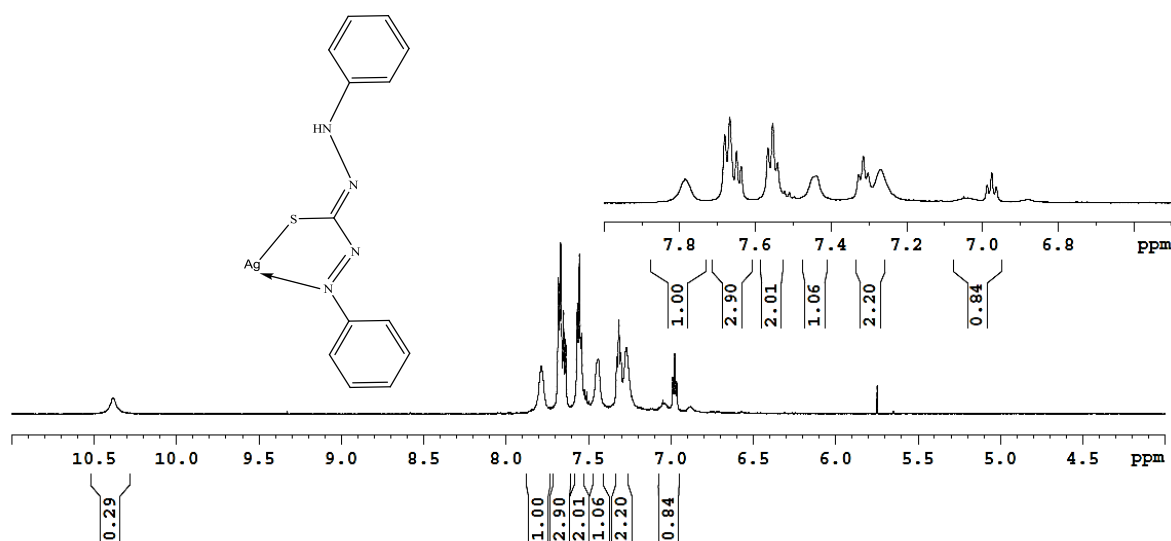


Figure 3.14. 1H NMR spectrum of dithizonato silver(I).

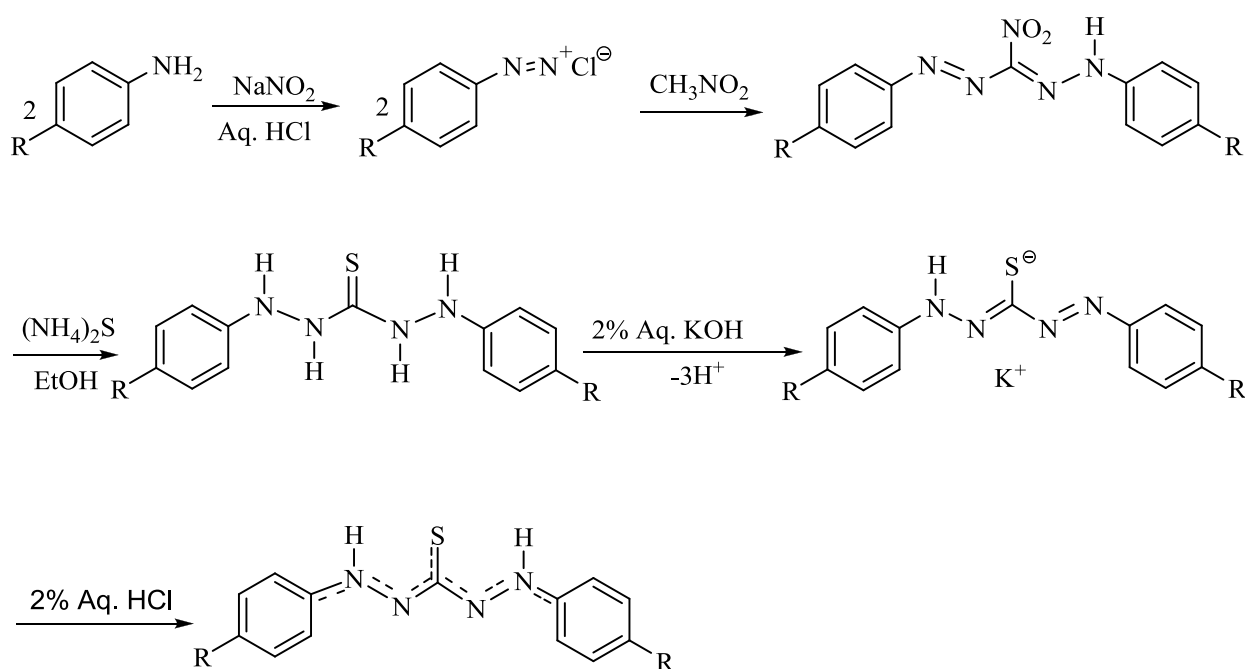
3.2.3. Discussion

3.2.3.1. Dithizone Derivatives

The main aim of this study was to synthesize dithizone derivatives, with symmetrically placed *para* substituents that enhance water-solubility. The synthesis method that was used was an adaption from that published method by Mirkhalaf *et al*¹¹⁷ - slightly modified to accommodate the aims of this study.

NITROFORMAZANS. The method begins with a water-soluble functionality *para*-substituted aniline dissolved in dilute acidic medium, followed by slow addition of sodium nitrite at sub-zero temperatures, forming a diazonium salt. Traditionally used volumes of aqueous acidic mixture of concentrated hydrochloric acid (15 mL) and water (25 mL) could be halved since these anilines are very soluble in water. However, it is worth mentioning that the altered ratios of aniline to sodium nitrite, nitromethane and also the volumes of acid and water mentioned in paragraph 3.2.1, gave best yields. Sodium nitrite has to be added slowly and in small portions to avoid temperature increase, because if the temperature exceeds 5 °C the diazonium salt usually does not form. This diazonium intermediate product is dirty white or yellowish white. Separately, in a large beaker an acidic buffer is prepared by addition of sodium acetate trihydrate to aqueous glacial acetic acid, stirring vigorously to prevent the formation of a hard solid mass. With the starting aqueous acidic mixture volume halved, the volumes and mass used to prepare the buffer solution is also halved, saving on chemicals. The diazonium solution is then added to the acidic buffer solution and stirred to homogeneity. It has been observed that if the reaction at the buffer step is kept below 20 °C, yields do increase. Nitromethane is added to couple the two diazonium molecules, forming a brick red precipitate. The slurry is then stirred for 3 hours to ensure reaction completion, with water periodically added since the slurry thickens over time. The mixture is filtered through a sintered glass funnel, equipped with filtering paper, because fine products sometimes pass through. An alternative is to re-filter the first 100 mL of the solution after bigger particles have already formed a layer that traps smaller particles. The brick-red or dark orange (in some compounds) nitroformazan precipitate is washed with copious amounts of cold water and dried at 60 °C in an oven overnight. All three compounds; the carboxylic acid, sulfanilic acid and sulfacetamide, were characterized and proved to be successful up to this step, with good yields ranging from 59 up to 94%. The latter two nitroformazan derivatives were also, and only successfully characterized up to this step, since follow-up steps failed. These compounds were not washed with water, because they are very soluble even in cold water. Alternatively the red precipitate was stirred in glacial acetic acid, ensuring all the excess salts are dissolved, then washed with cold ethanol upon filtration, to rid remaining precipitate of acetic acid.

¹¹⁷ F. Mirkhalaf, D. Whittaker, D. J. Schiffrin, *J. Electro. Anal. Chem.*, 203, 452 (1998).



Scheme 3.1. Synthesis of water-soluble dithizones. R = -COOH, SO₃H & SO₂NHCOCH₃.

¹H NMR spectrum of *p*-sulfonic acid-nitroformazan confirms the presence of the two phenyl rings in the nitroformazan compound, by the two peaks at 7.76 and 7.87 ppm each integrating for 4 aromatic protons. The imine proton is observed at 14.48 ppm, which is in agreement with NMR data published as part of crystallographic reports for other nitroformazans. The sulfacetamide nitroformazan is also confirmed, namely by the 6 methyl protons of the substituents at 1.95 ppm, and presence of the aromatic protons at 8.09 ppm integrating for 8 protons. The two substituent imine protons are at 12.21 ppm and that of the nitroformazan backbone at 14.03 ppm. The carboxylic acid nitroformazan has its aromatic protons at 8.3-7.4 ppm, integrating for 8 protons, with the carboxylic protons showing a broad peak at 13.2 ppm and the imine proton a sharp peak at 14.25 ppm.

DITHIZONES. The second step was to begin with the dried powder of the synthesized nitroformazan derivative dissolved in absolute ethanol. For best yields of dithizonone product it is important to make sure that nitroformazyl is well dissolved, and if necessary the temperature can be elevated to 30 °C, followed by reduction of the nitroformazan with the addition of 20 % ammonium sulphide, (NH₄)₂S, to produce the thiocarbazide, H₄Dz, intermediate product. (NH₄)₂S has to be added into a lightly stoppered Erlenmeyer flask and stirred in a fume hood to prevent the spreading of the foul smell. A large excess (6x) of (NH₄)₂S produces significantly increased yields. The observed colour change is from orange-red going to yellow, as the nitro group is exchanged for sulfur. Once this colour change is observed, the solution is placed on a cooling stirrer (*ca* 5 °C) for about 5 minutes, to promote precipitation. Traditionally, the solution

is poured on ice to promote precipitation, but ice would dissolve the water-soluble derivatives. The thiocarbazine, H_4Dz , solution is then filtered off by using a sintered glass funnel, after which 2% aqueous potassium hydroxide solution was used to dissolve and wash out the thiocarbazine, forming the oxidized orange-red potassium dithizonate salt, K^+HDz^- . During the former dissolution process the K^+HDz^- precipitate is to be stirred gently with a spatula, while it washes through the sintered glass funnel. To this K^+HDz^- solution, 5 °C cold 2 % aqueous hydrochloric acid is added to protonate and precipitate it as the green dithizone product, H_2Dz . However, the substituents are also affected by the addition of base and acid, i.e. altering between COO^-K^+ and $COOH$. Due to the very high solubilities of the *p*-sulfacetamide and *p*-sulfonic acid derivatives the dithizone product did not precipitate out. However, resulting green solutions were indicative of successfully synthesized products. Unfortunately the green solutions were not stable for long, after a while turning to a milky yellow colour. The same was observed with the use of other dilute acids like nitric and glacial acetic acid.

The (*p*-COOH)dithizone was successfully synthesized and characterized. The last purification acid base step was repeated five times. Initially the formed precipitate is very fine and may pass through the sintered glass funnel, thus a centrifuge was used. By repeating this acid base step it helps purify the required product and avoids the use of tedious silica column purifications. Finally, once the dried purified product is obtained, it is poured into warm DCM and washed twice (removing the top yellow band observed in the TLC plate, the product is insoluble in DCM). The product *p*-COOH- H_2Dz gave a good yield of 72% after purification.

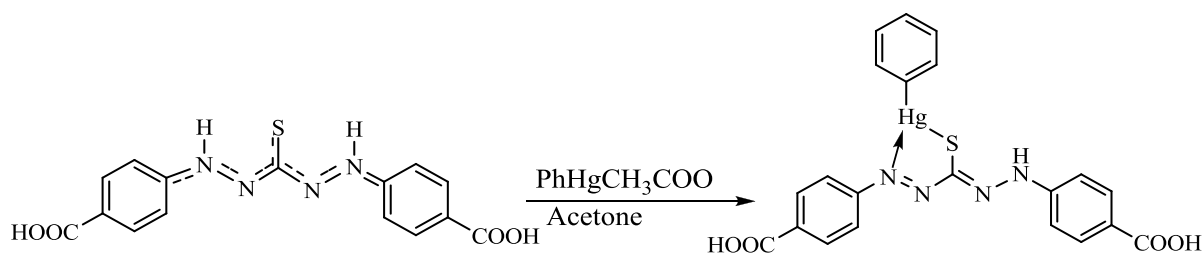
1H NMR spectrum of the carboxylic acid derivatives and complexes did not give good resolution, although being done on a 600 MHz instrument. This is ascribed to the many different isomers and/or tautomers that this particular compound may give rise to in solution. Additionally, proton exchange on/from hydroxy groups, as also present here, result in widened ill-defined peaks, as typically seen in the 1H NMR spectra of alcohols. The phenyl atoms are observed at 7.7 to 8.1 ppm, while those of the two carboxylic hydroxy groups are suspected to be the small peaks at 9.8 and 10.2 ppm.

3.2.3.2. Metal Dithizonates

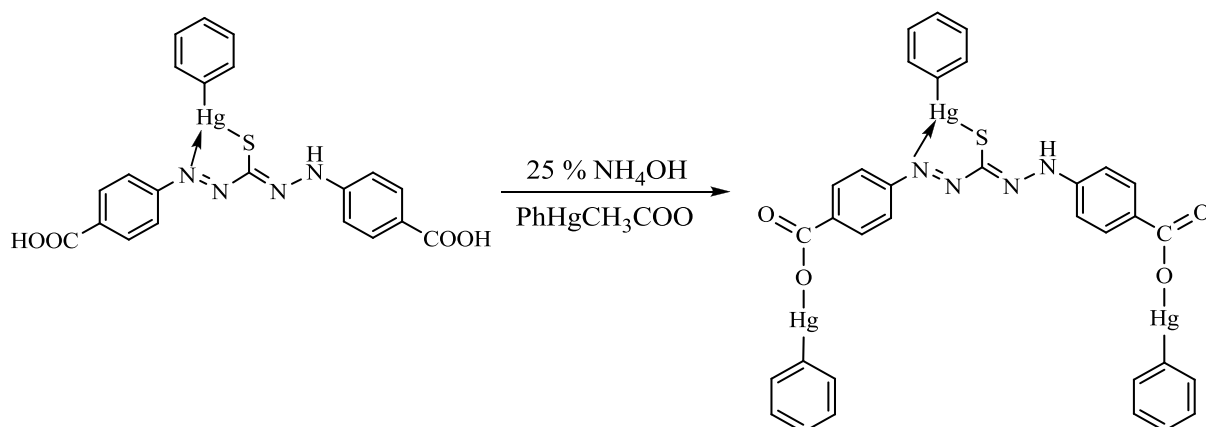
The synthesis of metal dithizonates ensued with the complexation of *p*-COOH- H_2Dz with mercury. This complexation was done as reported by Von Eschwege *et al.*,¹¹⁸ but without addition of base. *p*-COOH- H_2Dz was dissolved in acetone and the temperature elevated to 30 °C to improve solubility. Phenyl mercury acetate was added in a ratio of *ca* 1:1 with the ligand. The solution immediately turned from green to red, indicating that the reaction was taking place and

¹¹⁸ K. G. von Eschwege, J. Conradie, J. C. Swarts, *J. Phys. Chem. A*, 221, **112** (2008).

no base being required to deprotonate the dithizone derivative. After an hour of stirring, acetone was removed under reduced pressure. When there was about one quarter volume of acetone remaining, water was added to keep the acetates (from phenyl mercury acetate) in solution, but precipitate the required product. Then finally all the remaining acetone was evaporated and the solution was filtered and washed with warm water to dissolve all unreacted material. After drying the product, $\text{PhHg}(p\text{-COOH-HDz})$, it was characterized spectroscopically. The product was dark-red and photochromic in THF and diethyl ether.



Scheme 3.2. Formation of phenyl mercury(II) dithizonate derivative, $\text{PhHg}(p\text{-COOH-HDz})$.



Scheme 3.2. Formation of phenyl mercury(II) dithizonate derivative, $\text{PhHg}(p\text{-COOPhHg-HDz})$.

Furthermore, $\text{PhHg}(p\text{-COOH-HDz})$ was dissolved in methanol, deprotonated with 25% NH_4OH and reacted with phenyl mercury at the ratio of *ca* 2:1 with $\text{PhHg}(p\text{-COOH-HDz})$. The purification method was the same as that of the first complex. The product, $\text{PhHg}(p\text{-COOPhHg-HDz})$, was obtained with two phenyl mercury moieties attached to the two $-\text{COO}^-$ substituents of the dithizone ligand. This was confirmed by means of ^1H NMR spectroscopy, i.e. the carboxylic proton peak at 11.0 ppm disappeared, while the two additional phenyls' proton signals appeared. The reason for having done this reaction, was for testing the metal to ligand ratio in employing this new ligand, as it may be relevant in future metal analyses. In most complexation reactions the metal to ligand ratio is 1 : X, where $X \geq 1$. However, in this fairly unique case, the M : L ratio is the other way around, namely 3 : 1. In event of using Hg(II) acetate instead of PhHg(II) acetate, a polymerization reaction is expected, as one metal will ligate two dithizonates,

and four additional metals are to form intermolecular bridges between the four complex carboxylic substituents and those of neighboring complexes. As opposed to the previous *mono*-Hg complex there was no sign of photochromic PhHg(*p*-COOPhHg-HDz). This product is dark purple-blue in colour and soluble in non-polar organic solvents like DCM.

The PhHg(*p*-COOH-HDz) complex has λ_{max} at 293 and 485 nm, while PhHg(*p*-COOPhHg-HDz) complex is slightly redshifted to λ_{max} 296 and 500 nm, see Figure 3.15. Such redshifts are typical for more electron rich mercury dithizonate species.¹¹⁹

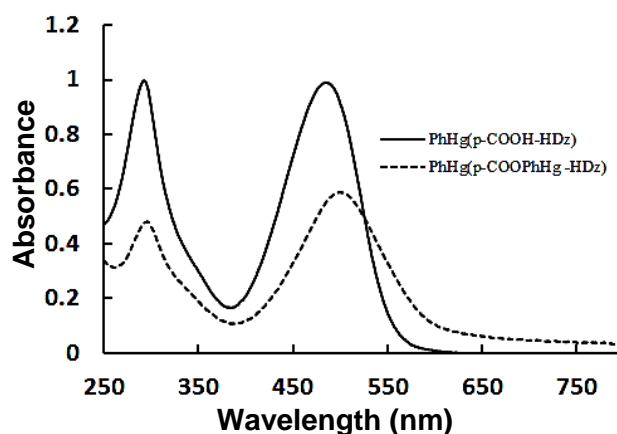
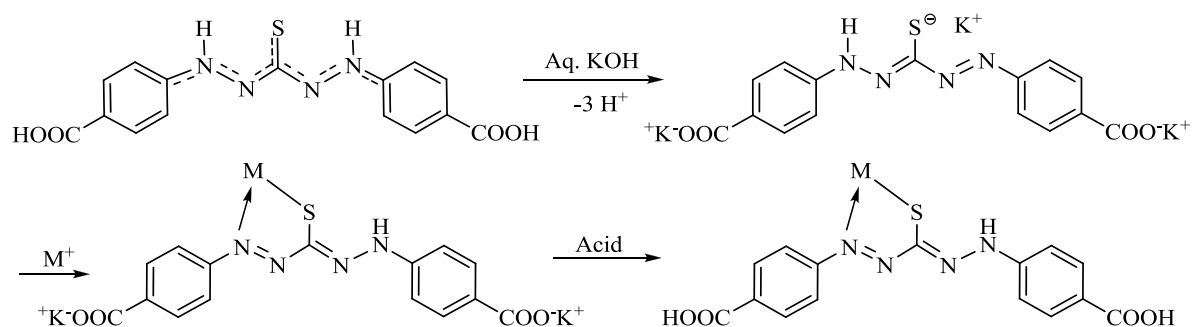


Figure 3.15. UV-vis spectra of PhHg(*p*-COOH-HDz) and PhHg(*p*-COOPhHg-HDz).

Henceforth will be discussed the metal dithizonate complexes forming the basis for spectrophotometric mole ratio and continues variation method studies reported on in Section 3.4. Dithizonate complexes with spectral properties suitable for determinations of this kind include only the metals; Co, Ni, Pb and Ag. These complexations were done in aqueous alkali medium.¹²⁰ Addition of metal salts change the colour of the orange-red *p*-COO⁻-HDz⁻ solution to dark purple when CoCl₂·6H₂O, blue-green when NiSO₄·6H₂O, and orange-red when Pb(CH₃COO)₂·3H₂O or AgNO₃ is added. After complexation glacial acetic acid is added to reprotonate the -COO⁻ anionic substituents. Stronger acids would cause reprotonation and precipitate out the liberated H₂Dz instead of its metal dithizonate. When complexing metals with H₂Dz, organic solvents were traditionally used to extract metal complexes. The difference here is that upon deprotonation H₂Dz only loses the imine proton, i.e. the proton that is replaced by a metal atom. In event of using *p*-COOH-H₂Dz, both the imine proton and the two acid protons are removed. A weak acid may be used to reprotonate the carboxylic acid groups after a metal is coordinated only at the traditional N,S ligand positions. Metal complexes formed from this acid derivative are insoluble in non-polar organic solvents. Scheme 3.3 illustrates the reaction.

¹¹⁹ K. G. von Eschwege, *J. Photochem. and Photobiology A: Chem.*, 159, **252** (2013).

¹²⁰ Part of the motivation for developing this water-soluble reagent and methods, is to introduce new alternatives to Job's method, etc., that will also be inexpensive and repeatable, and in aqueous medium, as opposed to costly organic media. These properties provide the option to utilize both the reagents and methods for training undergraduate students.



Scheme 3.3. Water-soluble metal dithizonate complexation. M – metal. For simplicity sake only one ligand is shown.

The nickel complex gave a stoichiometry of 1:2 when reacted with H_2Dz , forming $\text{Ni}(\text{HDz})_2$, which is in agreement with mass spectroscopy (see Figure 3.16) and crystal data.¹²¹ From the mass spectroscopy (MS) the molecular ion peak is observed at 569.5 (m/z , Da) which confirms the molar mass of two dithizonate ligands coordinated to a nickel atom, $\text{Ni}(\text{HDz})_2$, with a theoretical molar mass of 569.34 g/mol.

Contrary to expectation Ni-complexation with the $p\text{-COOH-H}_2\text{Dz}$ ligand resulted in a stoichiometric ratio of 1:3, i.e. $\text{Ni}(p\text{-COOH-HDz})_3$, as per the two spectrophotometric methods to be discussed in Section 3.4. The question here was if this increase in coordination number reveals an increase in oxidation number, from Ni^{II} to Ni^{III} , as is the case for $\text{Co}(\text{HDz})_3$, which auto-oxidizes from Co^{II} to Co^{III} during reaction with dithizone?¹²² ^1H NMR and MS were done to find independent evidence for this observation. From NMR data, the larger coordination number was not accompanied by an increase in oxidation number, from Ni^{II} to Ni^{III} . Since both complexes yielded signals at the same expected standard chemical shift values, ^1H NMR data indicates that both the $\text{Ni}(\text{HDz})_2$ and $\text{Ni}(p\text{-COOH-HDz})_3$ complexes are diamagnetic and thus of similar oxidation states, Ni^{II} . If the latter complex would have been Ni^{III} , then it would have been paramagnetic, with consequence that the H-signals would have shifted to way different and unexpected positions, as is typical for paramagnetic compounds. Oxidation state III is in general highly uncommon for nickel. The unaltered oxidation state therefore would not require an additional anion to balance the metal cationic charge. It is hence hypothesized that in the latter complex the 3rd ($p\text{-COOH-H}_2\text{Dz}$) ligand coordinate to Ni without loss of its imine proton, as is the case with other neutral ligands like phenanthroline, etc. This is possible, since ($p\text{-COOH-H}_2\text{Dz}$) may also coordinate through any or both of the $-\text{COOH}$ substituents. Additional experimental evidence for the *tris*-coordinated complex comes from mass spectrometry data (see

¹²¹ M. Laing, P. Sommerville, P. A. Aslop, *J. Chem. Soc. (A)*, 1247 (1971).

¹²² K. G. von Eschwege, L. van As, C. C. Joubert, J. C. Swarts, M. A. S. Aquino, T. S. Cameron, *Electrochimica Acta.*, 747, **112** (2013).

Figure 3.17), revealing the molecular ion peak (1088.5 m/z, Da), precisely as theoretically calculated (1088.71 g/mol). The peak at 743.9 (m/z, Da) is that of $\text{Ni}(p\text{-COOH-HDz})_2 = 745.37$ g/mol, with one proton removed. From this it is derived that the third ligand is only very loosely bound, which is understandable, since the oxidation state is not increased from II to III and therefore not increasing bond strength with the 3rd ligand. Lastly, the peak at 343.2 corresponds to the mass of a free ligand, $(p\text{-COO}^-)\text{-HDz}^- = 343.34$ g/mol.

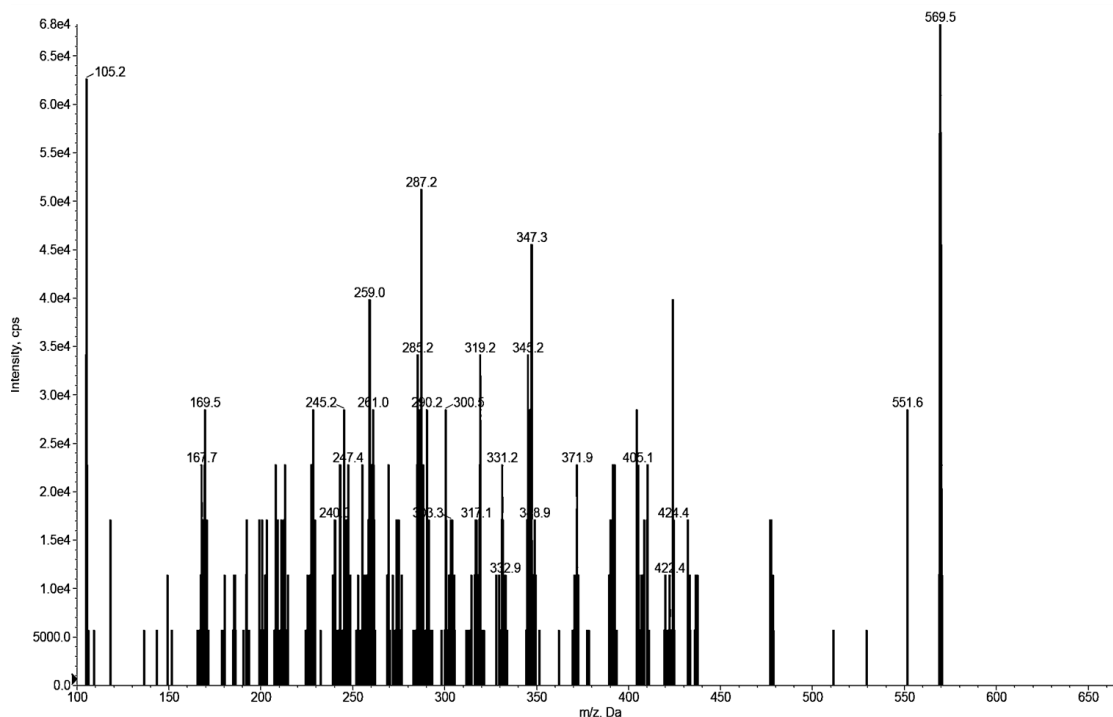


Figure 3.16. Mass spectrum of $\text{Ni}(\text{HDz})_2$.

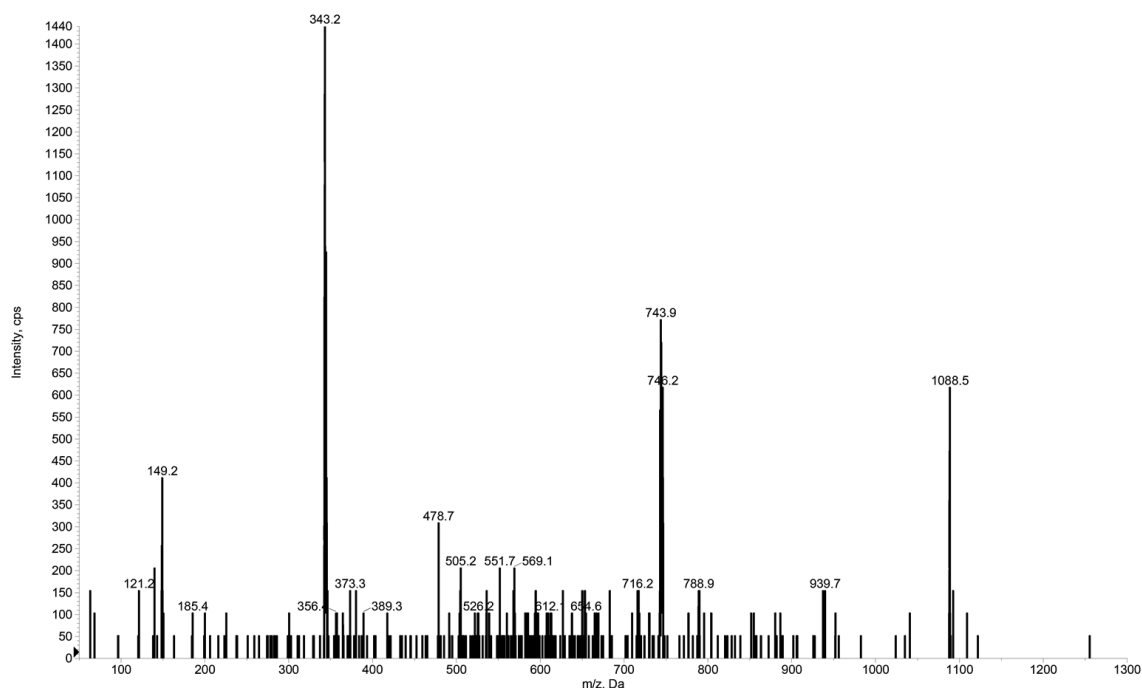


Figure 3.17. Mass spectrum of $\text{Ni}(p\text{-COOH-HDz})_3$.

Math and Freiser¹²³ reported structural changes in nickel dithizonate upon adduct formation giving rise to spectral changes in the UV-vis spectra. The spectrum of nickel dithizonate is very different to those of other metal dithizonates (Hg, Pb, Zn, etc), since it extraordinarily has four absorption bands in the visible region. This report illustrates how the absorption band at longest wavelength (above 520 nm) collapses upon addition of pyridine or other N-bases, causing the nickel dithizonate spectrum to resemble the spectra of other metal dithizonates. Similar behaviour is reported for other sulfur-containing ligands (di-*p*-tolylthiocarbazonate, di-2-naphthylthiocarbazonate and 8-mercaptoquinoline) that were tested for adduct formation. These observations are to be seen in comparison with the UV-vis spectra of our Ni(HDz)₂ and Ni(*p*-COOH-HDz)₃ complexes, see Figure 3.18 (left).

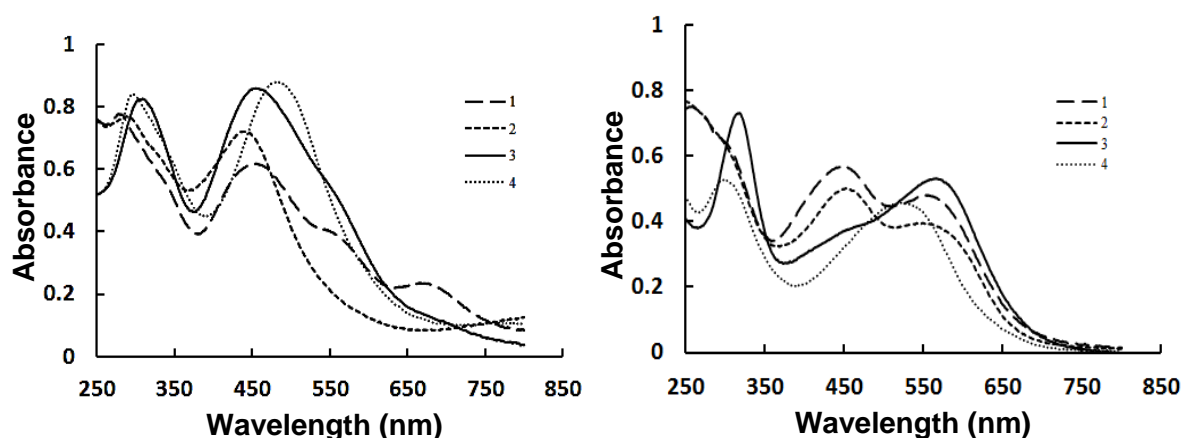


Figure 3.18. Nickel dithizonate UV-vis spectra in methanol (left) and cobalt dithizonate in the same solvent. Where 1 – Ni(HDz)₂, 2 – Ni(HDz)₂ + NH₃, 3 – Ni(*p*-COOH-HDz)₃, 4 – Ni(*p*-COOH-HDz)₃ + NH₃, the same for cobalt dithizonate.

The UV-vis spectra of the two Ni complexes were obtained with methanol as solvent. Ni(HDz)₂ has the 4-band absorption (279, 456, 560, 686 nm), while in Ni(*p*-COOH-HDz)₃ the long wavelength bands are seen to collapse completely (686 nm) or partially (560 nm). The low energy band collapsed as a consequence of the Ni(HDz)₂ square planar geometry transforming to trigonal bipyramidal or octahedral due to ligation of additional ligand(s). This long wavelength corresponds to the low energy absorption of the elongated HOMO orbital stretching along the entire length of the complex. The Ni(*p*-COOH-HDz)₃ 565 nm shoulder that coincides with the absorption band at 560 nm of the Ni(HDz)₂ could mean that there is still space for additional adduct formation in the Ni(*p*-COOH-HDz)₃ complex. This was tested by addition of NH₃ adduct; the shoulder did indeed disappear. The main visible region absorption bands for both these nickel dithizonates are shifted in opposite direction during adduct formation. For Ni(HDz)₂ a blue-shift is observed from 456 to 438 nm and that of Ni(*p*-COOH-HDz)₃ is red-shifted from 458 to

¹²³ K. S. Math, H. Freiser, *Anal. Chem.*, 1969, **41** (1969).

480 nm on addition of NH_3 . The adducts for the two nickel dithizonates were obtained by adding 1 mL of 25% NH_4OH in 25.0 mL volumetric flask to each, and diluting with methanol.

The spectra of the *tris*-coordinated cobalt dithizonate complex (see Figure 3.18, right), that have two absorption bands, show no significant change or absorption band collapse due to adduct formation in the presence of NH_3 . Some spectral shift is seen during addition of the base to the carboxylic acid derivative. This must be ascribed to significant change in electronic properties on the three coordinated ligands, due to deprotonation of $-\text{COOH}$ substituents and consequent salt formation.

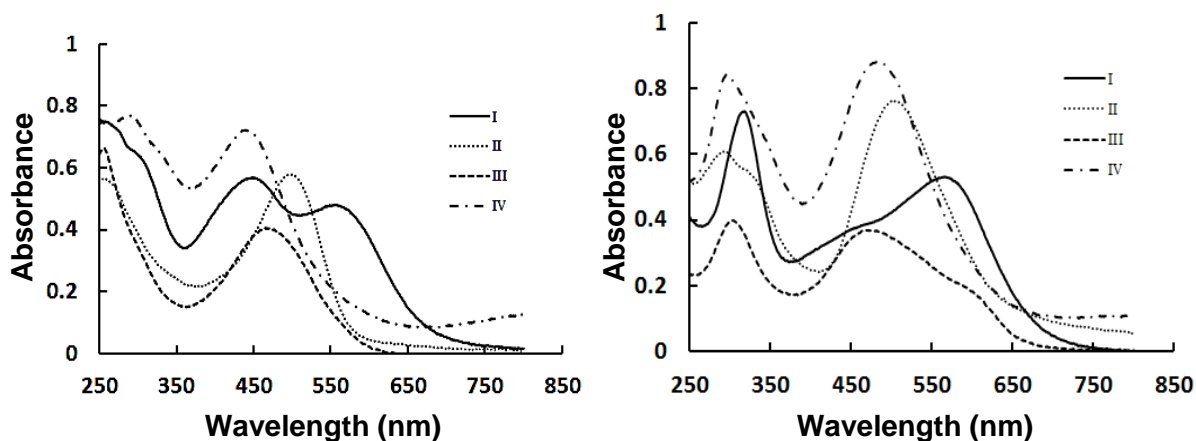


Figure 3.19. Comparative UV-vis spectra of all metal (Co, Ni, Pb and Ag)HDz (left) and *p*-COOH-HDz complexes (right) in methanol. I – $\text{Co}(\text{HDz})_3$, II – $\text{Pb}(\text{HDz})_2$, III – $\text{Ag}(\text{HDz})$, IV – $\text{Ni}(\text{HDz})_2 + \text{NH}_3$ and the same for *p*-COOH-HDz complexes (right).

UV-vis spectra of $\text{Co}(\text{HDz})_3$ revealed that there may be some reaction between the complex and methanol, as the absorption maximum is initially only at 550 nm. After some time a second maximum appeared at 450 nm. It remains unclear is to what reaction takes place, but may be ascribed to some form of chronochromism, related to what is reported in Section 3.5.7, at the end of this chapter. The change in spectra over time is illustrated in Figure 3.20.

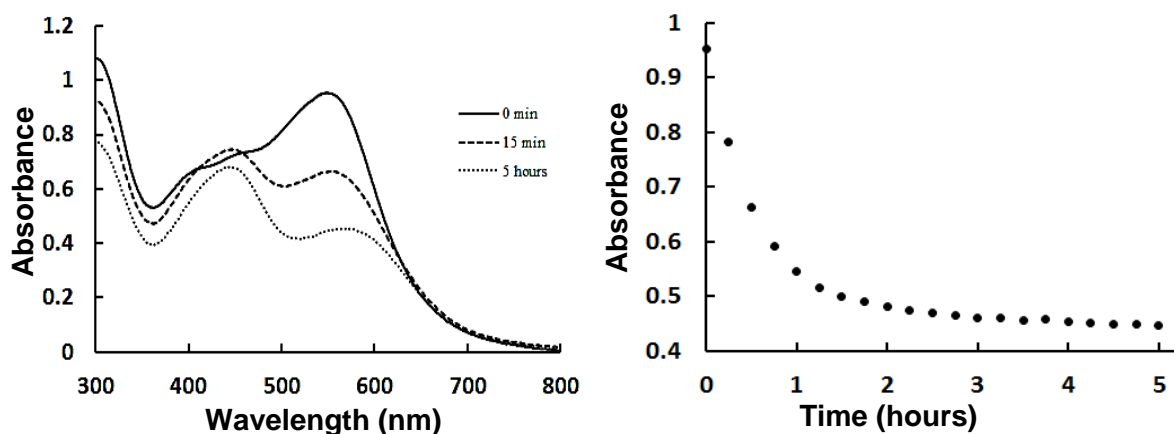


Figure 3.20. UV-vis spectra of $\text{Co}(\text{HDz})_3$ at 0 min, 15 min and 5 hours (left) and decay of λ_{max} 550 nm in methanol.

Also the lead carboxylic acid dithizonate complex (1:1) is an unexpected different stoichiometry to the unsubstituted dithizonate complex (1:2). Spectrophotometric methods in Section 3.4 gives evidence that Pb coordinates 1:1 with the carboxylic dithizonate, yielding $\text{Pb}(p\text{-COOH-HDz})$. MS fails to confirm these results, neither being indicative of either 1:1, 1:2 or 1:3 complexes. This may possibly be ascribed to dissociation during the MS ionization process. The spectrophotometric tests (Section 3.4) may however be trusted by extrapolation simply because the coordination ratio's of other metal dithizonates (Ni, Co, Ag) are proven to be correct, also by other means of characterisation. All other metal dithizonates (Co, Ag) gave the same coordination number, i.e. $\text{Co}(\text{HDz})_3$ and $\text{Co}(p\text{-COOH-HDz})_3$ and also $\text{Ag}(\text{HDz})$ and $\text{Ag}(p\text{-COOH-HDz})$, with their ^1H NMR yielding the expected number of aromatic protons.

3.3. X-Ray Crystallography

3.3.1 *p*-COOH(nitroformazan) crystal

For characterization and confirmation of the geometry and structure of the synthesized water-soluble derivatives of nitroformazan, dithizone, dithizinonatonphenylmercury and the other metal dithizonate complexes, sizeable crystals for single crystal X-ray were attempted to be grown. Out of all these compounds only the two nitroformazan derivatives, namely (*p*-sulfonylacetamide)nitroformazan and (*p*-COOH)nitroformazan, gave single crystals that were large enough to be characterized. Only crystal data of the latter was of good quality.

Before attempting to grow these crystals it has been observed that crystal quality improved when the nitroformazan derivatives were first washed with warm DCM and dried. The crystals were obtained in acetone overlaid with *n*-hexanes in a 1:1 ratio, at room temperature, but for (*p*-sulfonylacetamide)nitroformazan an additional two drops of methanol were required. However the crystals of these compounds did tend to decompose rapidly once they were out of solvent. This was prevented by adding more *n*-hexanes once the crystals have formed and the acetone level was very low.

The intensity data was collected on a Bruker X8 Apex II 4K Kappa CCD diffractometer equipped with graphite monochromated $\text{Mo } K\alpha$ radiation, at a wavelength of 0.71073 Å; with both ω - and ϕ -scans at 100 K. All the cell refinements were performed with SAINT-Plus¹²⁴ and the data reduction was done with SAINT-Plus and XPREP. The software package SADABS¹²⁵ that utilizes the Sheldrick multi-scan technique was used to apply absorption corrections. All the

¹²⁴ Bruker, SAINT-Plus, Version 7.12 (including XPREP), Bruker AXS Inc., Madison, Wisconsin, USA, (2004).

¹²⁵ Bruker, SADABS, Version 2004/1, Bruker AXS Inc., Madison, Wisconsin, USA, (1998).

structures were solved with the use of the SIR-97¹²⁶ package. Refinement was done with SHELXL-97¹²⁷ and WinGX¹²⁸ and the molecular graphics were completed with DIAMOND¹²⁹ and MERCURY.¹³⁰ All the structures are shown with thermal ellipsoids drawn at a 50% probability level and all non-hydrogen atoms were anisotropically refined, unless stated otherwise. Methyl, methylene, methine and aromatic hydrogen atoms were placed in geometrically idealized positions, C-H = 0.95 to 1.00 Å, and were constrained to ride on parent atoms, $U_{\text{iso}}(\text{H}) = 1.5 U_{\text{eq}}(\text{C})$ and $1.2 U_{\text{eq}}(\text{C})$

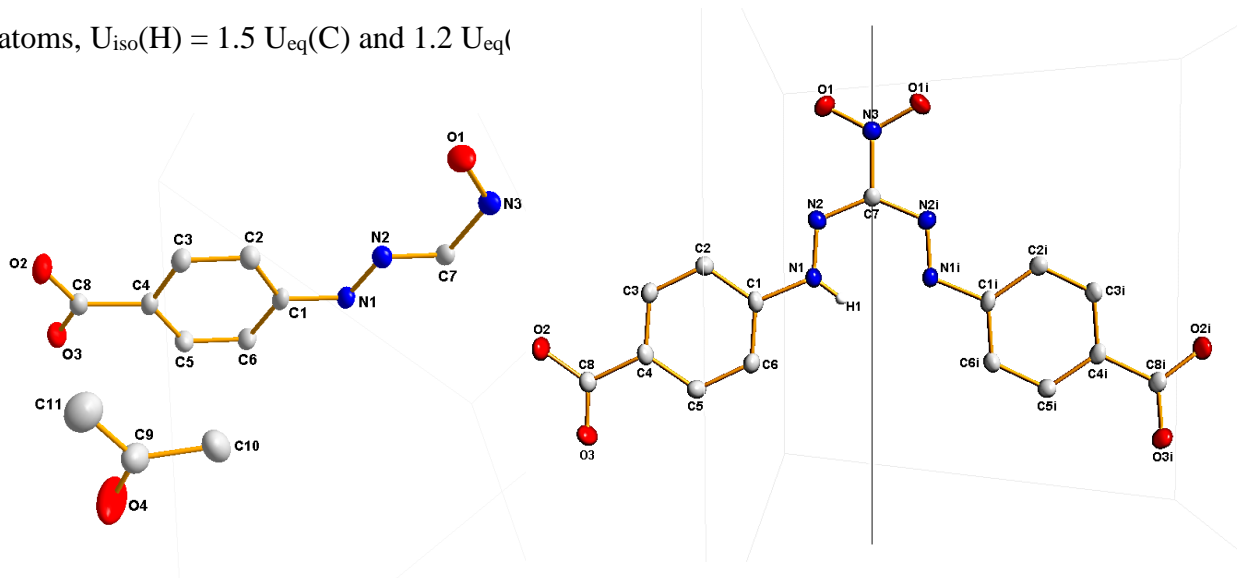


Figure 3.21. Illustration of the molecular structure of (*p*-COOH)nitroformazan in an asymmetric unit cell (left) and a full symmetry generated structure (right). Displacement ellipsoids are drawn at 50 % probability. Hydrogen atoms are omitted for clarity and the atoms of the symmetrically generated half are denoted by *i*. Displacement ellipsoids are drawn at 50 % probability.

The structure of (*p*-COOH)nitroformazan is shown in Figure 3.21(right) and corresponds to the schematic structure presented in Figure 3.1. The nitroformazan structure has a bent geometry and symmetrical in the solid state. The symmetry plane cuts through N3 and C7 which results in half (0.5) site occupancy factor's (SOF's) in the asymmetric unit cell. The symmetry plane also cuts through the H1 atom, which is arguably in between the N1 and N1*i* atoms. The induced symmetry results in electron density delocalization around the N1, N2, C7, N2*i*, N1*i* and H1 atoms mimics a resonance hybrid structure of a distorted 6-membered ring. The asymmetric unit

¹²⁶ A. Altomare, M. C. Burla, M. Camalli, G. L. Cascarano, C. Giacovazzo, A. Guagliardi, A. G. G. Moliterni, G. Polidori, R. Spagna, *J. Appl. Cryst.*, , 837, **32** (1999).

¹²⁷ G. M. Sheldrick, *SHELXL97*, Program for the refinement of crystal structures, University of Göttingen, Germany (1997).

¹²⁸ L. J. Farrugia, *J. Appl. Cryst.*, 837, 32 (1999).

¹²⁹ K. Brandenburg, H. Putz, *DIAMOND*, Release 3.0c, Crystal Impact GbR, Bonn, Germany (2008).

¹³⁰ I. Buno, J. A. Chisholm, P. R. Edgington, P. McCabe, E. Pidcock, L. Rodriguez-Monge, R. Taylor, J. van de Streek, P. A. Wood, *J. Appl. Cryst.*, , 466, 41 (2008).

contains half of the molecule, whereas the other half is symmetry generated, with one complete acetone molecule, see Figure 3.21(left). The complex crystallizes in a monoclinic crystal system in the $C2/c$ space group, with four formula units per unit cell ($Z = 4$).

Table 3.1. Crystal data and refinement parameters of (*p*-COOH)nitroformazan and structure.

	(<i>p</i>-COOH)nitroformazan
Empirical formula	$C_{10.5}H_{12}N_{2.5}O_4$
Formula weight	237.23
Temperature	100 K
Crystal system	monoclinic
Space group	$C2/c$
	$a = 17.797(3) \text{ \AA}$
	$b = 11.6932(16) \text{ \AA}$
	$c = 12.674(3) \text{ \AA}$
	$\alpha = 90^\circ$
	$\beta = 120.719(4)^\circ$
	$\gamma = 90^\circ$
Volume	$2267.4(8) \text{ \AA}^3$
Z	8
Density (calculated) ρ_{calc}	1.390 mg/mm^3
Absorption coefficient	0.108 m/mm^{-1}
F(000)	996.0
Crystal size	$0.581 \times 0.187 \times 0.066 \text{ mm}^3$
Radiation	Mo ($\lambda = 0.71073$)
2 Theta range for data collection	7.91 to 56°
Index ranges	$-23 \leq h \leq 23, -15 \leq k \leq 15, -16 \leq l \leq 12$
Reflections collected	27223
Independent reflections	2725[R(int) = 0.0430]
Data/restraints/parameters	2725/0/169
Goodness-of-fit on F^2	1.024
Final R indexes [$I \geq 2\sigma(I)$]	$R_1 = 0.0444, wR_2 = 0.1182$
Final R indexes [all data]	$R_1 = 0.0659, wR_2 = 0.1359$
Largest diff. peak/hole / $e \text{ \AA}^{-3}$	0.31/-0.29

The compound above exhibits potential multi-dentate ligand characteristics, with three possible bonding sites: carboxyl- and nitro-oxygen's as donors. The oxygen donor atoms from the nitro-group shows typical ambidentate-like behaviour. The equal bond distances of N3...O1 {1.223 (15) Å} and N3...O1i {1.223 (15) Å} suggests rather equal dipole moment inducing a hybrid resonance around the nitro group which is likely to break symmetry should there be any coordination of some sort at either O1 or O1i.

Table 3.2. Selected Bond angles and bond distances of (*p*-COOH)nitroformazan and structure.

Bond Types	Distance (Å)	Bond Types	Angles (°)
C7 - N2	1.339 (14)	C1 - N1 - N2	116.245 (118)
C7 - N2i	1.339 (14)		
N1 - N2	1.289 (17)	C1i - N1i - N2i	116.245 (118)
N1i - N2i	1.289 (17)		
C1 - N1	1.414 (18)	N1 - C1 - C6	116.505 (123)
C1i - N1i	1.414 (18)		
C1 - C2	1.394 (20)	N1i - C1i - C6i	116.505 (123)
C1i - C2i	1.394 (20)		
C1 - C6	1.391 (20)	N2 - C7 - N21i	134.353 (68)
C1i - C6i	1.391 (20)		

Two inter-molecular interactions of N—H...N and O—H...O are seen in (*p*-COOH)-nitroformazan, stabilizing the crystal as indicated in Table 3.3 and Figures 3.22 to 3.24.

Table 3.3. Observed N—H...N and O—H...O hydrogen bonding in L1.

Donor --- H...Acceptor	D - H (Å)	D...A (Å)	D - H...A (°)
N(1) --H(1) ..N(1) #1	0.78(3)	2.6361(18)	129(3)
N(1) --H(1) ..N(2) #1	0.78(3)	2.8584(18)	100(3)
O(2) --H(2) ..O(3) #2	1.21(3)	2.6161(16)	177(3)

Symmetry codes: #1 : -x+1,+y,-z+1/2; #2 : -x+1/2,-y+1/2,-z-1.

The organic framework, which lacks any metal atom coordinated to it, is tied up by several molecular hydrogen bonds, as observed in Figure 3.22 below. There are both intra- and inter-molecular interactions with no π - π stacking observed. The packing of the ligand is affected by the hydrogen bonding between the neighbouring symmetry generated molecules, forming sinusoidal shapes with distinct voids between molecules as viewed along the *c*-axis.

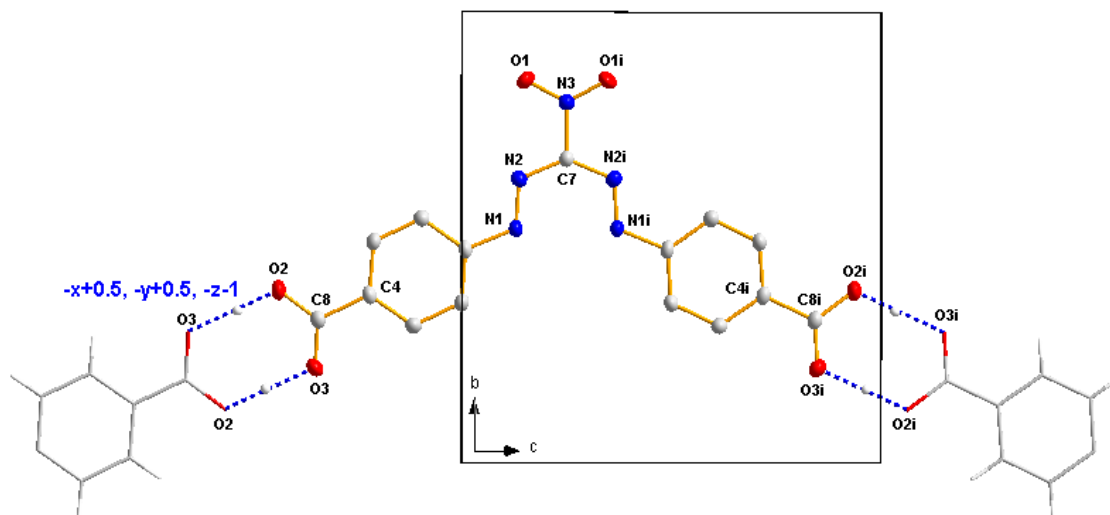


Figure 3.22. Illustration of hydrogen bonding in *(p*-COOH)nitroformazan. Hydrogen atoms are omitted for clarity.

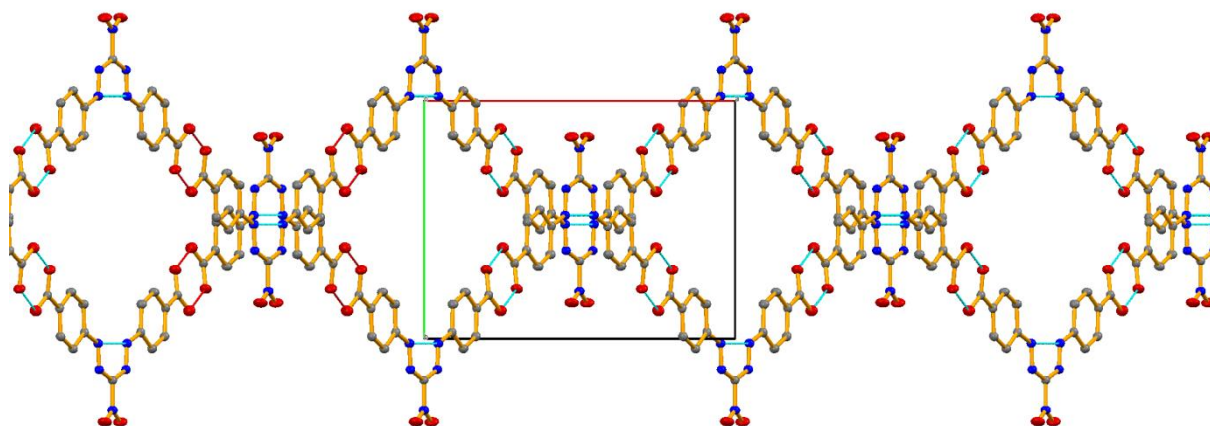


Figure 3.23. C-axis view of *(p*-COOH)nitroformazan, to illustrate alternating type of packing. Hydrogen's are omitted for clarity.

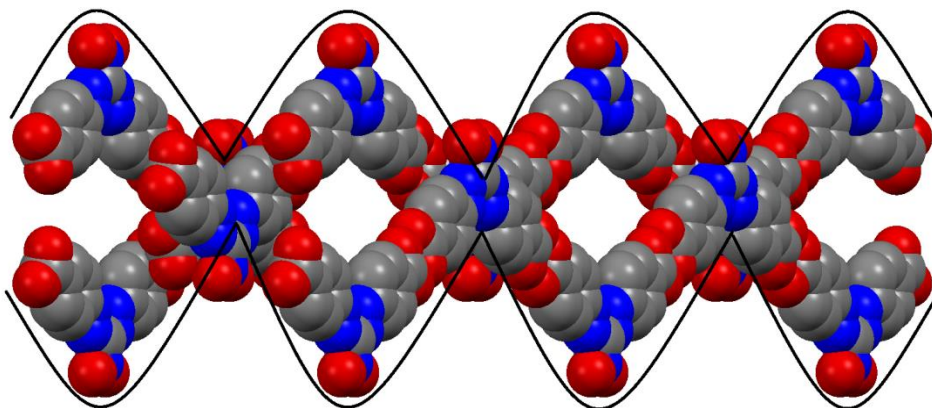
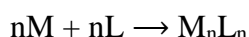


Figure 3.24. Space-fill view of *(p*-COOH)nitroformazan along the *c*-axis. Hydrogen's are omitted for clarity.

3.4. Spectrometric Determination of Complexes

3.4.1. Mole Ratio Method

The mole ratio method determines the stoichiometry of metal complexes from the plot of absorbance against mole ratio of the reactants. A series of ligand solutions with varied analytical concentrations are prepared, while the metal solution concentration is kept constant. The stoichiometry of a complex is determined at the endpoint of what may also in this case be called a spectrophotometric titration (see Figure 3.25), using the following equations:



Where M is the metal cation and L is the ligand used:

$$n_M = C_M \times V_M \text{ and } n_L = C_L \times V_L$$

given that,

$$C_M = C_L$$

then,

$$n_M : n_L \equiv V_M : V_L$$

n is the number of moles, C is the concentration, V_M is the volume, M and L denotes the metal and ligand respectively.

The aim here is to analytically determine the stoichiometry of particularly dithizonato metal complexes in aqueous medium. Since dithizone is not soluble in aqueous medium, but readily dissolves in aqueous alkali, two bases, KOH and NH_4OH , were used to dissolve the unsubstituted dithizone, H_2Dz , and its acid derivative, $p\text{-COOH-H}_2\text{Dz}$. During preparation of the dithizonate salts, HDz^- and $(p\text{-COO}^-)\text{-HDz}^-$, it was observed that the lower the concentration of base the more stable the solutions are over time, however the concentration of the base did not appear to have an effect on the stoichiometry of complexes. Very low base concentration (below 0.1 M) limits H_2Dz solubility, while KOH gives better solubility than NH_4OH . H_2Dz was first dissolved in small concentrated volumes of the base to get better dissolution, where after volumes were increased to final volume of 100.0 mL. 0.1 M NH_4OH concentration readily dissolves $p\text{-COOH-H}_2\text{Dz}$, which naturally is much more soluble than the unsubstituted parent molecule. Particular care was taken to obtain identical analytical concentrations through accurate weighing. H_2Dz solutions had to be prepared immediately prior to experiment, because of its lower stability and tendency to precipitate out again. The HDz^- anion and metal cation solutions were poured into burettes, for convenience. All glassware had to be clean and dried before use to avoid unintentional contamination or dilution. Absorbance measurements were taken at the indicated wavelengths for each experiment, thus chosen for best "titration endpoints" and experimental repeatability.

The experimental procedure given for $\text{Co}(\text{HDz})_3$ in Section 3.4.1.1 here below serves as general method for all complexes to follow.

3.4.1.1. $\text{Co}(p\text{-COOH-HDz})_3$ & $\text{Co}(\text{HDz})_3$

$p\text{-COOH-H}_2\text{Dz}$ (0.0176 g, 5.11×10^{-5} moles) was dissolved in *ca* 1 M KOH (0.5626 g in 10 mL) in 100.0 mL volumetric flask and fill up to the mark with water, to obtain 5.11×10^{-4} M ($p\text{-COO}^-$)-HDz $^-$ in 0.1 M aqueous KOH solution. $\text{CoCl}_2 \cdot 6\text{H}_2\text{O}$ (0.0121 g, 5.1×10^{-5} moles) was dissolved in 50 mL water in a 100.0 mL volumetric flask, then filled up to the mark with water to a concentration of 5.09×10^{-4} M. To each of the seven 50.0 mL volumetric flasks 2.00 mL of 5.09×10^{-4} M aqueous Co^{II} solution was added, and also 3.00, 4.00, 5.00, 6.00, 7.00, 8.00 and 9.00 mL of 5.11×10^{-4} M ($p\text{-COO}^-$)-HDz $^-$ respectively. A time of 40 min, with occasional swirling, was allowed for the reaction to complete, after which the flask was filled to the mark with aqueous 0.1 M KOH.

A full spectrum of absorbance readings were then taken for all seven solutions and plotted against corresponding mole ratios, see Figure 3.25.

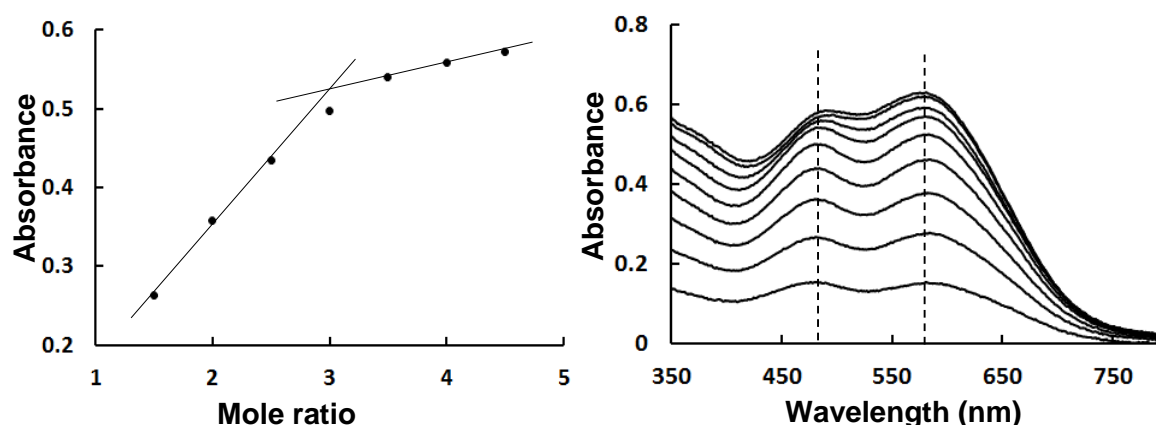


Figure 3.25. Left: Plot of absorbance vs mole ($p\text{-COO}^-$)-HDz $^-$ ligand per mole Co^{II} cation, in aqueous 0.1 M KOH at 490 nm (similar trend observed at 580 nm). Right: Overlay spectra, dashed lines correspond to data points used in mole ratio plot.

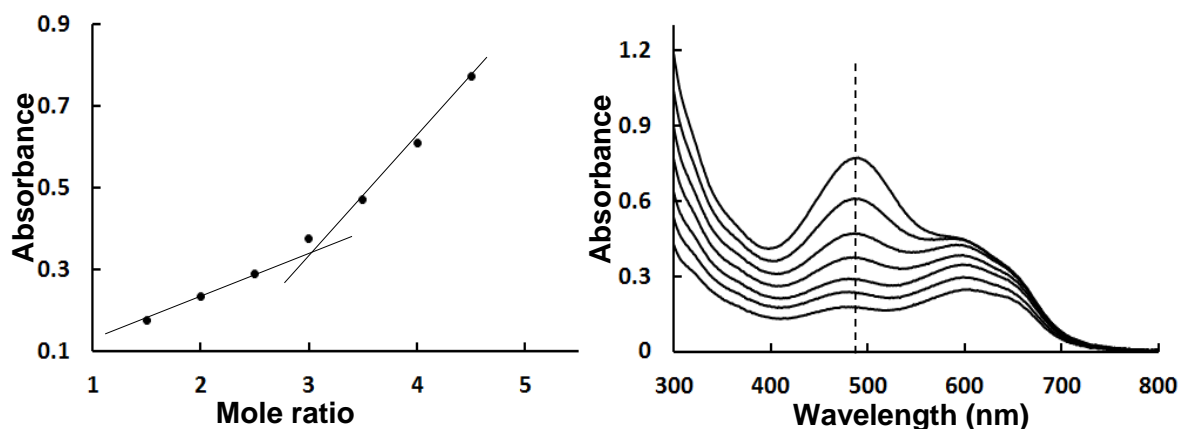


Figure 3.26. Left: Plot of absorbance vs mole ($p\text{-COO}^-$)-HDz $^-$ ligand per mole Co^{II} cation, in aqueous 0.1 M NH_4OH at 490 nm. Right: Overlay spectra, dashed line corresponds to data points used in mole ratio plot.

Results shown in Figures 3.25 and 3.26 are indicative of the Co^{II} cation reacting in a ratio of 1:3 with $(p\text{-COO}^-)\text{-HDz}^-$. These results are not affected by the type of base, namely NH_4OH or KOH . In aqueous 0.1 M KOH medium the overlay spectra have λ_{max} at 490 and 580 nm, corresponding to the purple blue solution going to orange-brown with increase in ligand concentration. In aqueous 0.1 M NH_4OH medium $\lambda_{\text{max}} = 490$ nm. These solutions are only light orange-brown, which intensifies with increase in ligand concentration.

Also the unsubstituted H_2Dz was observed to complex in the 1:3 ratio, $\text{Co}(\text{HDz})_3$, with $\lambda_{\text{max}} = 470$ and 570 nm, see Figure 3.27. Quality repeatable results were obtained when using 0.1 M aqueous KOH as medium. As was the case and seen in Figure 3.26, when using aqueous 0.1 M NH_4OH , only one λ_{max} at 470 was observed, resulting in a similar coordination ratio.

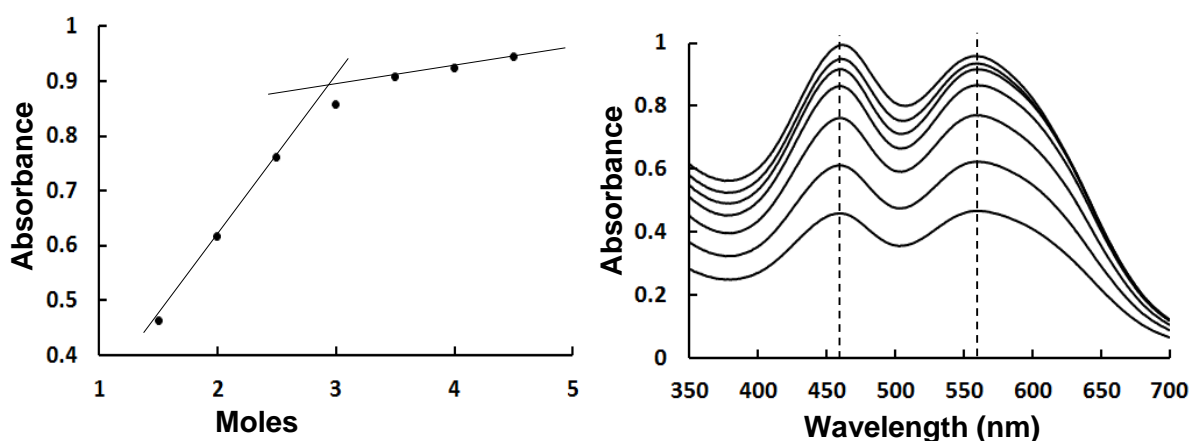


Figure 3.27. Left: Plot of absorbance vs mole HDz^- ligand per mole Co^{II} cation, in aqueous 0.1 M KOH at 570 nm (similar trend observed at 470 nm). Right: Overlay spectra, dashed lines correspond to data points used in mole ratio plot.

3.4.1.2. $\text{Ni}(p\text{-COOH-HDz})_3$ & $\text{Ni}(\text{HDz})_2$

The prepared solution of 5.11×10^{-4} M $(p\text{-COO}^-)\text{-HDz}^-$ in 0.1 M aqueous KOH reacted with an aqueous solution of 5.10×10^{-4} M Ni^{II} from $\text{NiSO}_4 \cdot 6\text{H}_2\text{O}$ (0.0134 g, 5.10×10^{-4} moles). A clear 1:3 ratio is observed in the reaction of Ni^{II} with $(p\text{-COO}^-)\text{-HDz}^-$ (see Figure 3.23). Both the λ_{max} absorbance values at 465 and 690 nm could be used equally successfully. Only 0.1 M aqueous KOH medium results are presented for this reaction, because aqueous 0.1 M NH_4OH medium gave two slopes that were too similar, with the consequence that the point of stoichiometric equivalence may not readily be determined.

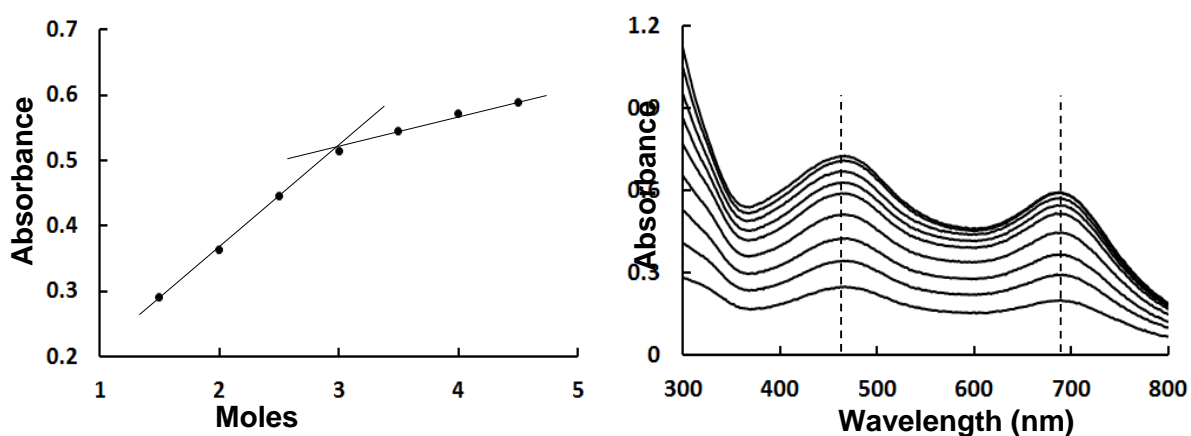


Figure 3.28. Left: Plot of absorbance vs mole ($p\text{-COO}^-$)-HDz $^-$ ligand per mole Ni II cation, in aqueous 0.1 M KOH at 690 nm (similar trend observed at 465 nm). Right: Overlay spectra, dashed lines correspond to data points used in mole ratio plot.

Due to the unexpected 1:3 coordination ratio found for the Ni(II) complex, this experiment was also repeated in a polar **organic solvent**, namely acetone, and without the presence of base. The ligand, ($p\text{-COOH}$)-H $_2$ Dz (0.0176 g, 5.11×10^{-5} moles) was dissolved in acetone in a 100.0 mL volumetric flask. An ultrasonic bath was used, obtaining the 5.11×10^{-4} M ($p\text{-COOH}$)-H $_2$ Dz solution. NiSO $_4 \cdot 6\text{H}_2\text{O}$ (0.0134 g, 5.10×10^{-5} moles) was dissolved in warm methanol in a 100.0 mL volumetric flask, then filled up to the mark to get a solution of 5.10×10^{-4} M. To each of the seven 50.0 mL volumetric flasks, 2.00 mL of 5.09×10^{-4} M methanolic Ni II solution was added and also 1.00, 2.00, 3.00, 4.00, 5.00, 6.00 and 7.00 mL of 5.11×10^{-4} M $p\text{-COOH}$ -H $_2$ Dz solution respectively. A time period of 40 minutes was allowed, with occasional swirling, for the reaction to complete, and the flasks were then filled to the mark with acetone. In the absence of base (KOH or NH $_4$ OH) the nickel complex now yielded a 1:2 ratio, Ni($p\text{-COOH}$ -HDz) $_2$, see Figure 3.29. Here, the COOH substituents are not deprotonated and thus not readily available for complexation. Typically here the Ni complex has three absorption peaks (465, 560 and 690 nm). Although the slopes of the two straight lines giving the combining ratio differ not much, it is nevertheless seen that the ratio of the Ni II cation to ($p\text{-COO}^-$)-HDz $^-$ ligand is 1:2. This reaction (Figure 3.29) serves as prove for the argument given in paragraph 3.2.3.2 under the discussion of metal dithizonates for the coordination of Ni II cation with ($p\text{-COO}^-$)-HDz $^-$ ligand, where it was also shown that from MS results a third ($p\text{-COO}^-$)-HDz $^-$ is coordinated to Ni, most probably via a -COO^- phenyl substituent.

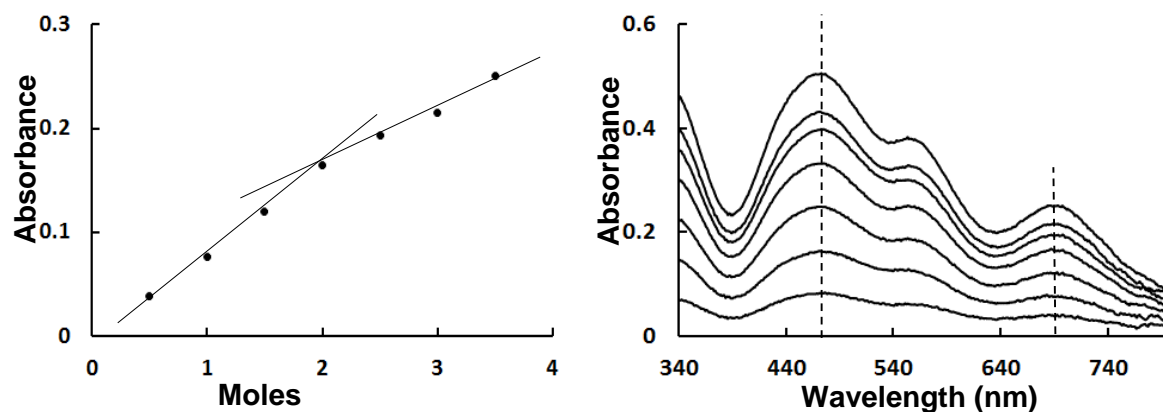


Figure 3.29. Left: Plot of absorbance vs mole (*p*-COOH)-H₂Dz ligand per mole Ni^{II} cation, in acetone at 690 nm (similar trend observed at 465 nm). Right: Overlay spectra, dashed lines correspond to data points used in mole ratio plot.

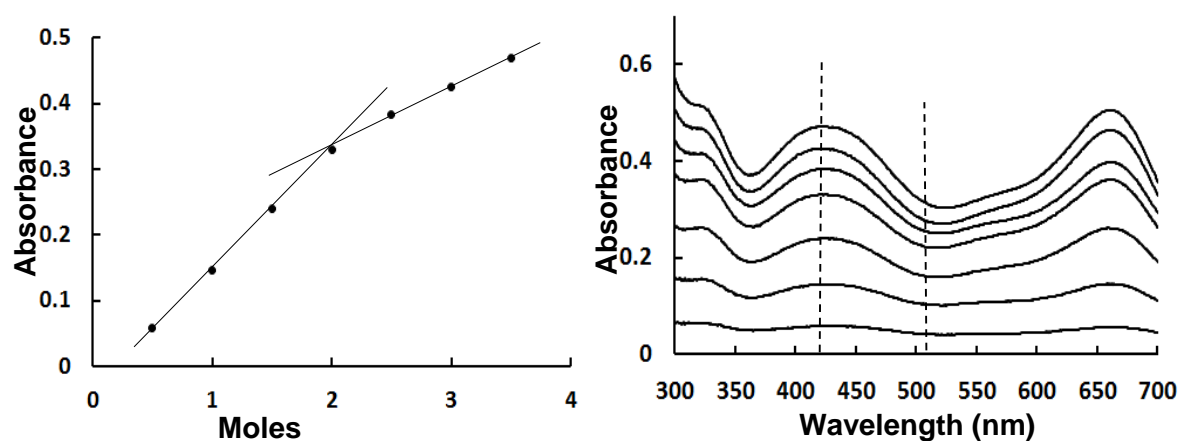


Figure 3.30. Left: Plot of absorbance vs mole HDz⁻ ligand per mole Ni^{II} cation, in aqueous 0.1 M KOH at 420 nm (similar trend observed at 510 nm). Right: Overlay spectra, dashed lines correspond to data points used in mole ratio plot.

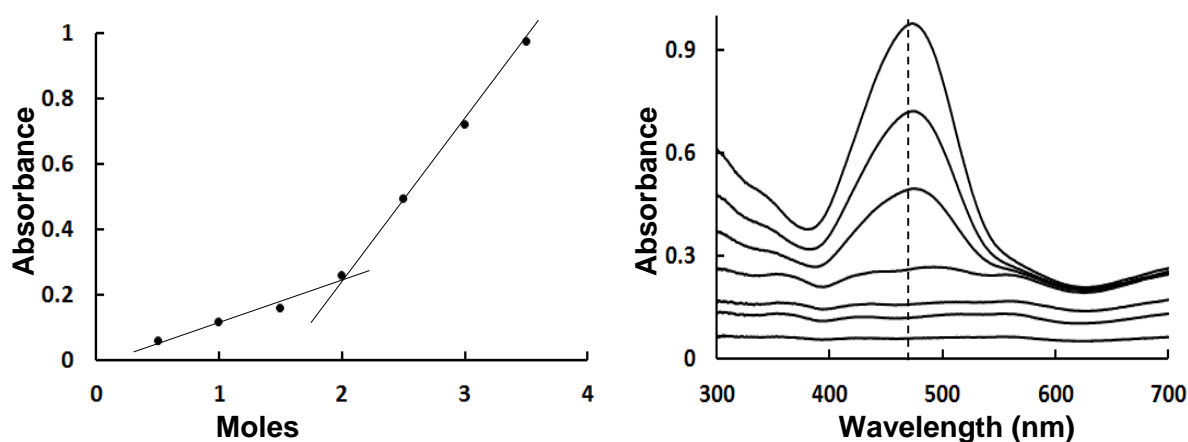


Figure 3.31. Left: Plot of absorbance vs mole HDz⁻ ligand per mole Ni^{II} cation, in aqueous 0.1 M NH₄OH at 470 nm. Right: Overlay spectra, dashed line corresponds to data points used in mole ratio plot.

In using the unsubstituted $\mathbf{H_2Dz}$, a 1:2 ratio, $\text{Ni}(\text{HDz})_2$, was observed in both bases, KOH and NH_4OH . The role of the carboxylate anion is therefore evident in coordination ratio's involving nickel. The overlay spectra in Figure 3.30 has $\lambda_{\text{max}} = 420$ and 660 nm for the $\text{Ni}(\text{HDz})_2$ complex. Repeatable results were only obtained at 420 and 510 nm, while absorbance data taken at 660 nm were not consistent. Also when using 0.2 M instead of 0.1 M aqueous NH_4OH , the exact same spectra were observed, with the orange colour not changing; the intensity merely increases in a non-linear fashion with increase in HDz^- concentration.

3.4.1.3. $\text{Pb}(p\text{-COOH-HDz})$ & $\text{Pb}(\text{HDz})_2$

A $(p\text{-COO}^-)\text{-HDz}^-$ solution of 5.11×10^{-4} M in 0.1 M of NH_4OH was reacted with equimolar solution of aqueous $\text{Pb}(\text{CH}_3\text{COO})_2 \cdot 3\text{H}_2\text{O}$. To each of the eight 50.0 mL volumetric flasks, 2.50 mL of the 5.11×10^{-4} M aqueous Pb^{II} solution was added, and also 0.50, 1.00, 1.50, 2.00, 2.50, 3.00, 3.50 and 4.00 mL of the 5.11×10^{-4} M HDz^- solution. A time of 30 minutes, with occasional swirling, was allowed for the reaction to complete, and the flasks were filled to the mark with 0.1 M NH_4OH solution. NH_4OH was preferred over KOH, since the latter gave ratio plot gradients for the two lines that are too similar. Figure 3.32 shows the Pb^{II} cation reacting with $(p\text{-COO}^-)\text{-HDz}^-$ at a ratio of 1:1, with absorbance data taken at $\lambda_{\text{max}} = 490$ nm.

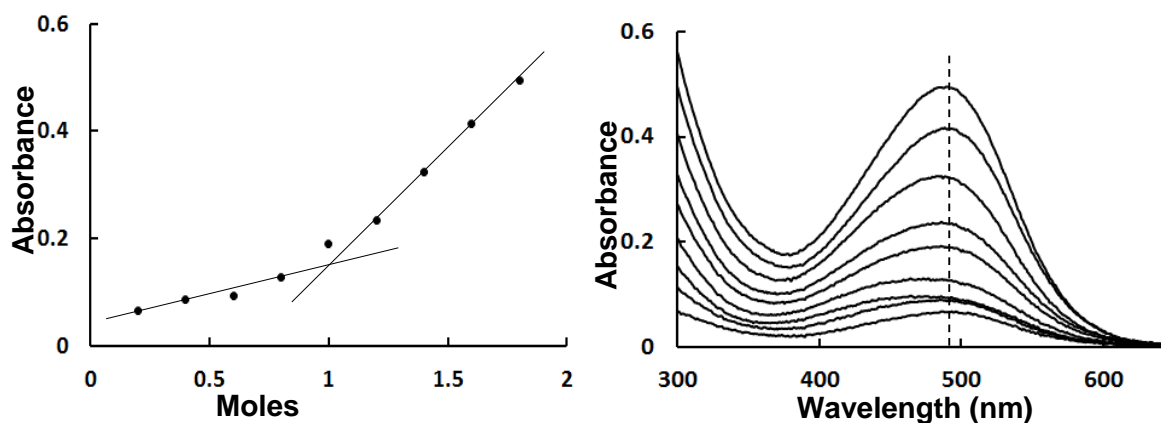


Figure 3.32. Left: Plot of absorbance vs mole $(p\text{-COO}^-)\text{-HDz}^-$ ligand per mole Pb^{II} cation, in aqueous 0.1 M NH_4OH , at 490 nm. Right: Overlay spectra, dashed line corresponds to data points used in mole ratio plot.

The prepared solution of 5.11×10^{-4} M HDz^- in 0.1 M aqueous NH_4OH reacted with an aqueous solution of 5.11×10^{-4} M Pb^{II} from $\text{Pb}(\text{CH}_3\text{COO})_2 \cdot 3\text{H}_2\text{O}$ (0.0121 g, 5.11×10^{-5} moles). To each of the seven 50.0 mL volumetric flasks, 2.00 mL of 5.11×10^{-4} M aqueous Pb^{II} was added and also 1.00, 1.50, 2.00, 2.50, 3.00, 3.50 and 4.00 mL of the 5.11×10^{-4} M HDz^- solution. A time of 30 minutes was given, with occasional swirling, for the reaction to complete, and the flasks were filled to the mark with aqueous 0.1 M NH_4OH . HDz^- reacts with Pb^{II} in a ratio of 1:2, $\text{Pb}(\text{HDz})_2$, at $\lambda_{\text{max}} 470$ nm (see Figure 3.33), agreeing perfectly with MS data.

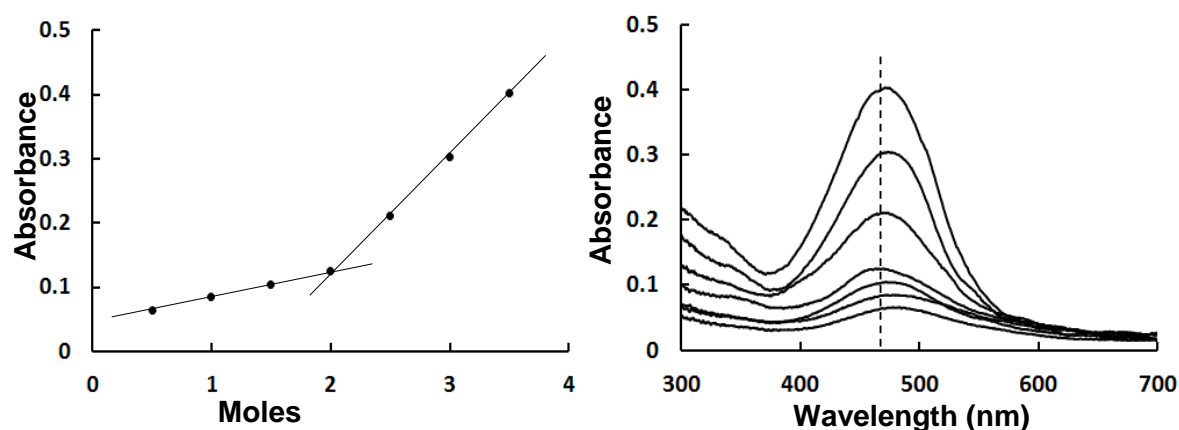


Figure 3.33. Left: Plot of absorbance vs mole HDz^- ligand per mole Pb^{II} cation, in aqueous 0.1 M NH_4OH at 470 nm. Right: Overlay spectra, dashed line corresponds to data points used in mole ratio plot.

3.4.1.4. $\text{Ag}(p\text{-COOH-HDz})$ & $\text{Ag}(\text{HDz})$

A solution of 5.11×10^{-4} M $(p\text{-COO}^-)\text{-HDz}^-$ in 0.1 M aqueous NH_4OH reacted with an aqueous solution of 5.06×10^{-4} M Ag^I from AgNO_3 (0.043 g, 2.53×10^{-4} moles). To each of the eight 50.0 mL volumetric flasks, 2.50 mL of 5.06×10^{-4} M aqueous Ag^I was added and also 0.50, 1.00, 1.50, 2.00, 2.50, 3.00, 3.50 and 4.00 mL of 5.11×10^{-4} M $(p\text{-COO}^-)\text{-HDz}^-$ solution. A time of 40 minutes was allowed, with occasional swirling, for the reaction to complete and the flasks were filled to the mark with aqueous 0.1 M NH_4OH . Results are presented in Figure 3.34, clearly showing a ratio of 1:1 between Ag^I cation and $(p\text{-COO}^-)\text{-HDz}^-$ ligand, $\text{Ag}(p\text{-COO}^-)\text{HDz}$. $\lambda_{\text{max}} = 500$ nm, with a shoulder at 590 nm. Consistent and repeatable results were obtained from the shoulder, while data from the λ_{max} position gave line slopes that were too similar for clearly determining the combining ratio. Also when using KOH as reaction medium, a similar inconclusive data set was obtained, and is thus not reported.

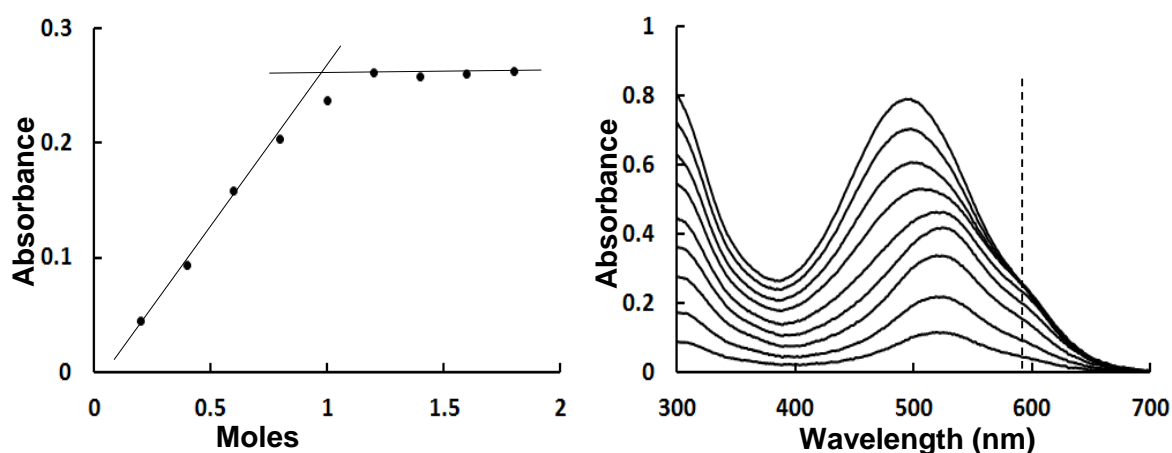


Figure 3.34. Left: Plot of absorbance vs mole $(p\text{-COO}^-)\text{-HDz}^-$ ligand per mole Ag^I cation, in aqueous 0.1 M NH_4OH , at 590 nm. Right: Overlay spectra, dashed line corresponds to data points used in mole ratio plot.

A solution of 5.11×10^{-4} M **HDz⁻** in 0.1 M aqueous KOH reacted with aqueous of 5.06×10^{-4} M **Ag^I** from **AgNO₃** (0.043 g, 2.53×10^{-4} moles). To each of the seven 50.0 mL volumetric flasks, 4.00 mL of 5.09×10^{-4} M aqueous **Ag^I** was added and also 1.00, 2.00, 3.00, 4.00, 5.00, 6.00 and 7.00 mL of the 5.11×10^{-4} M **HDz⁻** solution. A time of 40 minutes was allowed, with occasional swirling, for the reaction to complete, and the flasks were filled to the mark with aqueous 0.1 M **NH₄OH**. The coordination ratio observed for **HDz⁻** was not different from that obtained for **(p-COO⁻)-HDz⁻**, namely 1:1. Here, KOH was the only base that gave good repeatable results, at λ_{\max} 470 nm, see Figure 3.35. Although the two bases, KOH and **NH₄OH**, differ for the two ligands, **HDz⁻** and **(p-COO⁻)-HDz⁻**, the combining ratio with **Ag^I** was the same.

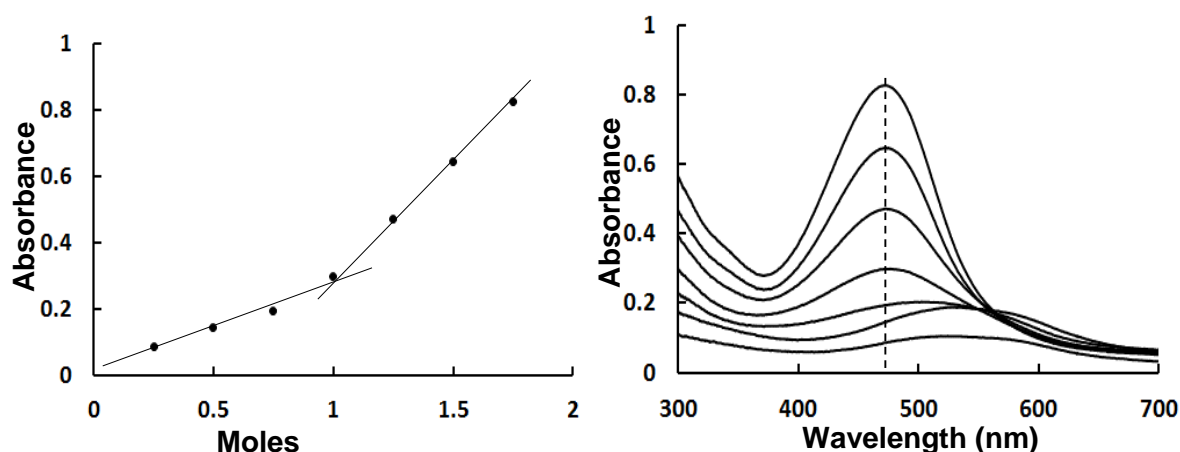


Figure 3.35. Left: Plot of absorbance vs mole **HDz⁻** ligand per mole **Ag^I** cation, in aqueous 0.1 M **KOH** at 470 nm. Right: Overlay spectra, dashed line corresponds to data points used in mole ratio plot.

3.4.1.5. **Hg(p-COOH-HDz)**

A solution of 5.11×10^{-4} M **(p-COO⁻)-HDz⁻** in 0.1 M aqueous **NH₄OH** reacted with an aqueous solution of 5.08×10^{-4} M **Hg^{II}** from **HgCl₂** (0.0138 g, 5.08×10^{-5} moles). To each of the eight 50.0 mL volumetric flasks 2.50 mL of 5.09×10^{-4} M aqueous **Hg^{II}** was added and also 0.50, 1.00, 1.50, 2.00, 2.50, 3.00, 3.50 and 4.00 mL of the 5.11×10^{-4} M **(p-COO⁻)-HDz⁻** solution. A time of 40 minutes, with occasional swirling, was allowed for the reaction to complete and the flasks were filled to the mark with aqueous 0.1 M **NH₄OH**. This complex was not initially part of this study, but is nevertheless reported to show that **(p-COO⁻)-HDz⁻** reacts with large metal cations in a ratio of 1:1, as was the case for **Pb**. The much larger ionic radii of these heavy metals most probably bring empty outer orbitals within reach of at least two anionic bonding sites on the ligand, i.e. at both **S⁻** (and **N**) and on one **-COO⁻** group, thus limiting the bonding ratio to 1:1. Such coordination would balance the 2+ charge on the cation, while at least a 2- charge remains. The ligand of course may readily be 3- at full deprotonation, i.e. 1- on the ligand backbone, and 2 x (2-) due to the two acid groups. Figure 3.36 shows the ratio 1:1 between **Hg^{II}** and **(p-COO⁻)-HDz⁻**, at λ_{\max} 548 nm.

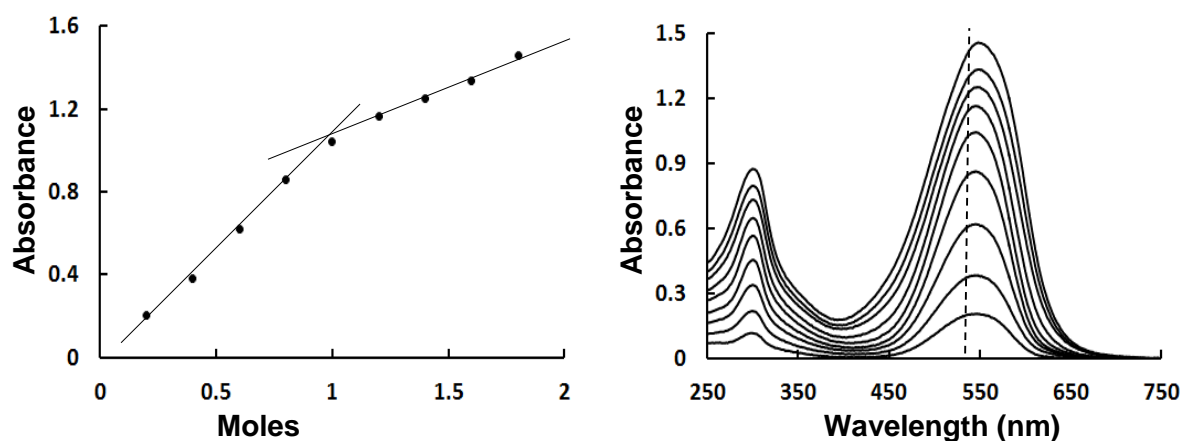


Figure 3.36. Left: Plot of absorbance vs mole ($p\text{-COO}^-$)-HDz $^-$ ligand per mole Hg^{II} cation, in aqueous 0.1 M KOH, and at 548 nm. Right: Overlay spectra, dashed line corresponds to data points used in mole ratio plot.

3.4.2. Method of Continuous Variation

The same goal mentioned under the previous section on the mole ratio method is also part of this method and the reaction conditions are the same. The results obtained from this method agrees with those of the previous method. However, some metal dithizonates did not yield conclusive results under this method, simply because the complex absorbs at the similar wavelengths to that of the reactants. Also, only results that were repeatable and consistent were reported.

In the method of continuous variation, the measured absorbance at a suitable wavelength is corrected for any absorbance the mixture might exhibit if no reaction had occurred, and then plotted against the volume fraction of one reactant. The absorbance is measured from solutions (metal cation and ligand) with identical concentrations that are mixed in different amounts such that the total volume of the mixture solutions and the total moles of reactant in each mixture stays constant. However, the mole ratio of reactants is varied systematically across the set of mixture solutions. The volume fraction of the metal cation that is plotted against the corrected absorbance is:

$$V_{\text{M}}/(V_{\text{M}} + V_{\text{L}})$$

V_{M} is the cation volume and V_{L} is the ligand volume in solution. The combining ratio of the cation and ligand in the complex is determined at a maximum volume ratio ($V_{\text{M}}/V_{\text{L}}$), assuming the complex absorbs more than the reactants.

3.4.2.1. $\text{Co}(p\text{-COOH-HDz})_3$

The solution of 5.11×10^{-4} M $(p\text{-COO}^-)\text{-HDz}^-$ in 0.1 M aqueous NH_4OH reacted with aqueous solutions of 5.09×10^{-4} M Co^{II} from $\text{CoCl}_2 \cdot 6\text{H}_2\text{O}$ (5.09×10^{-5} moles). To each of the thirteen 50.0 mL volumetric flasks, 0.00, 0.50, 1.00, 1.50, 2.00, 3.00, 4.00, 5.00, 6.00, 7.00, 8.00, 9.00 and 10.00 mL of 5.09×10^{-4} M aqueous Co^{II} was added and also 10.00, 9.50, 9.00, 8.50, 8.00, 7.50, 7.00, 6.00, 5.00, 4.00, 3.00, 2.00, 1.00 and 0.00 mL of 5.11×10^{-4} M $(p\text{-COO}^-)\text{-HDz}^-$ solutions, respectively. A time of 40 minutes was allowed, with occasional swirling, for the reaction to complete and the flasks were filled to the mark with aqueous 0.1 M NH_4OH . In Figure 3.37 the maximum absorbance volume ratio is observed at 0.25, which translates into the complex, $\text{Co}((p\text{-COO}^-)\text{-HDz})_3$. This 1:3 ratio of Co^{II} and $(p\text{-COO}^-)\text{-HDz}^-$ was obtained at λ_{max} 600 nm. When using KOH as base instead, results were not consistent.

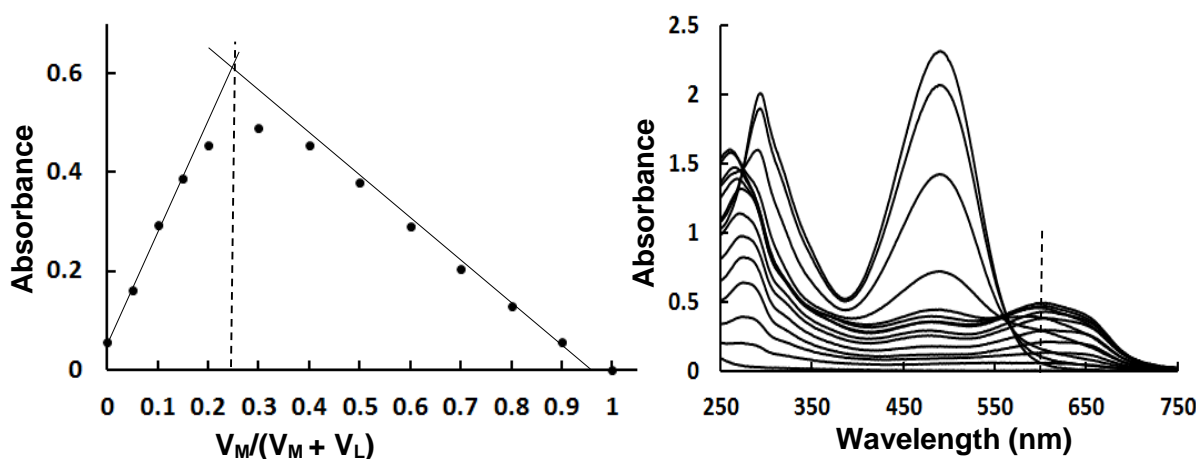


Figure 3.37. Left: Plot of corrected absorbance vs $(p\text{-COO}^-)\text{-HDz}^-$ volume fraction of Co^{II} cation, in 0.1 M NH_4OH , at 600 nm. Right: Overlay spectra, dashed line corresponds to data points used in continuous variation plot.

3.4.2.2. $\text{Ni}(p\text{-COOH-HDz})_3$ & $\text{Ni}(\text{HDz})_2$

The solution of 5.11×10^{-4} M $(p\text{-COO}^-)\text{-HDz}^-$ in 0.1 M aqueous KOH reacted with a solution of 5.11×10^{-4} M of Ni^{II} from $\text{NiSO}_4 \cdot 6\text{H}_2\text{O}$ (5.10×10^{-5} moles). To each of the twelve 50.0 mL volumetric flasks, 0.00, 0.50, 1.00, 1.500, 2.00, 3.00, 4.00, 5.00, 6.00, 7.00, 8.00, 9.00, and 10.00 mL of 5.09×10^{-4} M aqueous Ni^{II} was added and also 10.00, 9.50, 9.00, 8.50, 8.00, 7.50, 7.00, 6.00, 5.00, 4.00, 3.00, 2.00, 1.00 and 0.00 mL of 5.11×10^{-4} M $(p\text{-COO}^-)\text{-HDz}^-$ solution, respectively. A time of 40 minutes, with occasional swirling, was allowed for the reaction to complete and the flasks then filled to the mark with aqueous 0.1 M KOH. When using NH_4OH as base instead, results were not consistent. In Figure 3.38 the ratio between Ni^{II} and $(p\text{-COO}^-)\text{-HDz}^-$ is again seen to be 1:3, as seen from the maximum absorbance volume ratio at 0.25. This ratio was obtained by using absorbance data from the overlay spectra at λ_{max} 700 nm.

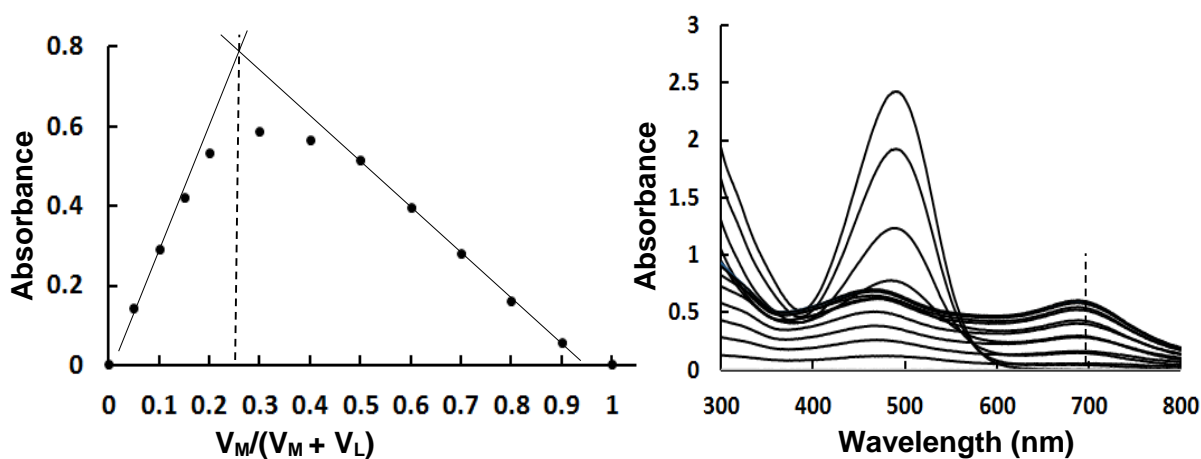


Figure 3.38. Left: Plot of corrected absorbance vs $(p\text{-COO}^-)\text{-HDz}^-$ volume fraction of Ni^{II} cation, in aqueous 0.1 M KOH, at 700 nm. Right: Overlay spectra, dashed line corresponds to data points used in mole ratio plot.

The solution of 5×10^{-4} M HDz^- in 0.1 M aqueous NH_4OH reacted with a solution of 5.1×10^{-4} M of Ni^{II} from $\text{NiSO}_4 \cdot 6\text{H}_2\text{O}$ (5.10×10^{-5} moles). To each of the eleven 50.0 mL volumetric flasks, 0.00, 2.00, 4.00, 6.00, 8.00, 10.00, 12.00, 14.00, 16.00, 18.00 was added and 20.00 mL of the 5.09×10^{-4} M aqueous Ni^{II} and also 20.00, 18.00, 16.00, 14.00, 12.00, 10.00, 8.00, 6.00, 4.00, 2.00 and 0.00 mL of 5.11×10^{-4} M $(p\text{-COO}^-)\text{-HDz}^-$ solutions, respectively. A time of 40 minutes, with occasional swirling, was allowed for the reaction to complete and the flasks were filled to the mark with aqueous 0.1 M NH_4OH . The overlay spectra in Figure 3.39 had to be plotted in the region that obeys Beer's Law at an absorbance 0.1 to 1.2, hence 25 % concentration values are presented here. The maximum volume ratio is at 0.33, meaning that the complex is in the form, $\text{Ni}(\text{HDz})_2$. There was no success in obtaining results with aqueous KOH.

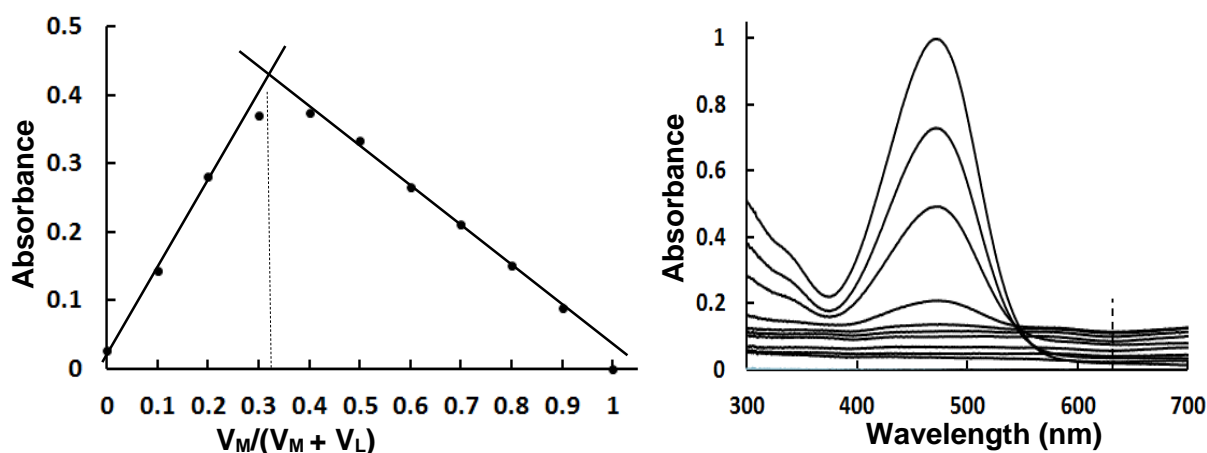


Figure 3.39. Left: Plot of corrected absorbance vs mole HDz^- volume fraction of Ni^{II} cation, in aqueous 0.1 M NH_4OH at 630 nm with the dashed line at maximum volume ratio. Right: Overlay spectra, dashed line corresponds to data points used in mole ratio plot.

In the continuous variation method, $(p\text{-COO}^-)\text{-HDz}^-$ could be used only in complexation with Co and Ni, and HDz^- only with Ni. Test results from other metals were inconclusive here.

3.5. Chromism

Chromism, the process whereby changes in the colour of a compound is induced by external stimuli, is usually associated with changes in mostly π - or d-electron states of atoms and molecules. A variety of external stimuli may be responsible for this phenomenon.

Here below are shown selected colour photographs of our discovered and/or investigated seven chromisms associated with dithizone, which is to be discussed in the ensuing section.

Solvatochromism

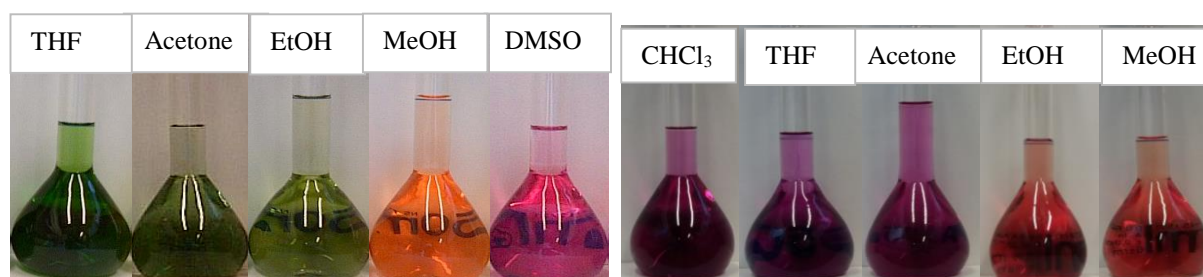


Image 3.1. Left: *p*-COOH-H₂Dz in various solvents. Right: S-Methylated-H₂Dz (the methyl group is on the ligand backbone sulphur) in various solvents.

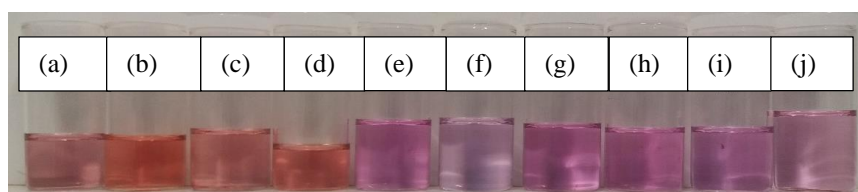


Image 3.2. S-Methylated-H₂Dz in (a) DMSO, (b) MeOH, (c) EtOH, (d) Acetonitrile, (e) Ethyl acetate, (f) Toluene, (g) Chloroform, (h) Diethyl ether, (i) THF, and (j) Acetone. Immediately after preparation, solutions with a dielectric constant below 21 changed to pink and those above 21 to orange.



Image 3.3. H₂Dz (left) and *p*-SCH₃-H₂Dz (right, the -SCH₃ group is on the *para* positions of the two phenyl groups) in various solvents (toluene, chloroform, THF, DCM, acetone, ethanol, methanol, and DMSO – from left to right).

Concentratochromism



Image 3.4. H₂Dz in MeOH at different concentrations (0.8, 1.6, 3.2, 6.5, and 9.7 × 10⁻⁵ M).



Image 3.5. *p*-COOH-H₂Dz in DMSO (left) and in MeOH (right) at different concentrations (13, 9.7, 6.5, 3.2, 1.6 and 0.8 × 10⁻⁵ M – from left to right).



Image 3.6. *p*-COOH-H₂Dz in EtOH (left) and in acetone (right) at different concentrations (13, 9.7, 6.5, 3.2, 1.6 and 0.8 × 10⁻⁵ M – from left to right).



Image 3.7. *p*-COOH-H₂Dz in THF at different concentrations (13, 9.7, 6.5, 3.2, 1.6 and 0.8 × 10⁻⁵ M – from left to right).



Image 3.8. (*p*-SCH₃)-H₂Dz in DMSO (left) and in MeOH (right), at different concentrations (0.8, 1.6, 3.2, 6.5, 9.7 and 13 × 10⁻⁵ M – from left to right).

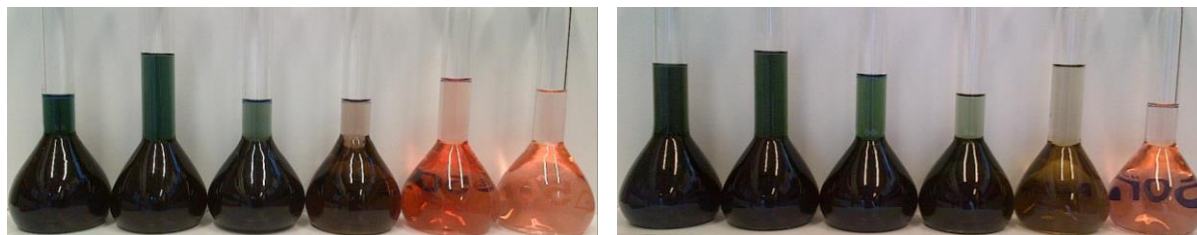


Image 3.9. (*p*-SCH₃)-H₂Dz in EtOH (left) and in THF (right), at different concentrations (13, 9.7, 6.5, 3.2, 1.6 and 0.8 x 10⁻⁵ M – from left to right).

Photochromism



Image 3.10: Left: PhHg(*p*-COOH-HDz) in THF:Tol (1:9); (a) without direct light exposure, (c) in ambient light, and (e) under direct irradiation with a mercury-halide lamp. PhHg(HDz) solution in THF:Tol (1:9) (b) without light shining, (d) in ambient light and (f) under direct irradiation. Right: PhHg(*p*-COOH-HDz) in (from left to right) ethanol, methanol, ethyl acetate, acetone, butan-2-ol, propan-2-ol, THF and diethyl ether, all under sunlight illumination. In the shade all eight solutions are orange.

Thermochromism



Image 3.11. *p*-SCH₃-H₂Dz in ethanol, changing color from orange ($T = 10\text{ }^{\circ}\text{C}$) to blue-grey ($T = 70\text{ }^{\circ}\text{C}$).

Chronochromism



Image 3.12. S-Methylated-H₂Dz in chloroform, changing from pink ($t = 0$) to orange ($t = 3\text{ hrs}$).

3.5.1. Photochromism and Reaction Kinetics

In this section, photochromism and reaction kinetics of phenylmercury dithizonates are reported. During these studies the two complexes, PhHg(HDz) and PhHg(*p*-COOH-HDz), were treated similarly as to obtain reliable comparative results on its photochromic nature. PhHg(*p*-COOH-HDz) was observed to be photochromic in THF (soluble) and diethyl ether (very limited solubility), see Image 3.10. The complex is insoluble in non-polar solvents, where-in the back reaction traditionally is the slowest, and thus readily measurable. To overcome this problem a mixture of solvents were considered; toluene was introduced to the THF solutions in varying ratio's. PhHg(HDz) (0.0101 g, 0.0185 mmol) was dissolved in THF, in 50.0 mL volumetric flasks. 4.00 mL aliquots of PhHg(HDz) solution were pipetted into four 50.0 mL volumetric flasks. To these volumetric flasks toluene was added in volumes; 45.00, 35.00, 20.00 and 0.00 mL, and the flasks filled to the mark with THF. The same procedure was followed when preparing PhHg(*p*-COOH-HDz) (0.0112 g, 0.0176 mmol) and diluted to 2.95×10^{-5} M in each of the four volumetric flasks.

For convenience a 400 W mercury-halide lamp was used to simulate sunlight. The colour change was from orange to blue when exposed to light. PhHg(HDz) has $\lambda_{max} = 478$ nm for the orange solution and 600 nm for the blue solution. Two isosbestic points are seen at 394 and 522 nm. PhHg(*p*-COOH-HDz) shows a redshift to $\lambda_{max} = 494$ nm for the orange-red solution and to 622 nm for the blue solution, with two isosbestic points at 400 and 552 nm. Effects that influence the spontaneous back reaction were studied at 600 nm for PhHg(HDz) and at 622 nm for PhHg(*p*-COOH-HDz) complex. Image 3.10 shows that even under ambient light conditions there is already some isomerization taking place.

SOLVENTS. UV-vis spectra of each of the four solutions, with different ratios of toluene and THF, were taken before and after being exposed to sunlight, spectra are shown in Figure 3.40. From these two sets of spectra it may be seen that the largest population of the blue photo-induced isomer for both complexes could be obtained when the largest percentage of non-polar toluene was used. Polar solvents are known to speed up the photochromic back reaction,¹³¹ and this was also the case when using polar THF as a solvent. In Figures 3.41 it is again seen that the photo-excited blue isomer population of the PhHg(*p*-COOH-HDz) complex is directly proportional to the percentage of toluene in THF. This means that the back reaction is so fast that already during the time of transfer between light exposure and placing the cuvette inside the spectrometer chamber and starting the scan, a large portion of the blue isomer population has already reverted back to the orange ground state. For this complex the polar substituent, -COOH,

¹³¹ K. G. von Eschwege, *J. Photochem. and Photobiology A: Chem.*, 159, **252** (2013).

does speed up the spontaneous radiationless thermal back reaction, similar to what is seen when traces of acid, base, impurities or polar solvents are present. The PhHg(HDz) return reaction appears to be largely unaffected by this solvent ratio. All reaction kinetics were thus to be done in the 9:1 Tol:THF solvent ratio.

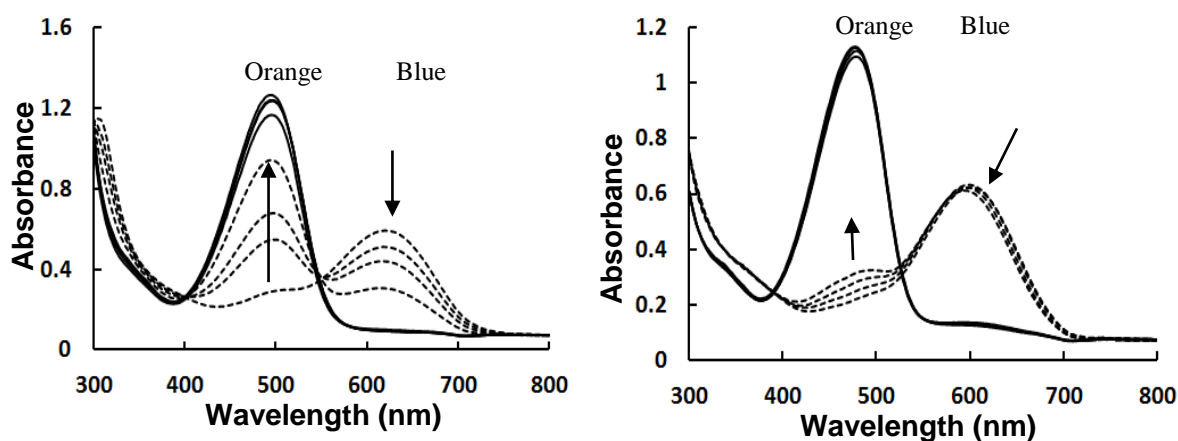


Figure 3.40. Spectra of photochromic 2.81×10^{-5} M PhHg(*p*-COOH-HDz) (left) and 2.95×10^{-5} M PhHg(HDz) (right) in the following Tol:THF solvent ratio's: 90:10 (max. blue population), 70:30, 40:60, 0 & 100. Solid lines represent orange solutions and dashed lines mostly blue solutions, immediately after photo-excitation, at 20 °C.

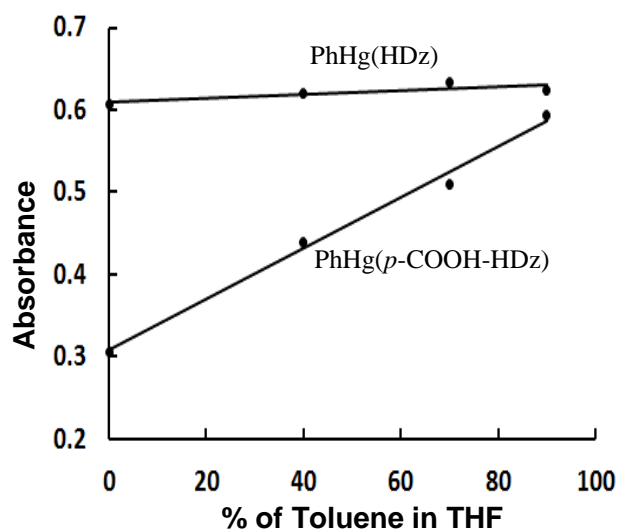


Figure 3.41. Maximum absorbance immediately after photo-excitation for various ratio's of Tol:THF for 2.81×10^{-5} M PhHg(*p*-COOH-HDz) at 622 nm and 2.95×10^{-5} M PhHg(HDz) at 600 nm. Data points to the right correspond to highest % toluene media.

CONCENTRATION: Another factor that does affect the thermal back reactions of photochromic complexes, is concentration, as also recently reported.¹³² The above two complexes were studied to determine the effect of concentration at 20 °C and in the optimum solvent mixture as derived above. The different concentrations used (1.44 , 2.17 , 2.89 , and 3.61×10^{-5} M) are within the

¹³² E. Alabaraoye, K. G. von Eschwege, N. Loganathan, *J. Phys. Chem. A*, 10894, **118** (2014).

absorbance range that obeys Beer-Lambert law for both complexes, as confirmed by a linear relationship between absorbance and concentration. Figure 3.42 shows the plots of $\ln[A_0/A_t]$ versus return reaction times for the photochromic reactions.

For $\text{PhHg}(p\text{-COOH-HDz})$ the plot of rate (k) against concentration gives a direct relationship with $R = 0.999$, see Figure 3.43. It confirms that this complex follows first order kinetics and also that the rate of the thermal back reaction from blue to orange increases with concentration. The same is true for $\text{PhHg}(\text{HDz})$. The rate increase for $\text{PhHg}(p\text{-COOH-HDz})$ with increase in concentration is more pronounced than is the case for the unsubstituted $\text{PhHg}(\text{HDz})$ complex. This result reflects what was seen for increase in polar solvent, and what is to be shown in the next paragraph where the effect of temperature will be discussed.

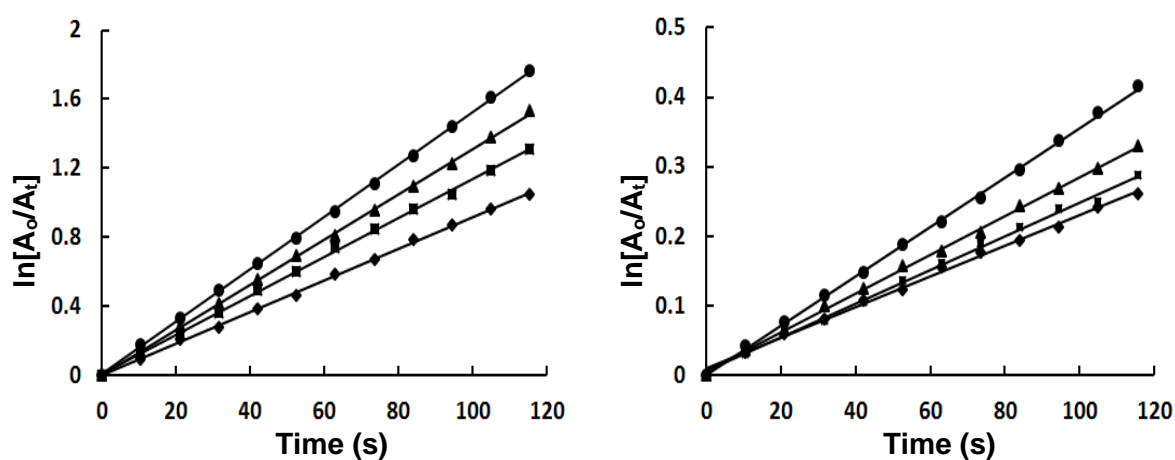


Figure 3.42. Kinetics of $\text{PhHg}(p\text{-COOH-HDz})$ at 622 nm (left) and $\text{PhHg}(\text{HDz})$ at 600 nm (right) for different concentrations at 20 °C, in 9:1 ratio of toluene:THF. (\bullet 3.61, \blacktriangle 2.89, \blacksquare 2.17, \blacklozenge 1.44) $\times 10^{-5}$ M concentrations.

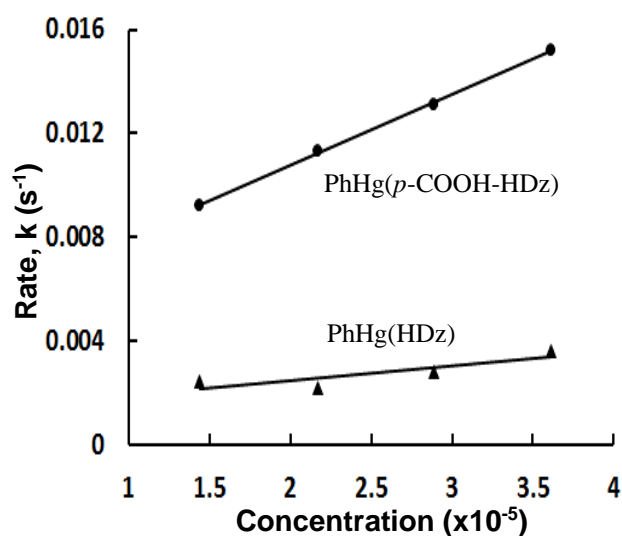


Figure 3.43. Rate of the spontaneous back reaction for different concentrations at 20 °C.

TEMPERATURE: Temperature also plays a vital role in the rate of the back isomerization of this photochromic reaction. In the 90:10 Tol:THF solvent mixture the temperature range was varied from 0 to 40 °C, in 10 °C interval steps. No problem with condensation around the cuvette at low temperatures was experienced, as these experiments were conducted during the dry season. Also, temperatures were kept low enough to avoid solvent evaporation. Similar temperatures and concentrations (2.81×10^{-5} M, and 2.95×10^{-5} M) were used for both complexes, PhHg(*p*-COOH-HDz) and PhHg(HDz) respectively.

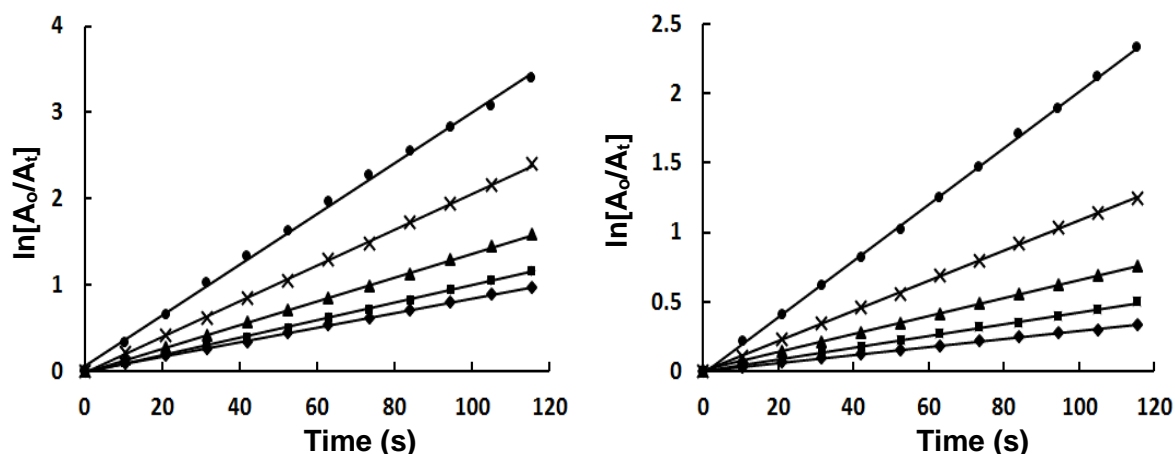


Figure 3.44. Kinetics of PhHg(*p*-COOH-HDz) at 622 nm (left) and PhHg(HDz) at 600 nm (right), at different temperatures in 9:1 ratio of toluene:THF. (♦ - 0, ■ - 10, ▲ - 20, X - 30, ● - 40) °C

The kinetic data that were obtained are represented in Figure 3.44, where $\ln[A_0/A_t]$ is plotted against time in seconds for each temperature set. The slope at each temperature is indicative of reaction rate. A plot of the rate, k (s^{-1}), against temperature shows an exponential increase of the rate with an increase of temperature for both complexes, see Figure 3.45.

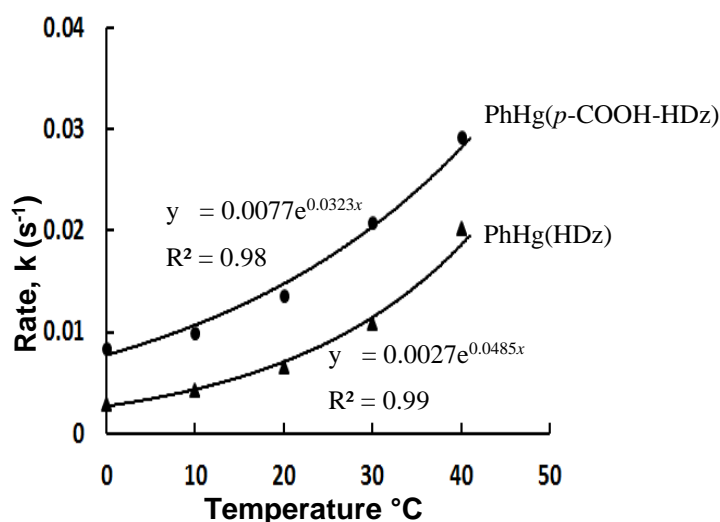


Figure 3.45. Rate of the spontaneous back reaction at different temperatures, in 9:1 ratio of Tol:THF.

Overall, the PhHg(HDz) thermal back reaction is slower, varying from $k = 0.0029 \text{ s}^{-1}$ at $0 \text{ }^{\circ}\text{C}$ to $k = 0.0203 \text{ s}^{-1}$ at $40 \text{ }^{\circ}\text{C}$, in comparison with PhHg(*p*-COOH-HDz) where $k = 0.0084 \text{ s}^{-1}$ at $0 \text{ }^{\circ}\text{C}$ to $k = 0.0293 \text{ s}^{-1}$ at $40 \text{ }^{\circ}\text{C}$. Over the temperature range of 0 to $40 \text{ }^{\circ}\text{C}$ PhHg(HDz) rates vary by 0.0174 s^{-1} . Similarly, PhHg(*p*-COOH-HDz) has a difference of $k = 0.0209 \text{ s}^{-1}$, which is only 0.0035 s^{-1} more than the rate for the unsubstituted complex.

Data from Figure 3.45 may consequently be used to determine the half-life of a solution at a given temperature, for this particular mixture of solvents.

From the equation:

$$y = 0.0027e^{0.0485x} \text{ for the PhHg(HDz) complex, where } y = k \text{ (s}^{-1}\text{) and } x = T \text{ (}^{\circ}\text{C),}$$

the half-life of this complex at $20 \text{ }^{\circ}\text{C}$, with $k = 0.0065 \text{ s}^{-1}$, can be determined by

$$\begin{aligned} t_{1/2} &= \ln 2/k \\ &= 1.8 \text{ minute} \end{aligned}$$

A combination of the latter two equations makes it possible to determine the required temperature if for instance $t_{1/2} = 1 \text{ day}$:

$$\ln 2/ t_{1/2} = 0.0027e^{0.0485T}$$

then

$$T = -120 \text{ }^{\circ}\text{C} \text{ will be required to slow the back reaction down to } t_{1/2} = 1 \text{ day.}$$

Similarly, if, on the other hand, the temperature would be increased to $114 \text{ }^{\circ}\text{C}$, a half-life for the back reaction of 1 second would result.

These results are in agreement with literature reports where the increase of temperature has been shown to speed up the photochromic back-reactions, and *vice versa*.^{133,134} The same calculations may be done for the PhHg(*p*-COOH-HDz) complex, where

$$y = 0.0077e^{0.0323x}$$

Here the half-life at $20 \text{ }^{\circ}\text{C}$ with $k = 0.0137 \text{ s}^{-1}$ is 51 seconds , which is about twice the rate of PhHg(HDz) at the same temperature. The required temperature for

$$t_{1/2} = 1 \text{ day, is } -213 \text{ }^{\circ}\text{C,}$$

and if the temperature would be increased to $93 \text{ }^{\circ}\text{C}$ then

$$t_{1/2} = 1 \text{ s.}$$

Although the singly protonated free ligand, S-methylated-dithizone, SCH₃-HDz, was not originally within the scope of this study, coincidental discovery of its photochromic nature in two polar solvents, ethanol and DMSO, it was decided to include its kinetic study also here. This is interesting, because metal dithizonates are visibly photochromic in less polar or non-polar

¹³³ L.S. Meriwether, E.C. Breitner, C.L. Sloan, *J of the American Chemical Society*, 4441, **87** (1965).

¹³⁴ H.M.N.H. Irving, Dithizone, *Analytical Sciences Monographs*, The Chemical Society, London, 1977, p. 39

solvents, while more polar solvents speed up the back reaction so much so that it no longer is observable to the naked eye.¹³⁵

The synthesis method for this compound was reported by Von Eschwege, who also supplied the chemical compound itself.¹³⁶

Preparation of solutions for the kinetic study of its photochromic return reaction is as follows: S-methylated-dithizone (0.0110 g, 0.0405 mmol) was dissolved in ethanol in a 50.0 mL volumetric flask, to obtain a concentration of 8.11×10^{-4} M. 2.00 mL SCH₃-HDz solution was pipetted into a 50.0 mL volumetric flask, to obtain a concentration of 3.24×10^{-5} M. The latter solution was used to study the photochromic nature of this compound. The colour changes in ethanol solution is orange to pink when exposed to sunlight. The orange solution gives two absorption maxima at 410 and 540 nm, while the pink solution has only the 540 nm peak. After exposure to sunlight the peak at 410 nm disappeared completely, while the peak at 540 nm intensifies, see Figure 3.46. During the photochromic reaction isosbestic points occur at 350 and 474 nm.

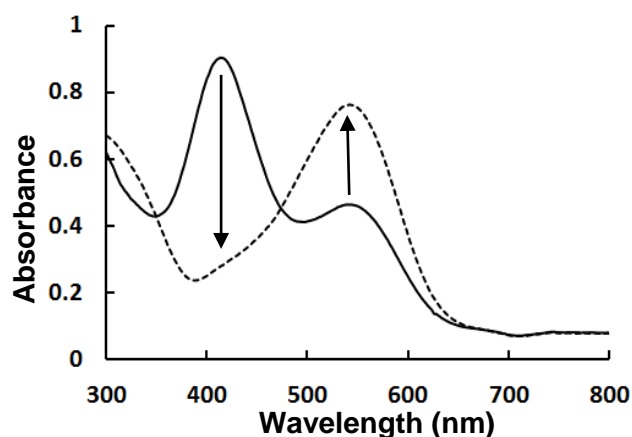


Figure 3.46. Photochromic reaction of 3.24×10^{-5} M S-methylated-dithizone in ethanol, at 20 °C. Solid lines represent the orange solution and dashed lines the pink solution.

Here it is illustrated how temperature affects the back reaction of S-methylated-dithizone, while other possible influences are left for future studies. Kinetic runs were investigated at temperatures varying from 10 to 50 °C. Different to the exponential relationship between rate and temperature observed for the metal dithizonates, a plot of rate, k , against temperature shows a linear relationship here. The temperature dependence nevertheless shows that also here the back reaction is thermal. Photochromism in this purely organic dithizone had never been observed before.

¹³⁵ H. Schworer, K. G. von Eschwege, G. Bosman, P. Krok, and J. Conradie, *ChemPhysChem*, 2653, **12** (2011).

¹³⁶ K. G. von Eschwege Ph.D. Dissertation, (2006).

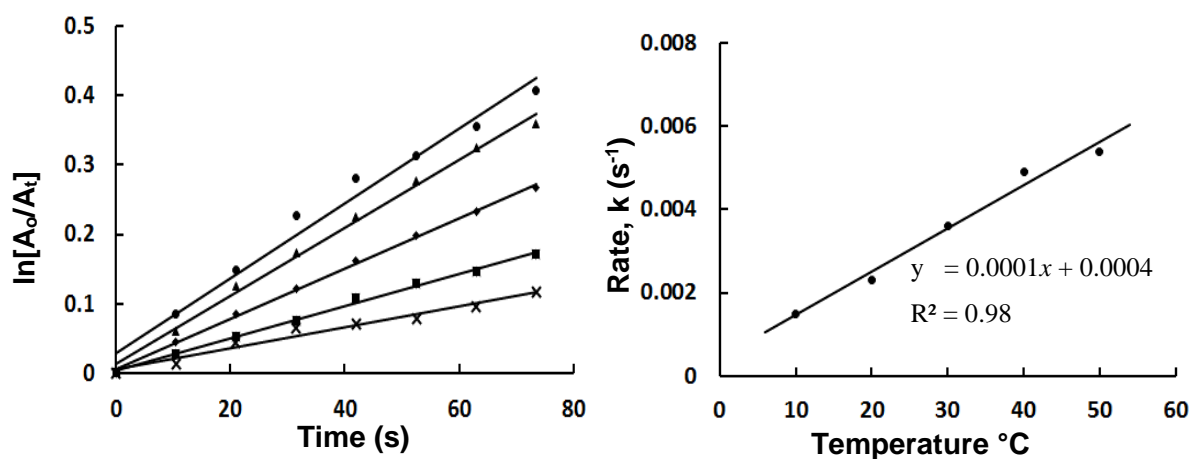


Figure 3.47. Kinetics of the spontaneous back reaction of SCH₃-HDz at different temperatures (left). Rate of the back reaction at different temperatures (right). (X - 10, ■ - 20, ◆ - 30, ▲ - 40, ● - 50) °C

This compound however is related to its metal complexes in that a covalent bond between sulphur and another atom or group of atoms exists. Discovery of photochromism in SCH₃-HDz now provides scope for new studies where a variety of chemical moieties may be substituted on the dithizone sulphur atom, and studied for new chromic responses and applications.

3.5.2. Solvatochromism

A comparative study of solvatochromism was done on four ligands; H₂Dz, *p*-COOH-H₂Dz, *p*-SCH₃-H₂Dz, and SCH₃-HDz. For interest sake the most electron rich dithizone derivative that had up to date been synthesized,¹³¹ *p*-SCH₃-H₂Dz, was added to this series. The SCH₃ groups that are located on the *para* positions of the two phenyl rings cause the largest redshift seen for dithizones, namely up to $\lambda_{max} = 667$ nm, as a consequence of its strong electron donating ability. Solvents that are representative of non-polar, polar aprotic and polar were used to study its effects on these ligands. However, since *p*-COOH-H₂Dz lacks solubility in non-polar solvents, the latter was studied only in polar aprotic and polar solvents. Conditions like concentration and temperature were otherwise kept constant.

The following general procedure was used to prepare these solutions:

H₂Dz (0.0104 g, 0.04 mmol) was dissolved in methanol, sonicating for 5 minutes (to aid dissolution) in a 50.0 mL volumetric flask to obtain a concentration of 8.11×10^{-4} M. 2.00 mL of this latter solution was pipetted into a 50.0 mL volumetric flask and filled to the mark with methanol, to obtain a concentration of 3.24×10^{-5} M. The same was done with acetone, ethanol, DMSO, DCM, chloroform, toluene, and THF. UV-vis spectra were recorded at room temperature (25 °C), in all the mentioned solvents, see Figures 3.48 to 3.50.

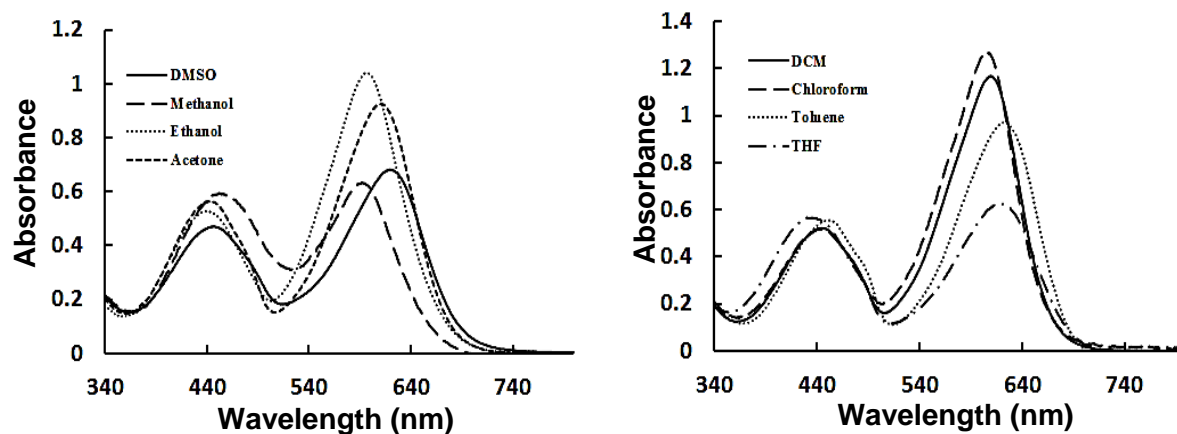


Figure 3.48. $3.24 \times 10^{-5} \text{ M H}_2\text{Dz}$ in solvents with dielectric constants above 20 (left) and solvents with dielectric constants below 20 (right).

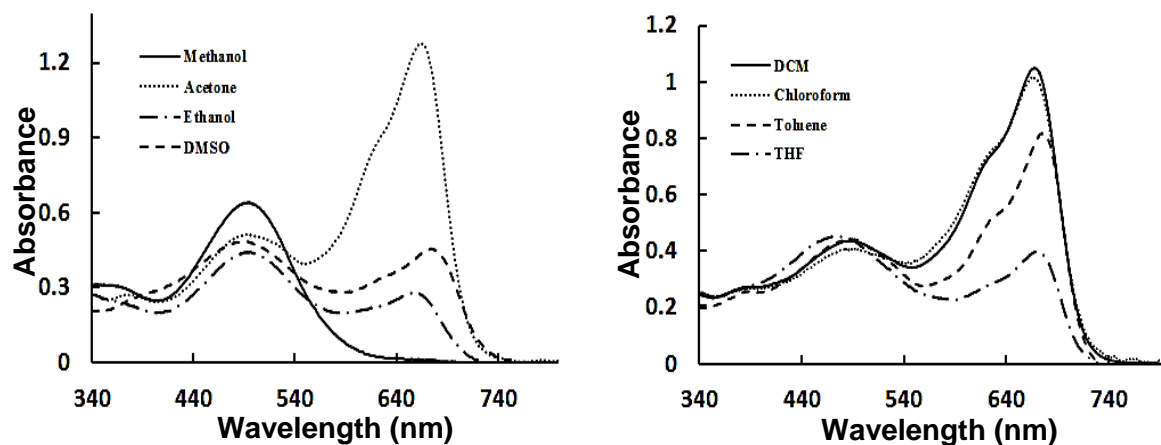


Figure 3.49. $3.22 \times 10^{-5} \text{ M } p\text{-SCH}_3\text{-H}_2\text{Dz}$ in solvents with dielectric constants above 20 (left) and solvents with dielectric constants below 20 (right).

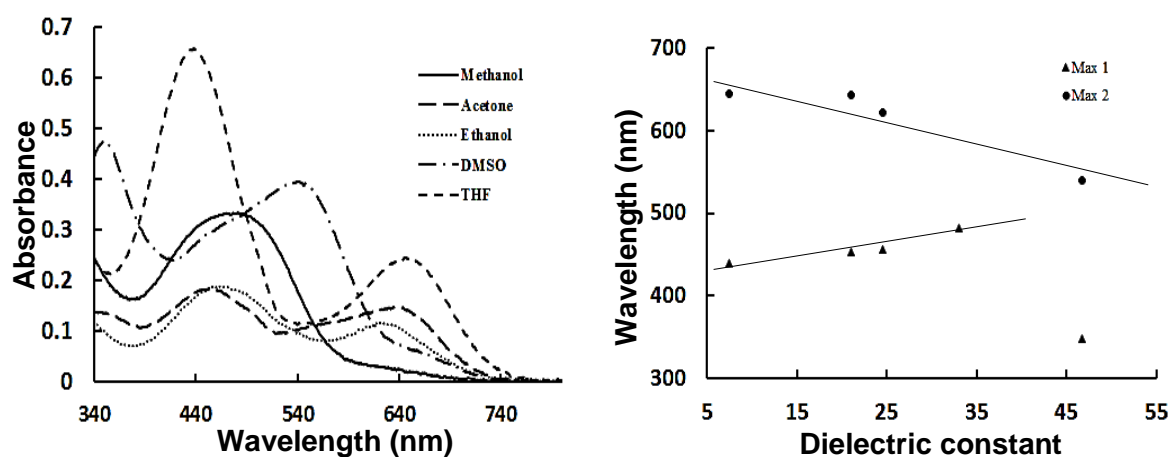


Figure 3.50. $3.23 \times 10^{-5} \text{ M } p\text{-COOH-H}_2\text{Dz}$ in solvents with dielectric constants above 20 (left). Plot of wavelengths of maximum absorption vs. dielectric constants (right).

For **H₂Dz**, as compared to the other species of this investigation, the least pronounced wavelength shifts are seen in the various solvents (Figure 3.48). λ_{\max} varies around 440 and 600 nm. Apart from small wavelength shifts the most significant difference is seen in relative intensities between the two absorbance bands. Both the methanol and THF solutions are observed to have almost similar molar extinction coefficients (ϵ) in both bands, whereas all the other solvents reveal a significantly higher ϵ in the low energy band. All these solutions are still green, howbeit slight differences in particular shade, see Image 3.3 (left).

Solvatochromism in ***p*-SCH₃-H₂Dz** is more pronounced in comparison with its unsubstituted parent compound, see Figure 3.49. Similarly, no real peak shift occurs, however, there is a clear shift in ϵ of the two characteristic dithizone peaks. As non-polar solvent environment promotes larger H₂Dz ϵ at longer wavelengths, so is observed for ***p*-SCH₃-H₂Dz**, although much more so for the latter. Here, the long wavelength peak (~ 660 nm) is completely absent in polar methanol environment, while on the contrary the short wavelength peak (~470 nm) is reduced to a small shoulder in DCM. The colour of these solutions are also shades of green, except for DMSO and ethanol, which appears brownish (mixture of green and orange) and the methanol solution that is orange-red, see Image 3.3 (right).

As for ***p*-COOH-H₂Dz**, the solvatochromic effect is most pronounced. Here, although being able to use only polar solvents due to the compound's solubility, not just shifts in ϵ are seen, but also significant wavelength shifts, see Figure 3.50 (left). In both methanol and DMSO the long wavelength peak (> 600 nm) is reduced to virtually zero. λ_{\max} in methanol for this compound lies centered around 481 nm, while the corresponding peak in acetone represents the maximum blue-shift, being at 453 nm, and that of DMSO at 540 nm, i.e. the most red-shifted peak. From results in this study this gives a shift of 87 nm in total, caused by merely changing solvents. Image 3.1 colourfully illustrates the solvatochromism in this new compound, varying from shades of green to orange (methanol) and pink (DMSO). From Figure 3.50 (right) the interesting trend may be seen whereby λ_{\max} of the long wavelength peak decreases with increasing dielectric constant, while the opposite is true for the short wavelength peak. An outlier is seen in DMSO, with a high energy peak as low as *ca* 350 nm.

SCH₃-HDz was the last compound for which solvatochromism was investigated, see UV-vis spectra in Figure 3.51. Image 3.2 shows various shades of orange and pink. Where-as in the previous dithizones with substituents on the phenyl rings, the solvatochromic shifts here occur by disappearance of one of the two characteristic ~470 & ~620 nm dithizone bands. The S-methylated compound has only one visible absorbance band, which blue-shifts with increase in dielectric constant of the solvent. In chloroform, THF and acetone only one peak is

seen at *ca* 540 nm. In methanol and ethanol this peaks disappears, although not completely, and reappears at *ca* 410 nm.

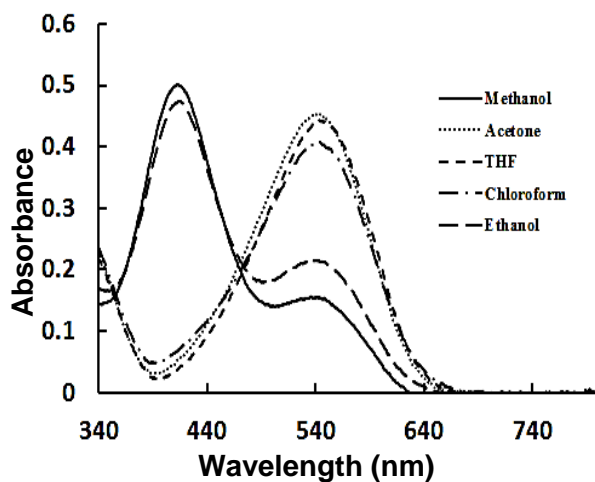


Figure 3.51. Spectra of 3.24×10^{-5} M S-methylated-dithizone in various solvents.

Earlier, by means of Density Functional Theory calculations, it was conclusively shown that the solvatochromic effect may be ascribed to different tautomers (tautomers 1 and 2, see Section 2.3.2 and Figure 3.40) in solution.¹³⁷ The colour change was attributed to intramolecular proton transfer from the backbone N to the central S.

In SCH₃-HDz one proton is essentially replaced by a methyl group. The consequence is that due to now absence of typical backbone π -conjugation, this compound no longer has two absorbance bands, but only one, at lower wavelengths. Different isomers may also here exist in solution, and also at different ratio's. The incomplete disappearance of the 540 nm peak in alcohols (Figure 3.51) is ascribed to the existence of a tautomeric equilibrium in solution, in an approximate ratio of 1:3, as roughly judged by relative peak heights. The exact geometries of these tautomers/isomers have as yet not been established, and remain outstanding as future computational chemistry project, whereby combined Time-Dependant Density Functional Theory and relative computed energies should resolve this matter.

¹³⁷ K. G. Von Eschwege, J. Conradie, A. Kuhn, *J. Phys. Chem. A*, 1463, **115** (2011).

3.5.3. Electrochromism

Comparative cyclic voltammetry (cv) and spectro-electrochemistry studies of the H₂Dz and *p*-SCH₃-H₂Dz ligands, and the PhHg(HDz) and PhHg(*p*-SCH₃-HDz) complexes are presented in this section. As reviewed in the Literature chapter, cv studies on PhHg(HDz)¹³⁸, Co(HDz)₃, H₂Dz¹³⁹ and its derivatives had already been reported by our group, also spectro-electrochemical characterization of the two Hg and Co complexes. Spectro-electrochemistry investigation into the electrochromic properties of the free ligands, H₂Dz and *p*-SCH₃-H₂Dz, and the PhHg(*p*-SCH₃-HDz) complex is now also for the first time reported here. (The *p*-COOH derivatives were not included in this particular section, as initial tests revealed complexity that is beyond the scope of this investigation. Observed overlapping redox waves are ascribed to the two carboxylic acid substituents.)

Before characterizing the electrochromic properties of the former compounds it is necessary to first explain the sections of the cyclic voltammograms that relate to corresponding spectro-electrochemistry scans (Figures 3.54 to 3.56), i.e. only the initial positive quarter of the cv's, and only initial negative scan quarters. Figure 3.52 gives the positive and negative cv scans of H₂Dz and *p*-SCH₃-H₂Dz, while corresponding peak potentials are listed in Table 3.4. Scheme 3.4 indicates electrochemical changes of species involved, with wave numbers corresponding to the cv's. Relevant oxidation peaks are indicated in Arabic numerals while Roman numerals denote reduction waves.

H₂Dz is seen to undergo two oxidations, at 624 and 1026 mV, the former being representative of disulphide formation. In *p*-SCH₃-H₂Dz the first reduction peak occurs, as expected due to the electron-donating ability of the -SCH₃ substituents, at the smaller potential of 430 mV. Instead of seeing only the two backbone oxidations, there are now two additional oxidation waves, which are ascribed to the two SCH₃ groups. It may however not unambiguously be said which of the remaining three peaks are centered around which molecular fragment. Scheme 3.4 places the two substituent centered oxidations in the 3rd and 4th positions.

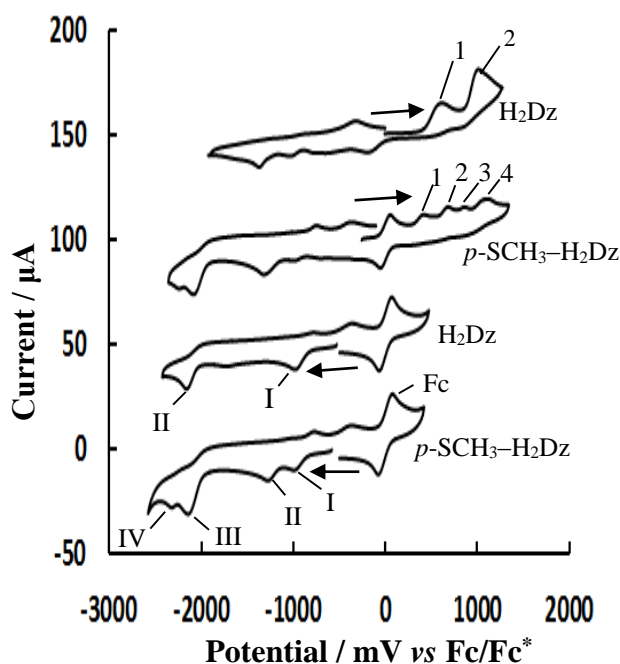
Figures 3.54 and 3.55 show the color changes (changes in absorbance spectra) during both oxidation (left) and reduction (right) scans of the above two ligands. Although the spectra of the *p*-SCH₃ (Fig.3.55) derivative have some added shoulders, in both ligands the first significant color changes are observed at about the same potentials, namely at 625 and 600 mV. This potential is associated with disulphide formation. The second transitions are seen at 850 mV. In both cases essentially colorless decomposition products form at 1500 mV. In *p*-SCH₃-H₂Dz one additional color variation is noticed at 1275 mV. The less pronounced changes at higher potentials in the latter compound is indicative of substituent oxidations, which is expected to

¹³⁸ K. G. von Eschwege, L. van As, J. C. Swarts, *Electrochim. Acta*, 10064, **56** (2011).

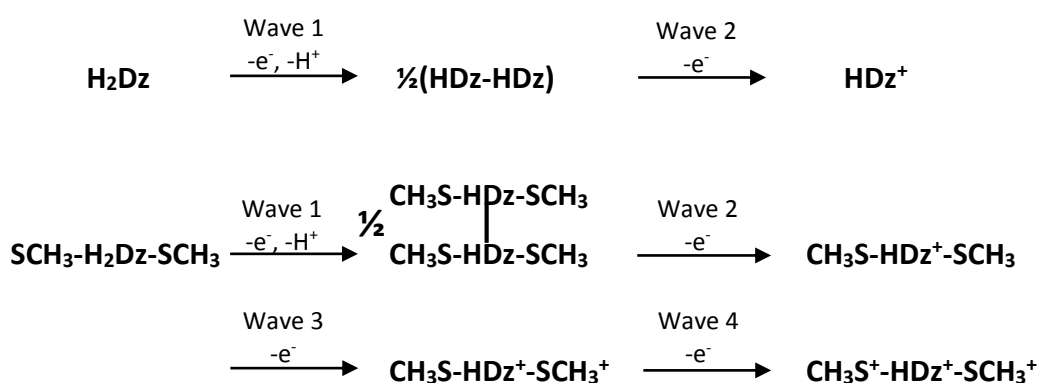
¹³⁹ K. G. von Eschwege, J. C. Swarts, *Polyhedron*, 1727, **29** (2010).

have a less significant effect on the color of the compound, as opposed to electronic changes that may occur along the π -conjugated backbone.

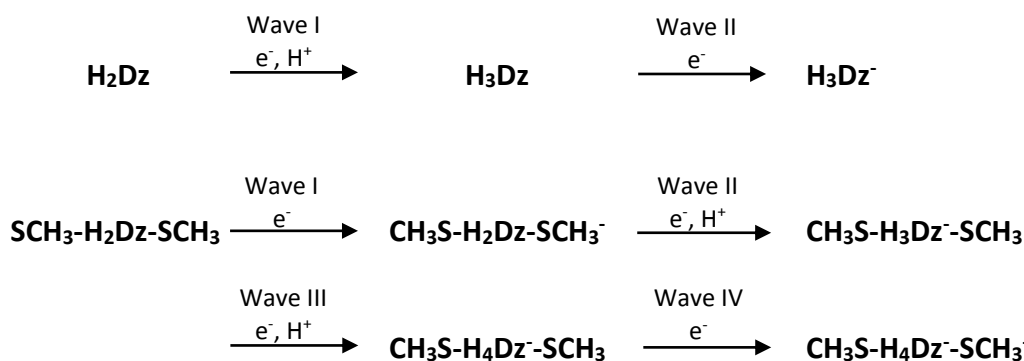
Figure 3.52. Cyclic voltammograms at 0.500 V s⁻¹ scan rates for 0.5 mM H₂Dz and *p*-SCH₃-H₂Dz in DCM, with 0.1 M [NBu₄][B(C₆F₅)₄] as supporting electrolyte, a glassy carbon working electrode and Pt reference and auxiliary electrodes. Positive and negative scans are indicated by arrows. The reversible redox wave centred around 0 mV is that of the internal reference standard, ferrocene. The H₂Dz cv is published, but inserted for comparison.¹³⁹



LIGAND OXIDATIONS (positive scans):



LIGAND REDUCTIONS (negative scans):



Scheme 3.4. Electrochemical oxidations (top) and reductions (bottom) of H₂Dz and *p*-SCH₃-H₂Dz.¹³⁹

Wave labels correspond to those in Figure 3.52.

Table 3.4. Anodic and cathodic peak potentials vs. Fc/Fc^+ for H_2Dz and $p\text{-SCH}_3\text{-H}_2\text{Dz}$ from a glassy carbon working electrode at 20 °C. Scan rate = 0.500 V s^{-1} , in DCM. Arabic numerals indicate oxidation peak potentials and Roman numerals reduction peak potentials.

Peak	Positive scans		Negative scans	
	H_2Dz (mV)	$p\text{-SCH}_3\text{-H}_2\text{Dz}$ (mV)	H_2Dz (mV)	$p\text{-SCH}_3\text{-H}_2\text{Dz}$ (mV)
1	624	430		
2	1026	730		
3		884		
4		1113		
I			-960	-987
II			-2142	-1273
III				-2119
IV				-2307

The negative scans in Figure 3.52 illustrate electrochromism during reduction. H_2Dz goes from green to orange at $E < -700 \text{ mV}$. The same is seen for the SCH_3 derivative, however at $E < -800 \text{ mV}$, which is expected, since this electron donating substituent resists reduction along the ligand back bone. Final color changes are seen at -1800 and -1900 mV respectively. $p\text{-SCH}_3\text{-H}_2\text{Dz}$ has, as may also be seen on the cv (Wave II), an additional reduction, which is reflected in the added color at -1275 mV .

It should be noted that spectro-electrochemical scans associated with color changes are often seen at potentials slightly different, however in the same region than what is seen on corresponding cv's. The reason for this is because spectro-electrochemical scans are obtained at very low scan rates, as compared to the very fast rates performed during cv's. The latter results in electrochemical response time variations, and therefore differences that may sometimes be seen between the two sets of data.

Figure 3.53. Cyclic voltammograms at 0.500 V s^{-1} scan rates for 0.5 mM $\text{PhHg}(\text{HDz})$ and $\text{PhHg}(p\text{-SCH}_3\text{-HDz})$ in DCM, with 0.1 M $[\text{NBu}_4][\text{B}(\text{C}_6\text{F}_5)_4]$ as supporting electrolyte, a glassy carbon working electrode, Pt reference and auxiliary electrodes. Positive and negative scans are indicated by arrows. The reversible redox wave centred around 0 mV is that of the internal reference standard, ferrocene. The $\text{PhHg}(\text{HDz})$ cv is published, but inserted for comparison.¹³⁸

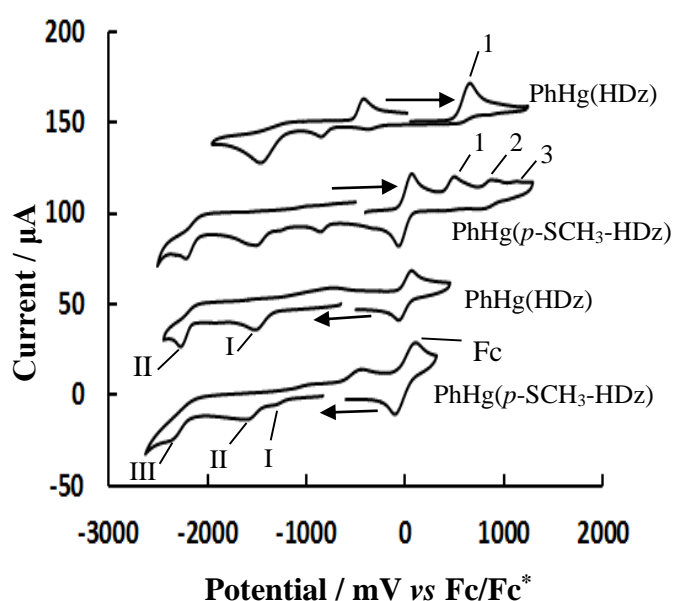
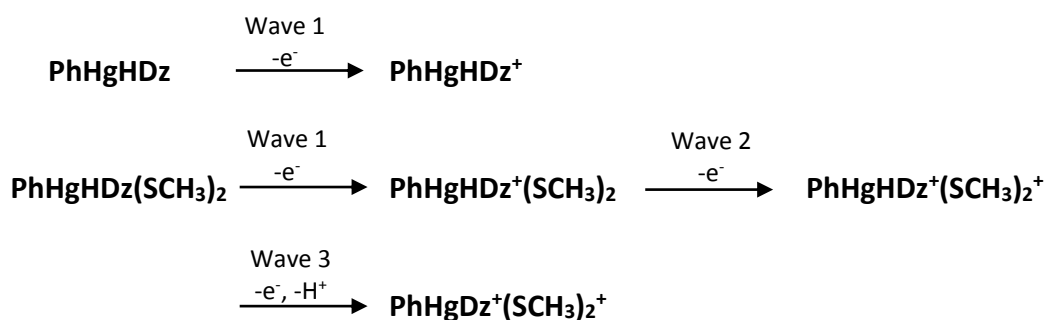


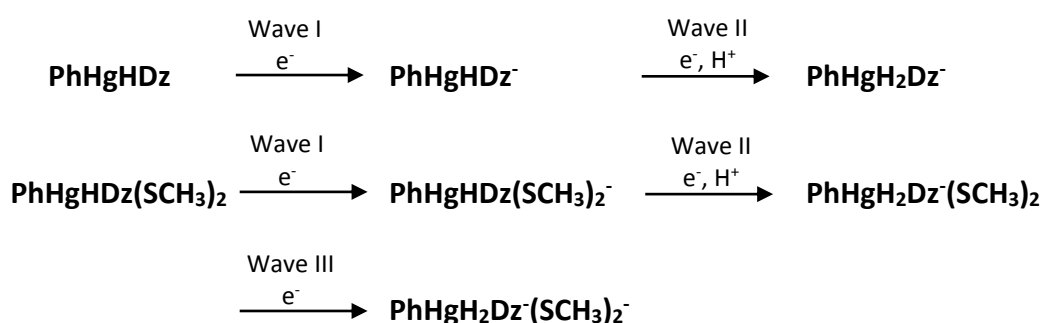
Table 3.5. Anodic and cathodic peak potentials vs. Fc/Fc⁺ for PhHg(HDz) and PhHg(*p*-SCH₃-HDz) from a glassy carbon working electrode at 20 °C. Scan rate = 0.500 V s⁻¹, in DCM. Arabic numerals indicate oxidation peak potentials and Roman numerals reduction peak potentials.

Peak	Positive scans		Negative scans	
	PhHg(HDz) (mV)	PhHg(<i>p</i> -SCH ₃ -HDz) (mV)	PhHg(HDz) (mV)	PhHg(<i>p</i> -SCH ₃ -HDz) (mV)
1	669	538		
2		910		
3		1164		
I			-1511	-1279
II			-2265	-1571
III				-2389

COMPLEX OXIDATIONS (positive scans):



COMPLEX REDUCTIONS (negative scans):



Scheme 3.5. Electrochemical oxidations (top) and reductions (bottom) of PhHg(HDz) and PhHg(*p*-SCH₃-HDz). Wave labels correspond to those in Figure 3.53.¹³⁸

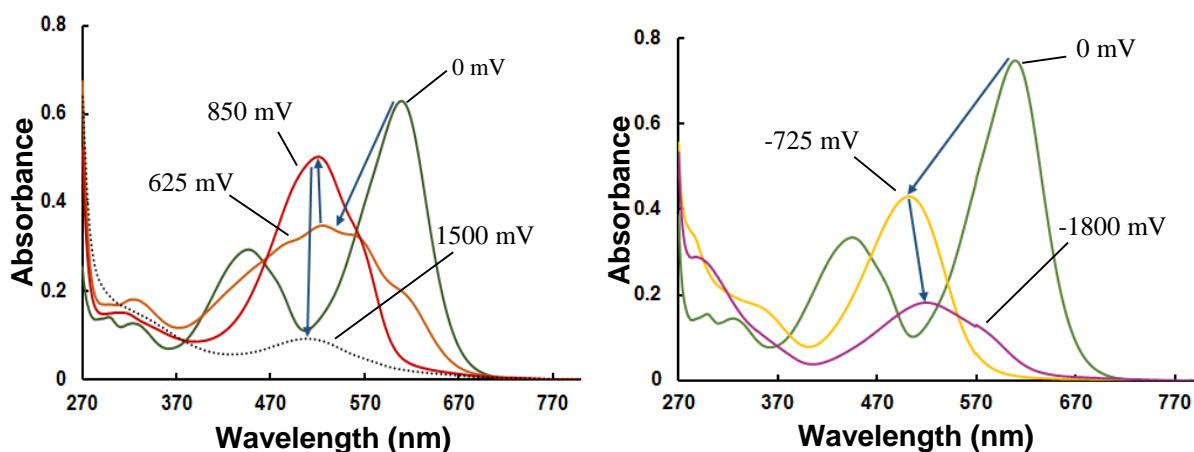


Figure 3.54. DCM solution of 1 mM H_2Dz for positive scan from 0 to 1500 mV (left) and negative scan from 0 to -1800 mV(right).

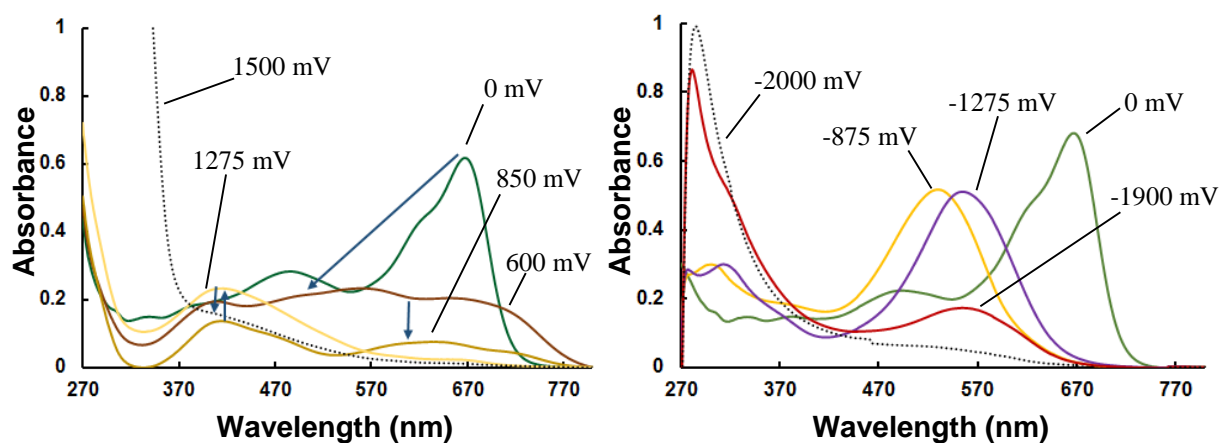


Figure 3.55. DCM solution of 1 mM $p-SCH_3-H_2Dz$ for positive scan from 0 to 1500 mV (left) and negative scan from 0 to -2000 mV(right).

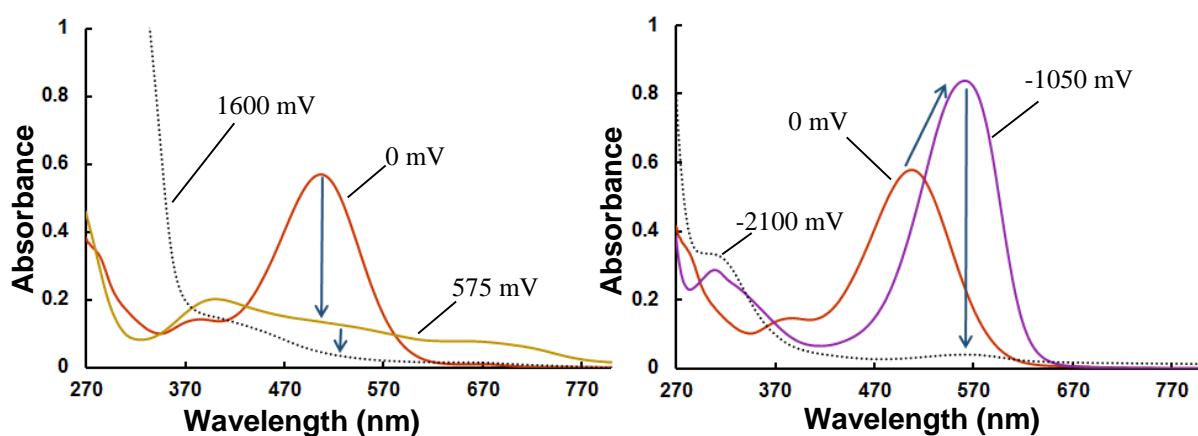


Figure 3.56. DCM solution of 1 mM $PhHg(p-SCH_3-HDz)$ for positive scan from 0 to 1600 mV (left) and negative scan from 0 to -1850 mV (right).

As opposed to the free ligand with two protons and thus two oxidations waves, the phenylmercury dithizonate complex has only one imine proton, and consequently also only one oxidation, wave at 669 mV. The two added SCH₃ groups also here in the complex give rise to two added oxidation waves, namely at 910 and 1164 mV. Its first oxidation is at 538 mV, 131 mV lower than in the unsubstituted complex. The more electron rich complex is indeed expected to more readily undergo oxidation.

Along the path of reduction two peaks are observed for PhHgHDz (-1511 & -2265 mV) and three for PhHg(*p*-SCH₃-HDz) (-1279, -1571 & -2389 mV). The first PhHgHDz reduction at -1511 mV is paralleled by the second (-1571 mV) reduction in the second compound, as the latter would be less readily reduced. This brought the conclusion that its first reduction wave, at -1279 mV, is ascribed to a substituent centred reduction.

Figure 3.56 shows the corresponding spectro-electrochemistry of PhHg(*p*-SCH₃-HDz) only, with positive (oxidation) scans at the left, and negative (reduction) scans at the right. (The spectro-electrochemistry of PhHgHDz is already published and discussed in the Literature chapter, and therefore not again shown here.) During oxidation the first significant color change occurs at 575 mV, after which decoloration, most probably due to decomposition, takes place at 1600 mV. No significant color changes associated with the two substituent oxidations are seen. The reduction pathway shows two major electrochromic color changes, namely at -1050 mV and decoloration at -2100 mV. Although more single-electron reductions evidently did take place, these were not all associated with color changes, and therefore most probably substituent-centered, as was seen along the oxidation path.

3.5.4. Halochromism

In this section on halochromism, H₂Dz, *p*-SCH₃-H₂Dz, *p*-COOH-H₂Dz, and *p*-CH₃-H₂Dz were involved. At the outset, obedience to Beer's law was tested over a large range of concentrations, as to ensure not taking measurements at concentrations where deviations impact negatively on results.

Typically, H₂Dz (0.0104 g, 0.04 mmol) was dissolved in methanol, with the help of an ultrasonic bath (15 min), in a 50.0 mL volumetric flask and filled to the mark, to obtain a 8.04 × 10⁻⁴ M stock solution. Then 2.00, 3.00, 4.00, 5.00, 6.00, and 7.00 mL aliquots were pipetted into a series of 50.0 mL volumetric flasks and filled to the mark with methanol, giving concentrations (3.2, 4.8, 6.4, 8, 9.7 and 11) × 10⁻⁵ M. Figure 3.57 shows the Beer-Lambert relationships for the four compounds under consideration, in methanol. No deviation is seen in absorbance values, even in absorbances as high as 3. The consequence is that such brightly coloured more concentrated solutions could with safety be used in tests to follow.

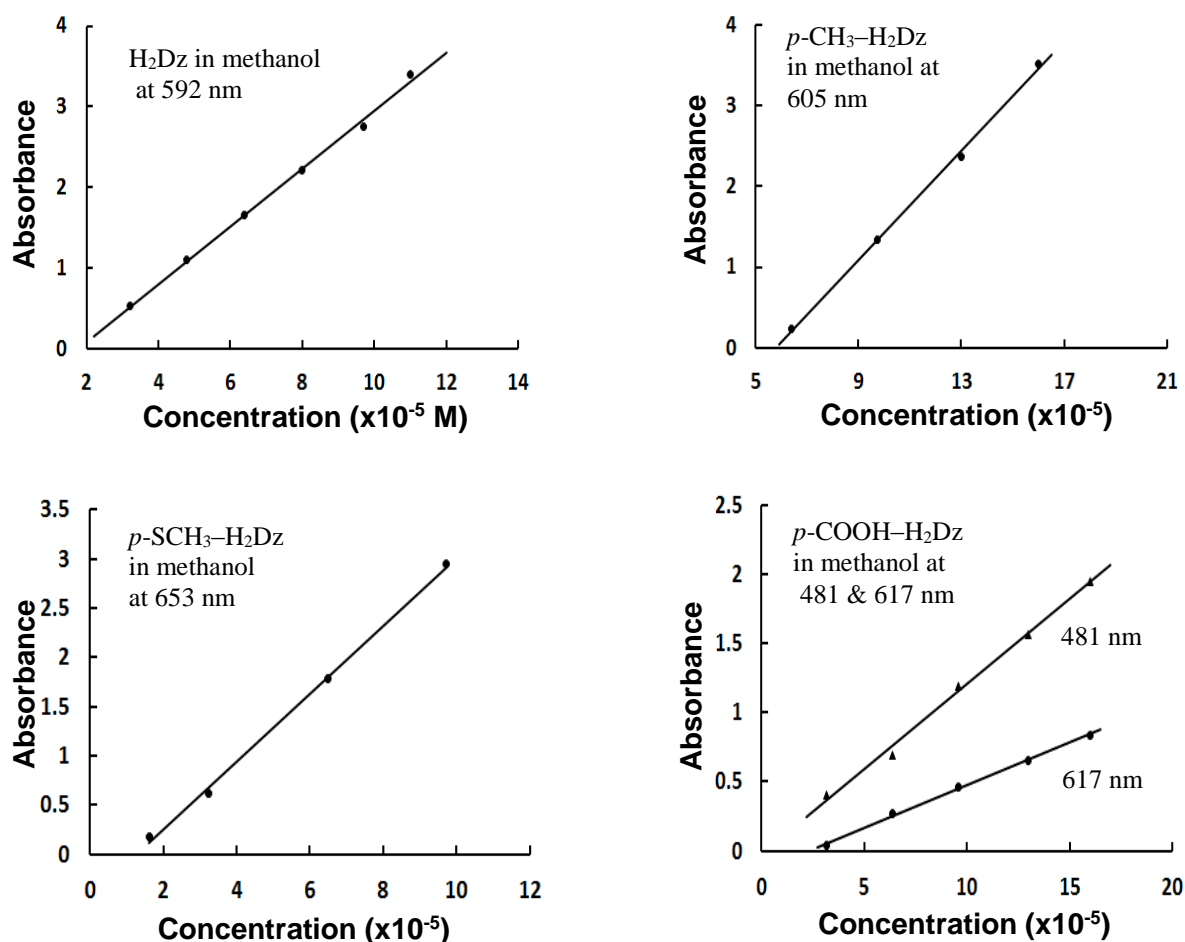


Figure 3.57. Beer's Law relationship for various dithizone concentrations.

The green methanolic solution of dithizone at a fairly high concentration was titrated with KOH and the colour change was from green to orange. Reversal was accomplished by titration of the orange dithizonate solution with methanolic HCl, with the colour changing back to green.

Typically of all four compounds; from the stock solution of 8.04×10^{-4} M H₂Dz, 6.00 mL was pipetted into a 50.0 mL volumetric flask and filled to the mark with methanol, to obtain a 9.65×10^{-5} M concentration. Then 25.0 mL of the latter solution was titrated against 9.65×10^{-5} M methanolic KOH solution. UV-Vis spectrophotometric titrations are presented in Figures 3.58 to 3.61 (left). H₂Dz peaks at λ_{\max} 450 & 592 nm disappear with the addition of KOH solution, while the HDz⁻ peak appears at 470 nm. The titration end point at close to 25 mL is seen in the spectrophotometric titration plot in Figure 3.58 (right).

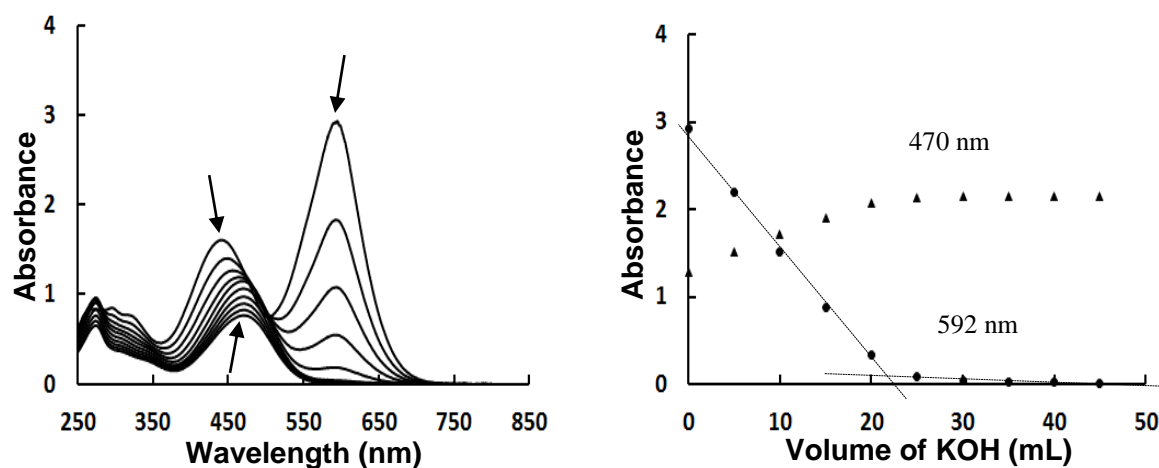


Figure 3.58. Titration of H_2Dz against KOH (left) in methanol. Corrected absorbance vs. V_{KOH} (right). Both concentrations were 9.65×10^{-5} M.

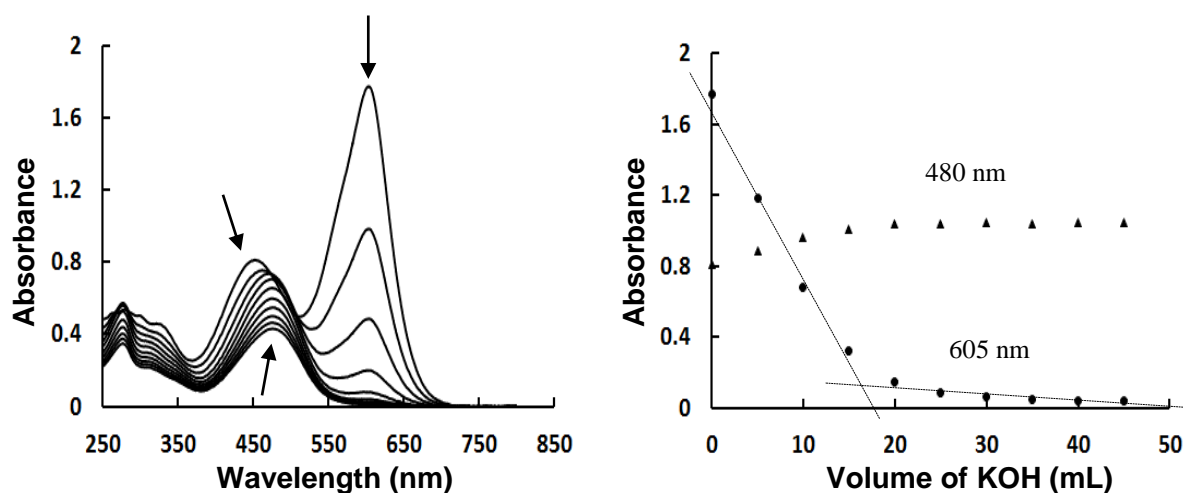


Figure 3.59. $p\text{-CH}_3\text{-H}_2\text{Dz}$ titrated against KOH (left) in methanol. Corrected absorbance vs. V_{KOH} (right). Both concentrations were 6.49×10^{-5} M.

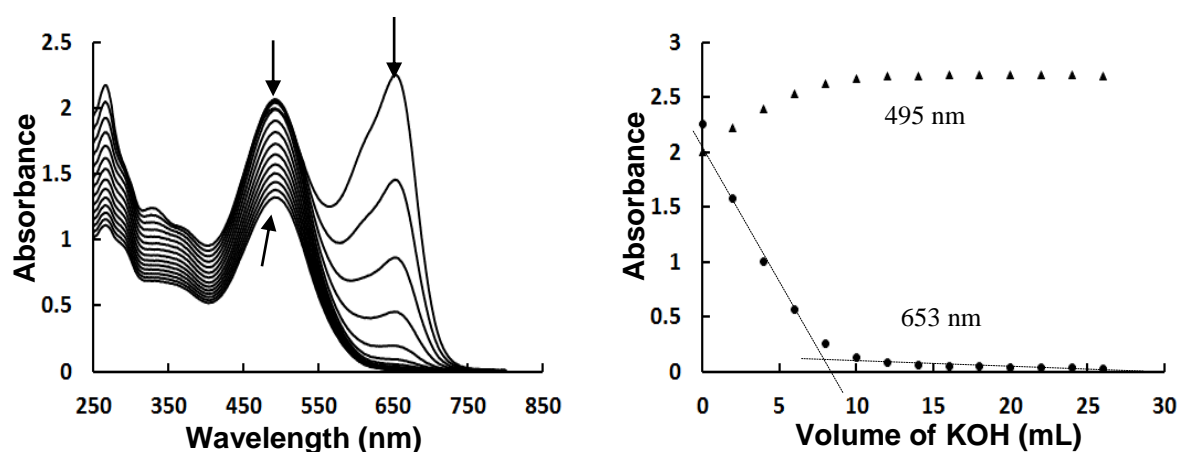


Figure 3.60. $p\text{-SCH}_3\text{-H}_2\text{Dz}$ titration against KOH (left) in methanol. Corrected absorbance vs. V_{KOH} (right). Both concentrations were 9.72×10^{-5} M.

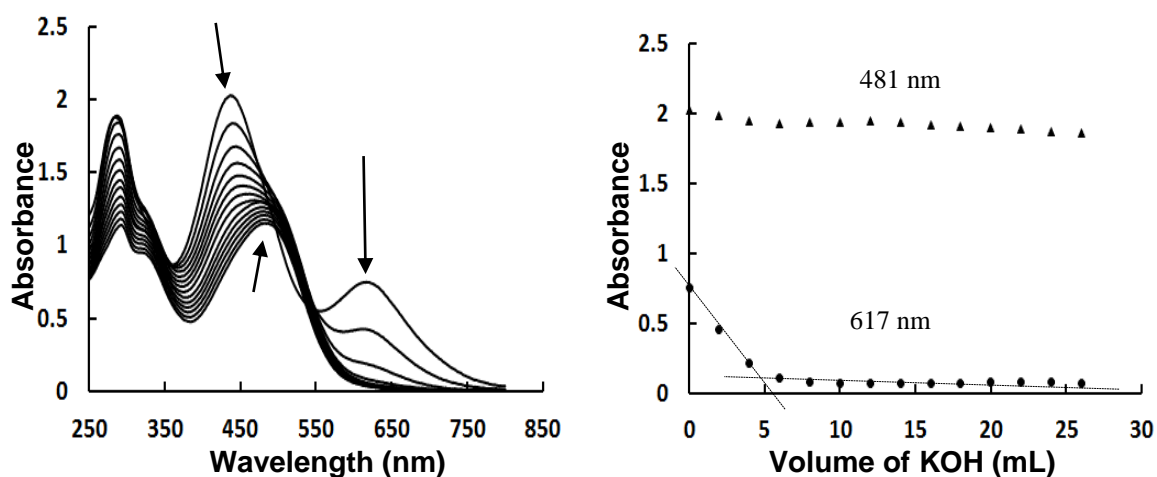


Figure 3.61: *p*-COOH-H₂Dz titration against KOH (left). Corrected absorbance vs. V_{KOH} (right). Both concentrations were 9.72×10^{-5} M.

The overall tendency for all the above derivatives of dithizone is to undergo reversible halochromism in the same way, however surprisingly, not at the same quantity of base added. The endpoint of the unsubstituted dithizone lies at almost 25 mL, i.e. close to stoichiometrically equivalent reagent amounts. For the *p*-CH₃ derivative less than 20 mL base was required for a complete color change, for *p*-SCH₃ less than 10, and for *p*-COOH less than 5 mL. Seen in isolation, this could have posed a serious problem to explain, for how could color changes be justified with the amount of base added being significantly less than what is stoichiometrically required for complete mono-deprotonation of all the H₂Dz molecules present? However, by now knowing how extremely sensitive dithizone is to a variety of external stimuli, i.e. *via* its characteristic intramolecular proton transfer to exist as either tautomer 1 or 2, it is now hypothesized that yet an additional form of chromism may come into play here, namely ionochromism.

Roughly, the group electronegativities of the four species in basic solution here are:



Color changes, as seen in the ratio of dithizone to OH⁻, are noted to follow the same trend:



Although uncertain at this stage, it is concluded that the mere generation of less than stoichiometric amounts of dithizonate anions during base addition results in these anions more readily catalyzing proton transfer in the still fully protonated parent compound (tautomer 1), to form tautomer 2. Addition of more base beyond this point will indeed continue the process of deprotonation, but this is not visible, as the spectra of tautomer 2 and that of the dithizonate anion, HDz⁻, overlap closely.

Also, two additional interesting first time observations were that of:

- methanolic solutions of *p*-COOH-H₂Dz changing from green to orange simply by sucking it up in a new pasteur pipette. The solutions however remain green if the pipette has prior been used, though cleansed before this test, and
- the same colour changes manifested when this solution was passed through new silica gel.

Figure 3.62 shows the colour changes as a consequence of various external contact surfaces.

These colour changes are suggested to also be halochromic by nature, as it is known that new glass surfaces and silica gel (both being silica oxides) are not pH neutral. Consequently the extreme sensitivity of dithizones to external stimuli of diverse kinds serves as a visibly very clear sensor for indicating surfaces that are – in this case, slightly basic.

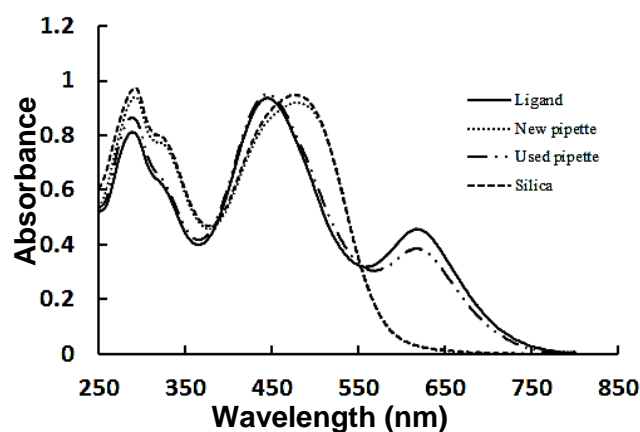


Figure 3.62. UV-vis of the methanolic solution of *p*-COOH-H₂Dz.

3.5.5. Concentratorchromism

In this section three dithizone derivatives were dissolved at different concentrations and UV-vis spectra recorded. All three ligands underwent changes of colour from orange to green with increase in concentration. Concentratorchromism was not observed in all solvents, for instance H₂Dz is only concentratorchromic in methanol, see Image 3.4. *p*-SCH₃-H₂Dz and *p*-COOH-H₂Dz, in turn, are concentratorchromic in most polar solvents, see Images 3.5 to 3.9.

Solutions were prepared by, for instance dissolving *p*-COOH-H₂Dz (0.0132 g, 0.04 mmol), with the aid of an ultrasonic bath (5 min), in 50.0 mL THF. Then was pipetted 0.50, 1.00, 2.00, 4.00, 6.00, and 8.00 mL into a series of 50.0 mL volumetric flasks and filled to the mark with THF. The same was done with ethanol, acetone, DMSO and methanol. Figure 3.63 shows the UV-vis spectra for different concentrations of *p*-COOH-H₂Dz in THF.

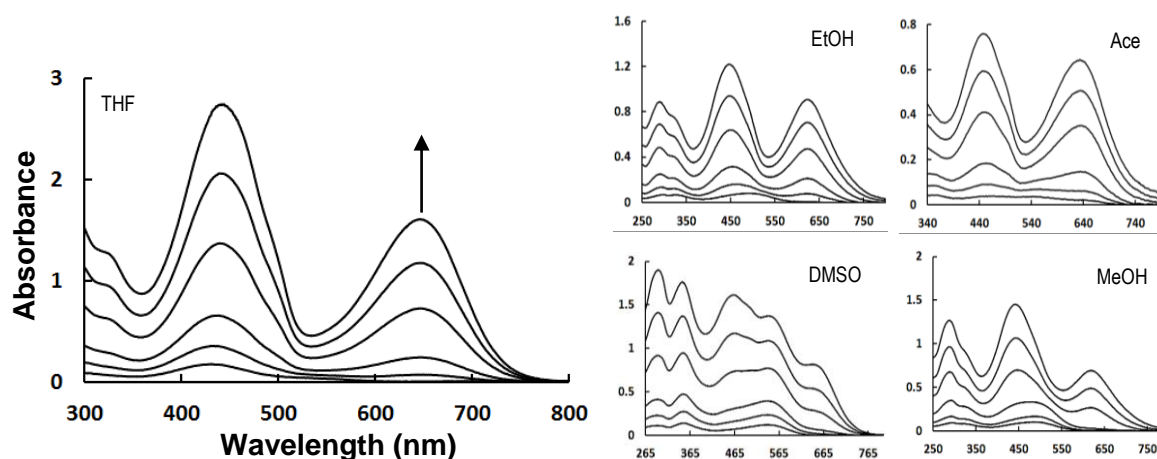


Figure 3.63. Spectra of *p*-COOH-H₂Dz in THF (left), with concentrations (0.8, 1.6, 3.2, 6.5, 9.7 & 13) × 10⁻⁵ M (from bottom to top). Related overlay spectra are also shown for ethanol, acetone, DMSO & methanol solutions.

Low concentration THF solutions of *p*-COOH-H₂Dz are orange in colour, with only one peak (440 nm) for low concentrations (0.8 to 1.6 × 10⁻⁵ M). A second absorption maximum emerges at 645 nm as the concentration increases from 3.2 to 13 × 10⁻⁵ M, and the solutions turn green. Similar colour changes were observed in ethanol, where the higher concentration second peak emerges at 622 nm. Colour changes are the same in acetone and methanol, the latter however being more yellow than orange. DMSO solutions differ by going from light pink to brown-red. It also gives rise to a new peak at longest wavelength, namely *ca* 655 nm.

p-SCH₃-H₂Dz solutions go from orange-red to blue-green with increase in concentration. In Figure 3.64 (left) the ethanol solutions clearly has only the one peak at 500 nm at low concentration, while at higher concentrations another peak starts growing around 657 nm, and becomes dominant. In *p*-COOH-H₂Dz solutions the long wavelength absorbance band never becomes dominant. Solvatochromism in *p*-SCH₃-H₂Dz is therefore more pronounced. The same tendency is seen for the other three solvents, THF, DMSO and methanol, see also Images 3.8 and 3.9. Clearly, as was the case for the *p*-COOH derivative, methanol also here is the solvent that stabilizes tautomer 2 (orange) most strongly, as may be seen by the orange colour that persists even at higher concentrations at which other solvents are already mostly green, having reverted to tautomer 1.

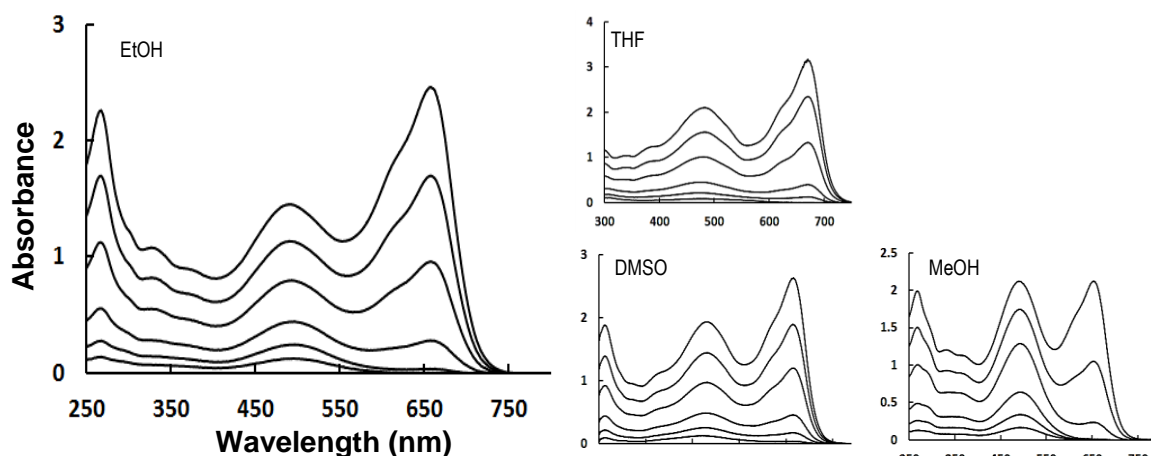


Figure 3.64. *p*-SCH₃-H₂Dz spectra in EtOH (left), with concentrations (0.8, 1.6, 3.2, 6.5, 9.7 & 13) × 10⁻⁵ M (from bottom to top). Related overlay spectra are also shown for THF, DMSO & methanol solutions.

Lastly, for purposes of comparison, H₂Dz and *p*-CH₃-H₂Dz were also investigated, in methanol solution. Also here, the concentratochromic response was very similar to the *p*-SCH₃-H₂Dz derivative, where the 452 nm peak is dominant at low concentration, and the 597 nm peak at high concentration, see Figure 3.65 and Image 3.4. The only difference is that the *p*-SCH₃-H₂Dz long wavelength peak starts growing at sooner than is the case for H₂Dz solutions.

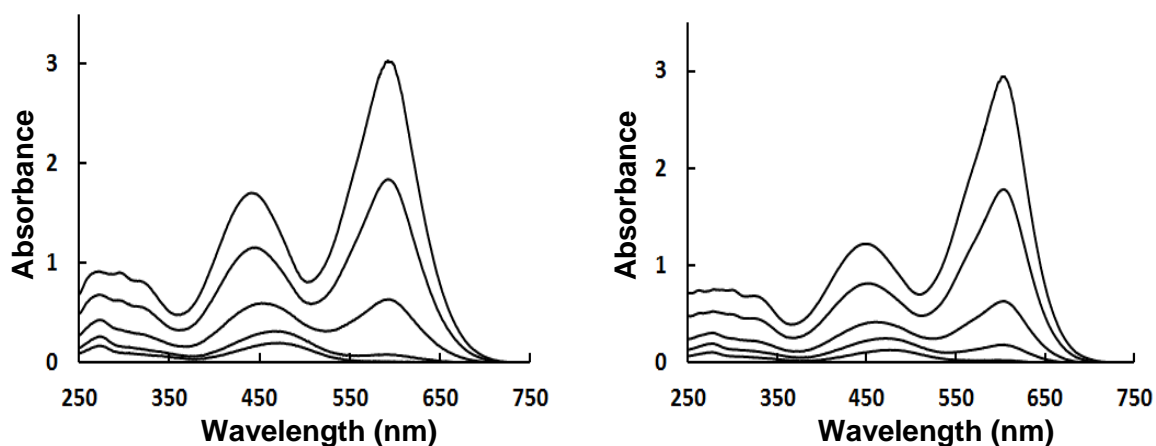


Figure 3.65. H₂Dz (left) and *p*-CH₃-H₂Dz (right) spectra, both in methanol, with concentrations (0.8, 1.6, 3.2, 6.5, & 9.7) × 10⁻⁵ M (from bottom to top).

In general then, as was elsewhere explained,¹³⁷ concentratochromism also here was observed for all four the present ligands, where the orange/yellow colour at low concentration is ascribed to tautomer 2 geometry where one imine proton on a nitrogen in the molecule backbone stays intact, while the other proton is intramolecularly transferred to the sulphur atom. Green solutions agree with tautomer 1, where both backbone protons are symmetrically placed on the two nitrogen atoms adjacent to the two phenyl rings. An exact explanation for this phenomenon occurring as a consequence of change in concentration is yet to be found.

3.5.6. Thermochromism

Of the three main dithizone ligands that were studied, namely H₂Dz, *p*-COOH-H₂Dz and *p*-SCH₃-H₂Dz, the latter was the only one that showed reversible thermochromism, and only in ethanol. Colour change due to temperature variation took place only at low concentrations of the ligand. A selected number of solvents, i.e. methanol, ethanol, acetone, THF and DMSO were tested for this type of chromism.

Solutions were prepared by dissolving *p*-SCH₃-H₂Dz (0.0139 g, 0.04 mmol) in 50.0 mL ethanol, with the aid of an ultrasonic bath (5 min), to obtain a concentration of 8×10^{-4} M. 1.00 mL of this solution was then pipetted into a 50.0 mL volumetric flask and filled to the mark with ethanol. The solution was heated from 10 to 70 °C and the observed colour change was from orange to green. In Figure 3.66 the orange solution shows λ_{max} at 495 nm partially disappearing, while the shoulder at 655 nm grows to almost 4 times its original height. There is an isosbestic point at *ca* 550 nm, indicative of one single species going to another, without the presence of intermediates. To test if the colour change was reversible, the green solution at 70 °C was allowed to cool to 25 °C. It reverted back to orange indeed. The heating and cooling cycles were successfully replicated three times to test repeatability. Based on previous arguments pertaining to solvato and concentratochromism, the conclusion is that the geometry change here is again; from that of tautomer 2 at low temperature to that of tautomer 1 at high temperature.

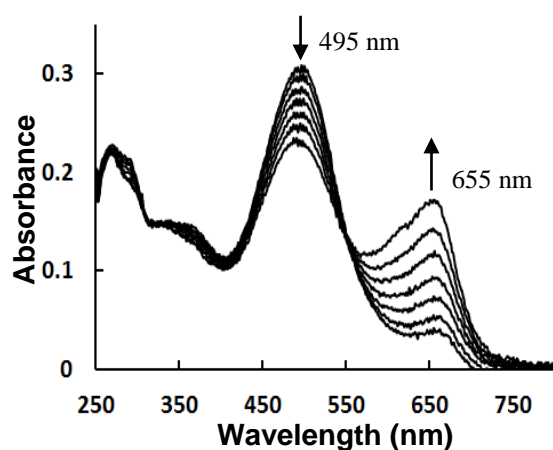


Figure 3.66. *p*-SCH₃-H₂Dz spectra in ethanol, while heating from 10 °C to 70 °C in 10°C steps.

3.5.7. Chronochromism

It was coincidentally discovered that solutions of SCH₃-HDz standing for a while gradually changes its colour in certain solvents. This led to the last form of chromism covered by this investigation, namely chronochromism, i.e. colour change that occurs over time. At low concentrations the change in colour was observed in chloroform. S-methylated-dithizone (0.0110

g, 0.04 mmol) was dissolved in chloroform in a 50.0 mL volumetric flask. 2.00 mL of this solution was pipetted into another 50.0 mL volumetric flask, to obtain a concentration of 3.2×10^{-5} M. For the sake of consistency, readings were taken at 20°C over a period of 5 hours. The colour of the solution changed from pink to orange within 3 hours, see Image 3.12. Figure 3.67 shows the absorption maxima at 416 and 545 nm, with isosbestic points at 350 and 474 nm. The rate of the return reaction is 0.0077, which is comparable to the related reaction in PhHg(HDz) at the same temperature, see Figures 3.68 & 3.43

The SCH₃-HDz chronochromic colour change in chloroform took place in exactly the same “direction” as that observed during its photochromic *reverse* reaction (Figure 3.46) in ethanol, namely from pink to orange. In polar ethanol therefore, a photon of light is required to isomerize the molecule to the pink state, from where it auto-reverts to the orange state, while in chloroform the initial state in solution is pink, which then slowly reverts to orange. This may lead to the suggestion that the solid compound is in the pink geometry, while the orange geometry is favoured in solution.

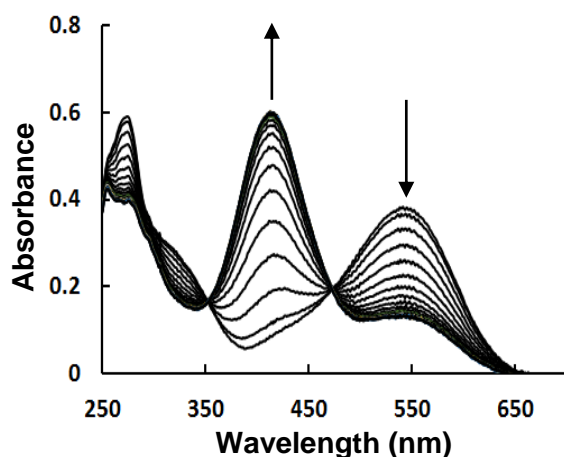


Figure 3.67. S-methylated-dithizone spectra in chloroform, observed over 5 hours.

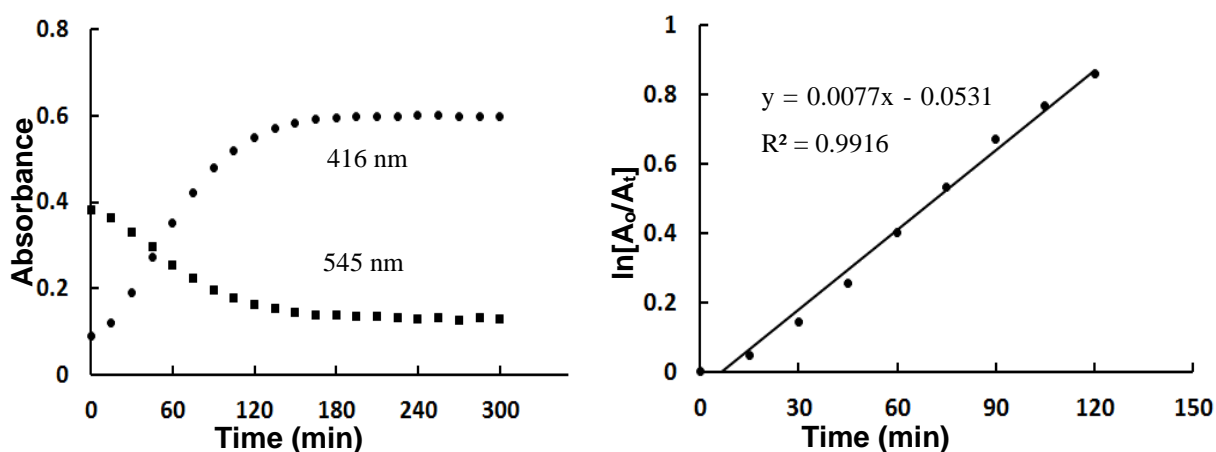


Figure 3.68. Kinetics of S-methylated-dithizone in chloroform, observed over 5 hours, at 416 and 545 nm.

4 ABSTRACT

Ever since discovery of the intensely colored dithizone ligand, H₂Dz, in the late 1800s it had been used extensively in aqueous solution trace metal analyses. However, hardly any effort had gone into developing the water-soluble derivative. The main aim of this study was to synthesize such derivatives by symmetrically placing *para* substituents that enhances water-solubility. The three substituents that were involved were the carboxylic acid, sulfanilic acid, and sulfonylacetamide groups. First step syntheses, up to nitroformazan formation, was successful for all three derivatives. Quality single crystals were grown for the former and latter species, but crystal data reported only for the carboxylic acid derivative, the only set being of publishable standard. The *p*-COOH derivative was the only one to be successfully synthesized and characterized up to the final dithizone and metal complex products. Spectral properties of both the free metals and ligands, as well as its complexes, limited the number of metals to be involved in consequent mole-ratio and continuous variation studies. These studies were embarked on, in order to find well-working and inexpensive undergraduate spectrometry practical's – in water media – that may be employed in training classes, apart from its wider analytical applications. The metals that were involved were Co, Ni, Pb, Hg and Ag, and for comparison purposes, the unsubstituted dithizone ligand was also employed, next to its *p*-COOH derivative. Resulting metal to ligand coordination ratio's were in agreement with mass spectrometry data, however, in some cases surprising, as discussed in detail in the Results chapter.

During these investigations seven chromisms associated with dithizone were observed, some expectantly and some unexpectedly. Presently there exists no other known compound with such varied and sensitive chromic behaviour. The new *p*-COOH-H₂Dz derivative gave rise to many of these discoveries. For comparison purposes the *p*-SCH₃-H₂Dz, *p*-CH₃-H₂Dz and unsubstituted derivatives were also employed where necessary. Also the derivative that are methylated at the backbone sulphur of the ligand, SCH₃-HDz, were brought into comparison. The former three were found to be halochromic, solvatochromic, electrochromic and concentratochromic as free ligands, while *p*-SCH₃-H₂Dz also revealed thermochromic behaviour, in ethanol alone. The mercury complexes of all three species were photochromic, as was the free SCH₃-HDz ligand itself – for the first time seen in a purely organic dithizone species. The latter was also chronochromic, i.e. changing color over time. The back reactions of the photochromic species were studied kinetically, during which solvent, concentration, temperature and varied substituents were compared.

5 FUTURE PERSPECTIVES

- The synthesis of the water-soluble dithizone is at its beginning stages, still leaving a variety of options yet to be pursued, i.e. revisiting the failed attempts in this investigation, but also employing different substituents.
- Based on what was observed for the $M_3 : L_1$ ratio in $\text{PhHg}(p\text{-COOPhHg-HDz})$, new options in multi-dentate dithizonate coordination patterns are hereby opened up, which may be further investigated.
- Other moieties, whether organic or inorganic, may be attached via the $-\text{COO}^-$ group, to form polymers or many-metal complexes, etc.
- Both the mole ratio and continuous variation methods/chemicals presented in this study may now be optimized for training undergraduate students in spectrometric techniques, as they are inexpensive and repeatable.
- Photochromism of the S-methylated dithizone now provides much scope for new studies where a variety of chemical moieties may be substituted on the dithizone sulphur atom, and studied kinetically, and for possible new chromic applications.
- In new evolving technologies, these chromisms may be applied as indicators, sensors, and tracers of metals.

Appendix

A. (*p*-COOH)nitroformazan

Table A2-1. Fractional Atomic Coordinates ($\times 10^4$) and Equivalent Isotropic Displacement Parameters ($\text{\AA}^2 \times 10^3$). U_{eq} is defined as 1/3 of the trace of the orthogonalised U_{ij} tensor.

Atom	x	y	z	U(eq)
O1	4749.4(8)	8489.0(9)	1524(1)	34.7(3)
O2	2533.8(7)	3821.3(10)	-4363.2(9)	31.0(3)
O3	2987.0(7)	2101.0(9)	-3490.8(10)	29.0(3)
N2	4568.9(7)	6294.1(10)	1367.4(10)	21.1(3)
N3	5000	7998.4(15)	2500	22.9(4)
N1	4537.2(8)	5193.9(11)	1290.9(11)	20.9(3)
C4	3301.1(9)	3711.7(12)	-2198.2(12)	20.7(3)
C7	5000	6738.4(17)	2500	19.4(4)
C3	3332.4(9)	4901.1(12)	-2097.0(12)	22.0(3)
C1	4095.1(9)	4730.3(12)	91.9(12)	20.0(3)
C5	3668.5(10)	3037.4(13)	-1145.8(13)	23.7(3)
C8	2913.5(9)	3166.5(12)	-3424.3(12)	20.6(3)
C6	4066.3(10)	3543.9(12)	3.5(13)	23.2(3)
C2	3729.6(9)	5416.7(13)	-954.4(13)	22.2(3)
C9	1146.8(12)	3413.8(15)	-2413.7(16)	35.1(4)
C10	1599.2(12)	4071.9(17)	-1240.3(17)	40.1(4)
C11	826.5(14)	4062.4(19)	-3575.8(19)	46.7(5)
O4	1042.5(14)	2395.9(13)	-2421.1(14)	73.5(6)

Table A2-2 Anisotropic Displacement Parameters ($\text{\AA}^2 \times 10^3$). The Anisotropic displacement factor exponent takes the form: $-2\pi^2[h^2a^{*2}U_{11} + \dots + 2hka \times b \times U_{12}]$

Atom	U11	U22	U33	U23	U13	U12
O1	53.4(8)	22.8(6)	23.8(6)	7.1(4)	16.8(5)	2.4(5)
O2	37.5(6)	31.1(6)	15.0(5)	-0.2(4)	6.5(5)	1.2(5)
O3	37.2(6)	23.9(6)	21.7(5)	-5.6(4)	12.0(5)	-2.6(5)
N2	22.8(6)	20.3(6)	19.8(6)	-1.8(4)	10.6(5)	0.1(5)
N3	27.4(9)	19.8(8)	20.0(8)	0	10.9(7)	0
N1	24.4(6)	21.7(6)	14.3(6)	-0.6(5)	8.2(5)	-0.2(5)
C4	20.6(7)	25.0(7)	15.0(6)	-2.6(5)	8.0(5)	-1.0(5)
C7	21.5(9)	19.3(9)	16.2(9)	0	8.8(8)	0
C3	23.7(7)	23.2(7)	15.1(6)	1.2(5)	7.0(6)	1.5(5)
C1	20.0(7)	25.0(7)	13.2(6)	-2.2(5)	7.2(5)	-0.8(5)
C5	29.8(8)	19.1(7)	19.9(7)	-0.6(5)	11.1(6)	-1.5(6)
C8	19.4(7)	23.6(7)	16.7(7)	-1.9(5)	7.6(5)	-0.9(5)
C6	28.0(7)	22.3(7)	15.7(7)	1.8(5)	8.5(6)	0.2(6)
C2	24.6(7)	20.6(7)	18.8(7)	-0.4(5)	9.1(6)	1.0(6)
C9	42.9(10)	32.6(9)	35.6(9)	-7.5(7)	24.3(8)	-4.9(7)
C10	41.3(10)	38.6(10)	42.6(10)	-14.4(8)	23.2(9)	-10.7(8)
C11	44.6(11)	51.2(12)	43.7(11)	6.0(9)	22.0(9)	9.2(9)
O4	139.3(17)	36.8(8)	46.4(9)	-14.3(7)	48.8(10)	-25.2(9)

Table A2-3 Bond Lengths.

Atom	Length/Å	Atom	Length/Å
O1 - N3	1.2225(13)	C4 - C8	1.4838(18)
O2 - C8	1.2796(17)	C7 - N2 ¹	1.3393(14)
O3 - C8	1.2602(18)	C3 - C2	1.3836(19)
N2 - N1	1.2892(17)	C1 - C6	1.391(2)
N2 - C7	1.3394(14)	C1 - C2	1.395(2)
N3 - O1 ¹	1.2226(13)	C5 - C6	1.386(2)
N3 - C7	1.473(3)	C9 - C10	1.493(2)
N1 - C1	1.4144(17)	C9 - C11	1.487(3)
C4 - C3	1.395(2)	C9 - O4	1.204(2)
C4 - C5	1.3918(19)		

Symmetrical transformation used to generate equivalent atoms:

$$^11-X,+Y,1/2-Z$$

Table A2-4 Bond Angles.

Atom	Angle/°	Atom	Angle/°
N1 - N2 - C7	116.54(13)	C6 - C1 - N1	116.51(12)
O1 - N3 - O1 ¹	124.02(17)	C6 - C1 - C2	121.16(13)
O1 - N3 - C7	117.99(9)	C2 - C1 - N1	122.30(13)
O1 ¹ - N3 - C7	117.99(9)	C6 - C5 - C4	120.19(13)
N2 - N1 - C1	116.25(12)	O2 - C8 - C4	117.32(13)
C3 - C4 - C8	119.99(12)	O3 - C8 - O2	123.57(12)
C5 - C4 - C3	119.97(12)	O3 - C8 - C4	119.09(12)
C5 - C4 - C8	119.98(13)	C5 - C6 - C1	119.28(13)
N2 ¹ - C7 - N2	134.35(19)	C3 - C2 - C1	119.03(14)
N2 ¹ - C7 - N3	112.82(9)	C11 - C9 - C10	117.55(16)
N2 - C7 - N3	112.82(9)	O4 - C9 - C10	121.32(17)
C2 - C3 - C4	120.37(13)	O4 - C9 - C11	121.13(17)

Symmetrical transformation used to generate equivalent atoms:

$$^11-X,+Y,1/2-Z$$

Table A2-5 Torsion Angles.

Atom (s)	Angle/°	A	Angle/°
O1 - N3 - C7 - N2 ¹	168.51(9)	C7 - N2 - N1 - C1	-178.86(10)
O1 ¹ - N3 - C7 - N2	168.51(9)	C3 - C4 - C5 - C6	-0.1(2)
O1 ¹ - N3 - C7 - N2 ¹	-11.49(9)	C3 - C4 - C8 - O2	-7.4(2)
O1 - N3 - C7 - N2	-11.50(9)	C3 - C4 - C8 - O3	171.29(13)
N2 - N1 - C1 - C6	179.38(13)	C5 - C4 - C3 - C2	0.2(2)
N2 - N1 - C1 - C2	1.5(2)	C5 - C4 - C8 - O2	175.49(13)
N1 - N2 - C7 - N2 ¹	0.22(9)	C5 - C4 - C8 - O3	-5.8(2)
N1 - N2 - C7 - N3	-179.77(9)	C8 - C4 - C3 - C2	-176.93(13)
N1 - C1 - C6 - C5	-177.82(13)	C8 - C4 - C5 - C6	177.08(13)
N1 - C1 - C2 - C3	177.85(13)	C6 - C1 - C2 - C3	0.0(2)
C4 - C3 - C2 - C1	-0.2(2)	C2 - C1 - C6 - C5	0.1(2)
C4 - C5 - C6 - C1	-0.1(2)		

Symmetrical transformation used to generate equivalent atoms:

$$^11-X,+Y,1/2-Z$$

Table 2A-6 Hydrogen Atom Coordinates ($\text{\AA}\times 104$) and Isotropic Displacement Parameters ($\text{\AA}^2\times 103$).

Atom	x	y	z	U(eq)
H3	3085	5350	-2802	26
H5	3647	2245	-1214	28
H6	4311	3095	708	28
H10A	1204	4625	-1232	60
H10B	2098	4457	-1173	60
H10C	1786	3557	-561	60
H11A	579	3541	-4256	70
H11B	1305	4465	-3551	70
H11C	389	4600	-3670	70
H2A	3765(11)	6220(16)	-885(15)	25(4)
H2	2300(20)	3370(30)	-5340(30)	126(12)
H1	4720(20)	4790(30)	1860(30)	143(16)